2017

Light Stimulation of Sensory Hair Cells

Julien Azimzadeh

LIGHT STIMULATION OF SENSORY HAIR CELLS

A Thesis Presented to the Faculty of

The Rockefeller University

in Partial Fulfillment of the Requirements for

the degree of Doctor of Philosophy

by

Julien Babak Azimzadeh

June 2017

LIGHT STIMULATION OF SENSORY HAIR CELLS

Julien B. Azimzadeh, Ph.D.

The Rockefeller University 2017

Hair cells are the mechanosensory detectors that underlie our senses of audition and balance. Their mechanosensitivity arises from direct gating of force-sensitive ion channels by the tension in tip links located at the tops of the stereocilia. The study of hair cells and their mechanically gated channels has heretofore required physical displacement of a hair bundle to open its mechanotransduction channels. The work presented here describes a novel method of hair-bundle stimulation: irradiation with light.

The original aim of this study was to elucidate the role of Ca^{2+} in fast adaptation, a process thought to underlie a hair bundle's ability to amplify stimuli. I aimed to do this by generating intracellular surges in Ca^{2+} concentration without altering the state of the mechanotransduction channel or its associated elements. This procedure would permit me to study the mechanical correlates of fast adaptation independently from those associated with transduction. I used a light-sensitive, Ca^{2+}-loaded cage compound to release Ca^{2+} in hair cells by ultraviolet irradiation. To my surprise, irradiation both in the presence and absence of the caged compound caused rapid motion of hair bundles towards their tall edge, a motion typically associated with excitatory stimulation.

Tight-seal, whole-cell recording disclosed that the motion was associated with rapid opening of mechanotransduction channels. Both the light-evoked movement and the channel gating disappeared when tip links were ruptured, indicating that the mechanotransduction apparatus is involved in a hair cell's response to light. Blockage of the mechanotransduction channels in their open state with gentamicin abolished the light-evoked electrical response but incompletely reduced the light-evoked dis-

placement, suggesting that channel gating is only partially responsible for light-evoked hair-bundle motion.

I sought to identify the cellular components underlying light-evoked hair-bundle motion. Using an illumination system containing a digital micromirror device, I localized the absorptive element responsible for hair-bundle motion to the region directly below the bundle. The absorbers appeared to be mitochondrial chromophores that release the absorbed energy as heat. In experiments combining ultraviolet and infrared irradiation, I found that heat pulses of 0.5 K are sufficient to elicit hair-bundle motion. These heat pulses may alter the mechanical properties of tip links, leading to hair-bundle motion and mechanotransduction-channel gating. Thus the hair bundle confers thermal sensitivity upon a hair cell. The ability to stimulate hair cells using light will benefit physiological investigations of hair-cell function, and may have a role in non0invasively boosting hair-cell function in patients with hearing loss.

Dedication

To my parents.

Acknowledgements

For my first visualizations of the microscopic living world I thank my mom. Her epic stories recounting the battles waging inside my body on sick days ignited my imagination. Thank you mom and dad for nurturing my passion and always being there to support me. To Mr. Stranathan I owe a great deal of my independence of thought. Thank you for making us think.

I am grateful to Steven Bernstein, who gave me my first glimpse of the beauty of nervous tissue and inspired me to discover how it works. That desire led me to the lab of Patrick Kanold, where I fell in love with physiology. Patrick's pronouncement on my first day, "it's just like a video game" would have attracted any undergraduate, but his contagious energy and curiosity were the ultimate magnet for my young mind. To Ray St. Leger I would like to say: thank you for keeping me humble. Your elaborate recountings of history showed me just how old our current concerns are.

My graduate education would not have been the same without the wonderful people of the Hudspeth lab. The familial, collaborative, and hard-working nature of our group make it an ideal place to explore the unknown. I especially would like to thank Tobi Bartsch, from whom I received a working understanding of optics, and Josh Salvi, who helped debug many of my ideas. Daibhid Ó Maoiléidigh and Florian Berger helped me understand my experimental results in mathematical terms, and Andrei Kozlov's razor-sharp reasoning guided the coherent interpretation of my

results.

None of the wonderful science that takes place in the Hudspeth lab would occur without the expert administrative support of Beth Dougherty. Beth, thank you for being so welcoming and supportive, and for just making everything work. My experience would also not have been the same without Brian Fabella, who wrote the LabVIEW code for the many different experiments I performed, and helped me build much of the custom equipment used in this study. Brian, thank you for being so talented, flexible, and wonderful to be around.

I also owe a debt of gratitude to the faculty of the inaugural Physical Biology of the Cell course at the Marine Biology Laboratory. Rob Phillips, Hernan García, Jané Kondev, and Julie Theriot: thank you for your patience and dedication. I wish to thank Olaf Andersen, Ruthie Gotian, Renee Horton, Elaine Velez, Ken Javier, and Hanna Silvast for making the MD/PhD program run as smoothly as it does. Likewise, I send a big thank you to Cris Rosario, Stephanie Fernandez, Marta Delgado, Kristen Cullen, Emily Harms, and Sid Strickland at the Dean's office at Rockefeller for all of their hard work.

My faculty committee members, David Gadsby, Sandy Simon, and David Christini provided valuable insight and guidance, as well as periodic boosts of confidence for which I am very grateful. I especially would like to thank my external examiner, Richard Rabbitt, for flying in from Utah to examine my graduate work.

Rebecca, you were instrumental in keeping me grounded and happy regardless of the state of my science. Thank you for all of your support, and for your uncanny ability to seed experimental ideas into my mind.

Finally I wish to thank Jim, the ultimate role model for an aspiring scientist. Jim, thank you for leading by example and allowing me wide latitude and independence. I have been inspired by your clarity of thought and expression, and deeply appreciate

the environment you have created in lab. Thank you for showing me how to design experiments around important questions (and not vice-versa), and for freeing me from any perceived limits of what is experimentally possible.

Table of Contents

List of Figures

List of Tables

Chapter 1

Introduction to Hearing

1.1 The Peripheral Auditory Pathway

Our sense of hearing endows us with the ability to detect pressure waves at frequencies ranging from 20 to 20,000 Hz. These waves are guided towards the inner ear by the pinna and external auditory canal, where they impinge upon the eardrum and set it into motion (Fig. 1.1). Vibrations of the eardrums are transmitted through a chain of three ossicles, the malleus, incus, and stapes, to the oval window of the cochlea. The cochlea is a bony spiral structure, named after the Greek word kokhlias, or "snail." Inside it lies the organ of Corti, an epithelial structure comprising a variety of cells, including the hair cells responsible for mechanoelectrical transduction. The organ of Corti lies atop the basilar membrane, a stiff membrane of connective tissue. The cochlea is liquid-filled and partitioned into three reservoirs by the organ of Corti and Reissner's membrane, a thin sheet of connective tissue (Fig. 1.2). The mechanical energy conferred to the cochlear fluid by motion of the oval window generates pressure waves that travel along the basilar membrane. These traveling waves set the organ of Corti into motion and peak at various positions along its length. The

mechanical properties of the basilar membrane change continuously along the length of the cochlea, conferring upon each segment a characteristic frequency of motion. Thus vibrations generated by pressure stimuli are spatially decomposed into their frequency components along the basilar membrane. High-frequency vibrations peak in the proximal portion of the organ of Corti, whereas low-frequency vibrations travel to its tip. A thin, gelatinous structure, the tectorial membrane, lies atop the organ of Corti just above the hair cells (Fig. 1.2a). The organ of Corti and its overlying tectorial membrane shear past each other in response to the traveling wave. This shearing motion stimulates hair cells, which then convert the mechanical energy into electrical signals (Fig. 1.2b). The electrical activity of hair cells is transmitted to spiral ganglion neurons, which carry the information to the cochlear nuclei of the brainstem.

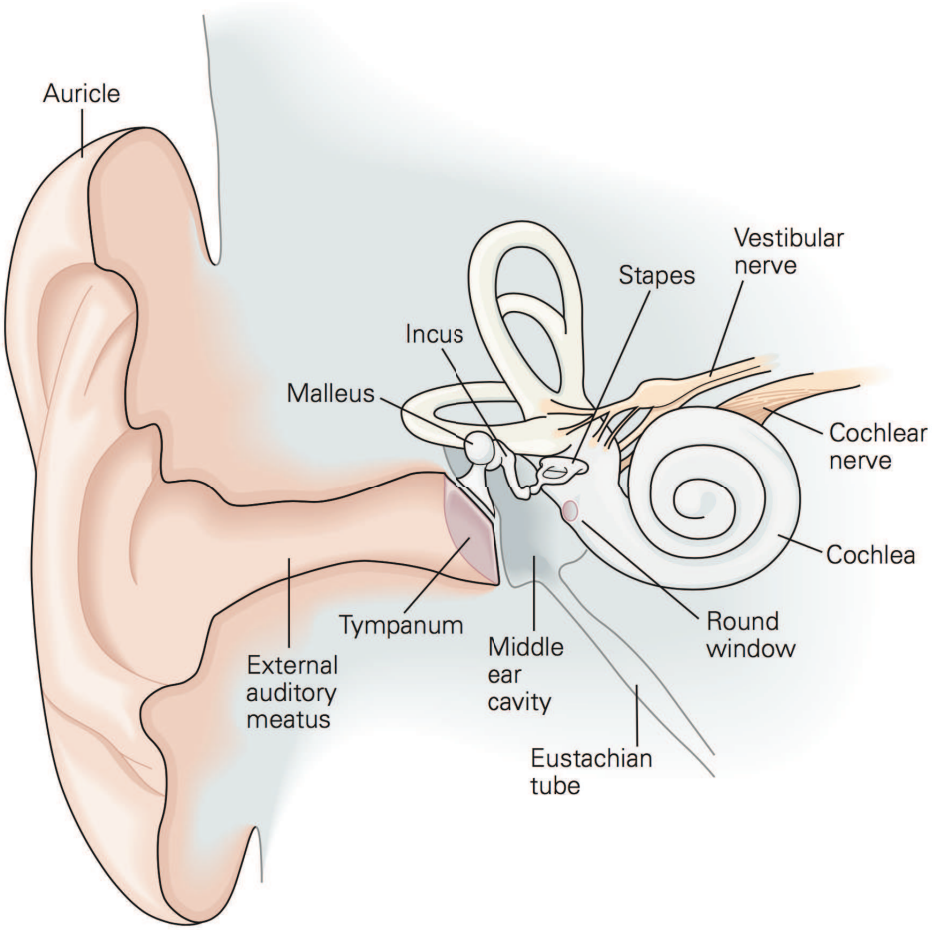

Figure 1.1: Peripheral auditory pathway. The external ear guides sound waves towards the tympanic membrane, setting it in motion. The three middle ear bones, the malleus, incus, and stapes, transmit the sound vibrations to the oval window of the cochlea. Image taken from *Principles of Neural Science*, 5^{th} ed., p. 655.

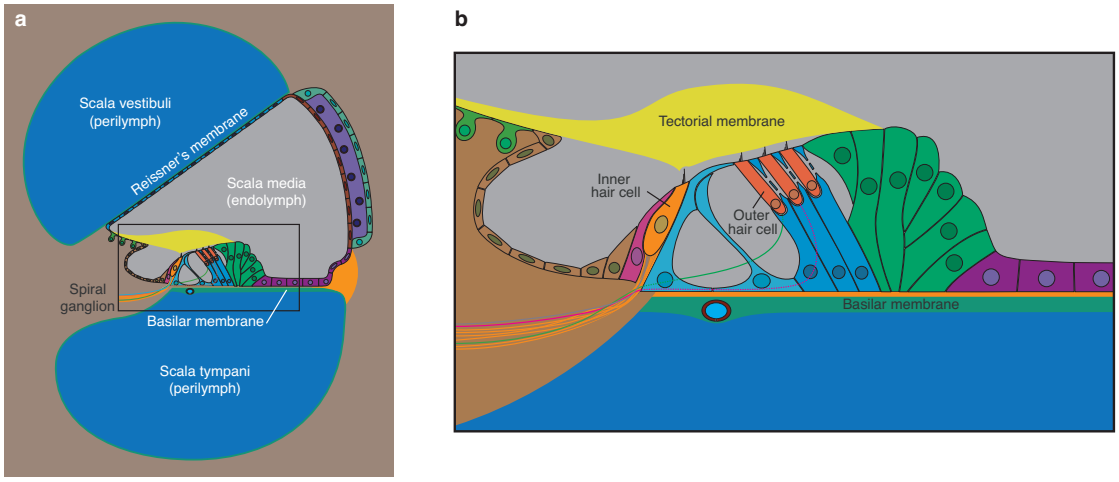

Figure 1.2: The organ of Corti. (a) The organ of Corti is an epithelial structure that lies between the scala media and scala tympani. (b) It rests atop the basilar membrane, a stiff layer of connective tissue. Pressure-induced travelling waves displace the organ of Corti and its overlying tectorial membrane, causing them to shear with respect to one another. This motion deflects the apical hair bundles of hair cells towards and away from the spiral ganglion, stimulating them. Hair cells are exposed to K^+-rich endolymph at their apical surface, and Na^+-rich perilymph on their basolateral surface. Figures adapted from [1]

The organ of Corti contains two types of sensory cells: inner and outer hair cells. Inner hair cells, of which there is a single row, are located towards the cochlea's spiral axis, and serve primarily as detectors of mechanical stimulation. They are innervated by afferent fibers of the spiral ganglion. Outer hair cells are present in three rows and are principally responsible for mechanical amplification. Unlike inner hair cells, they are chiefly innervated by efferent fibers, and have sparse afferent innervation. The mechanical amplification produced by outer hair cells is discussed in the next section.

1.2 The Active Process

The ear is exquisitely sensitive: its hair cells can detect movements close to $\pm$ 0.35 nm, on the order of the motion due to thermal noise [2, 3, 4]. The ear is also a remarkable frequency sensor, allowing us to distinguish tones that differ by only 0.2% [5]. However, both of these characteristics disappear within minutes after the cochlea is deprived of energy [6]. This has led to the hypothesis that an active process underlies the cochlea's extreme performance [3, 7].

The basis of the active process lies in two distinct forms of cellular motility. In the first, termed hair-bundle motility, motion of the basilar membrane is augmented by force produced by hair bundles. Hair-bundle motility is responsible for the entirety of the active process in amphibians and some reptiles, and for a portion of the mammalian active process. The second process, which is limited to mammals and perhaps some birds, is termed somatic motility or electromotility. In somatic motility, the length of a hair cell's soma changes in phase with basilar-membrane vibrations to supplement basilar membrane motion. Somatic motility is carried out by outer hair cells in the organ of Corti. Outer hair cells are uniquely suited for this function owing to their high membrane concentration of prestin, a protein that displays piezoelec-

tricity. Prestin undergoes a conformational change in response to alterations in the membrane potential. The concerted rearrangement of millions of prestin molecules in the cell membrane generates force in the organ of Corti and amplifies the motion detected by inner hair cells. Hair-bundle and somatic motility likely work in tandem, the first setting the timing for amplification and the second providing most of the power gain [1, 8, 9].

1.3 Other Mechanosensitive Organs Including Hair Cells

In addition to their role in the cochlea, hair cells mediate mechanotransduction in a variety of other mechanosensitive organs. For example, they underlie the detection of linear and angular acceleration in the vestibular system and water motion in the lateral line of fish. Saccular hair cells of the American bullfrog (*Rana catesbeiana*) have proved especially useful in the study of hair-cell physiology. The sacculus is a mixed-function organ performing both low-frequency hearing and seismic sensation (Fig. 1.3). The otolithic membrane, a thin gelatinous sheet, rests on top of hair cells of the sacculus. The otolithic membrane is loaded with crystals of calcium carbonate that provide an inertial load that displaces the membrane upon stimulation.

The sacculus' extraordinary use to physiologists stems from several characteristics. First, it is readily accessible because unlike the cochlea, it is not encased in a brittle shell of bone. Its hair cells are remarkably robust and can remain healthy at room temperature for several hours. The hair bundles of saccular hair cells are large and easily visualized thanks to the thinness of the organ. Finally, the sacculus' low curvature allows easy mounting and manipulation with electrophysiological and micromechanical implements [10]. I performed this study in the American bullfrog's

sacculus because of the advantages listed above and our group's extensive experience with this system.

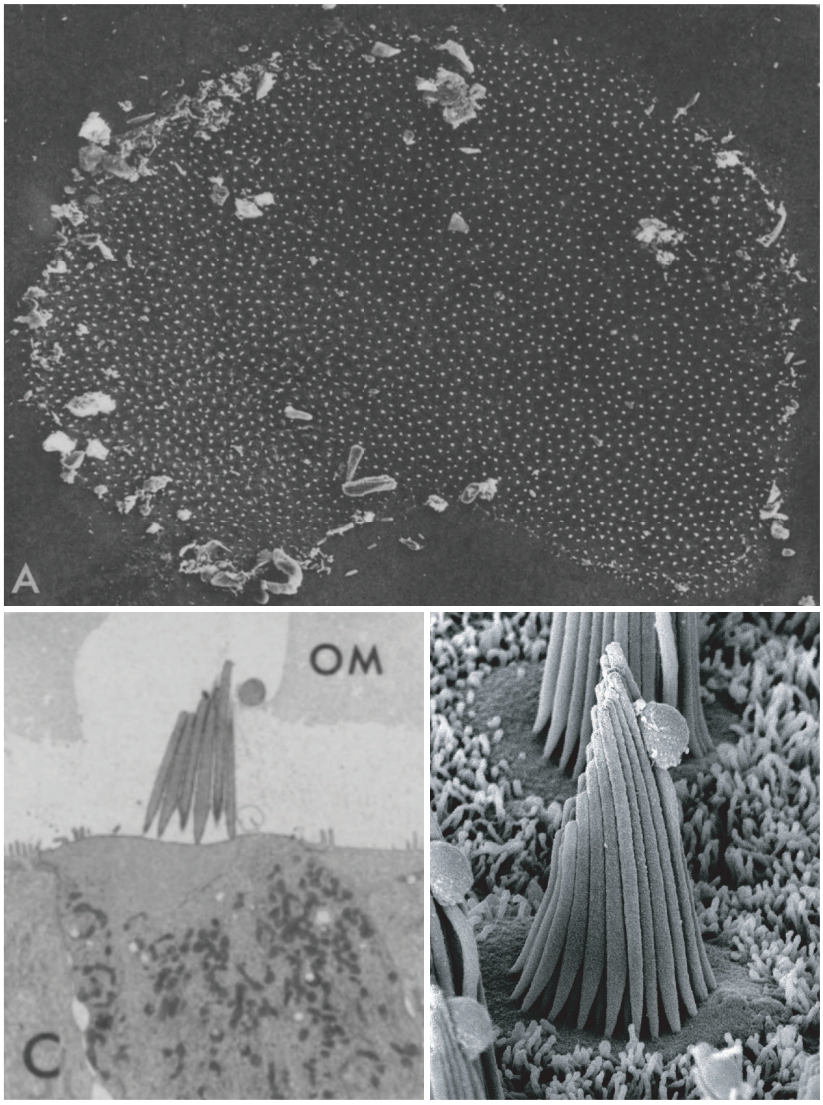

Figure 1.3: The bullfrog sacculus. Top: Scanning electron micrograph of the sacculus of the American bullfrog, *Rana catesbeiana*. The tectorial membrane was removed before processing to allow visualization of hair bundles (seen here as small, regularly-spaced white punctae). Bottom left: Transmission electron micrograph of the apical portion of a hair cell. The attachment of the kinociliary bulb to the otolithic membrane (labelled "OM") is seen. Bottom right: Scanning electron micrograph of a bullfrog saccular hair bundle. Top and bottom left images from [11]. Bottom right image unpublished, personal communication from Dr. Hudspeth.

1.4 Hair-Bundle Structure

Hair cells are named for their apical organelle, the hair bundle. A hair bundle consists of tens to hundreds of stereocilia, rigid rod-like protrusions filled with paracrystalline actin (Fig. 1.3). Stereocilia emerge from an apparently rigid actin-filled structure at the apex of each hair cell named the cuticular plate. Although the function of the cuticular plate is still uncertain, it is thought to provide a stable anchor to the hair bundle. The bundle's stereocilia are arranged in a staircase pattern, with the tallest row of stereocilia abutting a single true cilium, the kinocilium. In some organs, such as the organ of Corti, the kinocilium degenerates after development, leaving only the staircase arrangement of stereocilia. Each stereocilium tapers in diameter at its insertion into the cuticular plate. Because of this, mechanical stimulation causes each stereocilium to bend only at this insertion point, which is termed the stereociliary pivot. The pivoting motion of stereocilia leads to shearing at the hair-bundle tip in response to mechanical stimulation.

Figure 1.4: Hair cell and hair bundle structure. (a) The hair bundle extends from the apical surface of the hair cell, where it is anchored in the actin-containing cuticular plate. Each stereocilium tapers in diameter at its insertional point, the stereociliary pivot. A single "true" microtubule-filled cilium, the kinocilium, is present on the tall side of the hair bundle. In the bullfrog sacculus, the kinociliary bulb is attached to the otolithic membrane. It conveys stimuli to stereocilia through small proteinaceous links between itself and the tallest row of stereocilia. (b) When a hair bundle is forced towards its tall edge, tension in its tip links pulls mechanically-gated transduction channels open. The resulting K^+ and Ca^{2+} influx depolarizes the cell and increases its synaptic release of glutamate. (c) Adaptation motors control the tension in the tip link by climbing or slipping on the actin core of stereocilia. Panels **b** and **c** adapted from [1].

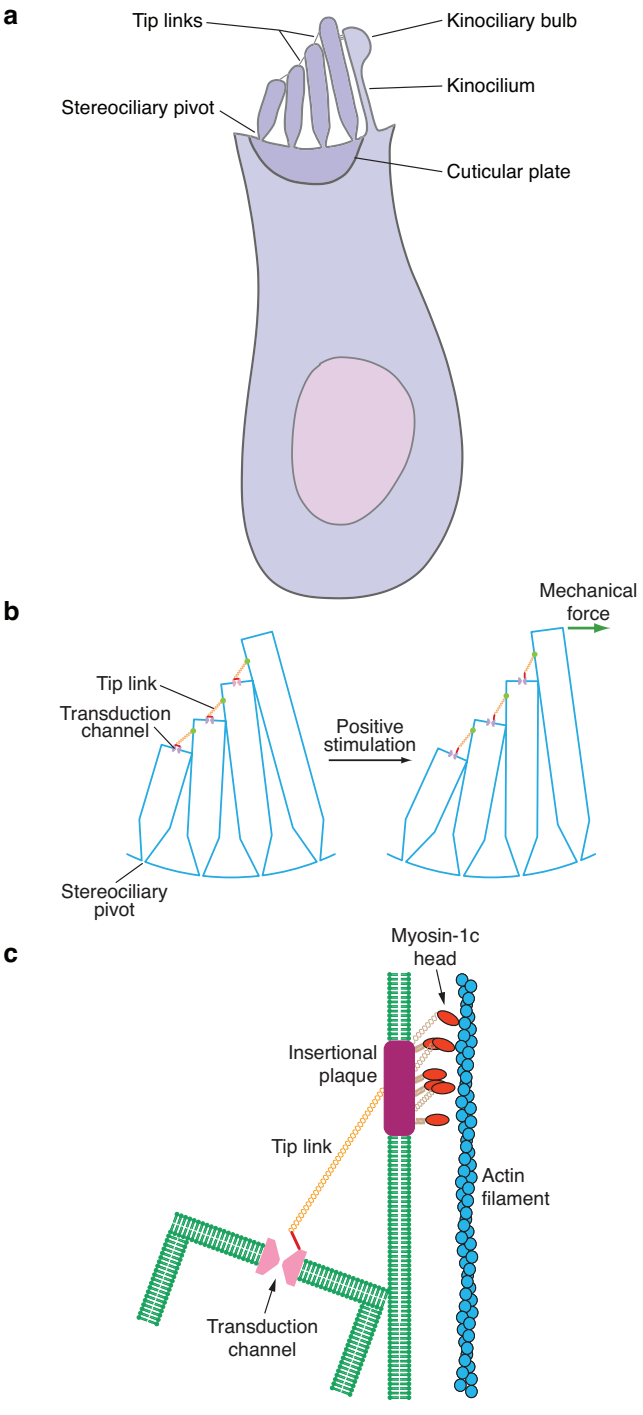
a
Tip links
Kinociliary bulb
Kinocilium
Stereociliary pivot
Cuticular plate
b
Mechanical force
Tip link
Transduction channel
Positive stimulation
Stereociliary pivot
c
Myosin-1c head
Insertional plaque
Tip link
Actin filament
Transduction channel

1.5 Hair-Bundle Function

Each stereocilium is connected to its tallest neighbor through a thin filamentous linkage termed the tip link. When a hair bundle is pushed towards its tall edge, the resulting shear at the tips of its stereocilia tenses the tip links, causing force-gated channels at the top of each stereocilium to open (Fig. 1.4). The exact number of channels per stereocilium is not known, but the closest estimates suggest that there are only one or two [12]. The channel, which has not yet been identified, has a large-conductance (100 pS), cation-selective pore and can thus be transiently blocked by large positively charged molecules such as aminoglycoside antibiotics. Each tip link comprises a dimer of cadherin 23 bound end-on to a dimer of protocadherin 15 [13]. These filamentous proteins require Ca^{2+} both to properly fold and to interact with each other. Thus tip links can be disrupted by lowering the external Ca^{2+} concentration to several hundred nanomolar. A hair bundle with disrupted tip links does not respond to mechanical stimuli [14].

1.6 Direct Gating and Gating Compliance

Mechanical deflection of a hair bundle towards its tall edge results in a graded receptor potential that adapts within several tens of milliseconds (Fig. 1.5). This receptor potential stems from the receptor current carried by mechanotransduction channels, which develops within 40 μs of stimulation [15]. The short latency of this current provides the first clue that transduction is directly mediated by mechanical tension. Enzymatic turnover rates are in general too slow to account for the rapid onset of current observed in hair cells [16]. The direct mechanical gating hypothesis is supported by the observation that a bundle's stiffness is not linear with displacement [17]. Instead, a bundle's stiffness is smaller in the range of displacements over which

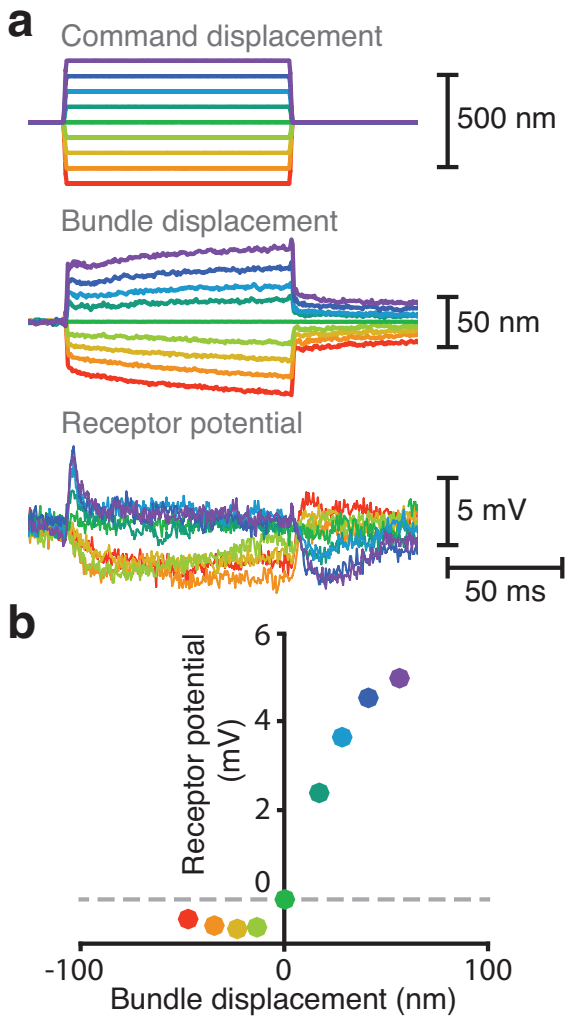

Figure 1.5: Receptor potential. (a) The tip of a glass stimulus fiber was coupled to the kinociliary bulb of a hair bundle and the fiber's base was subsequently displaced across nine discrete steps. The bundle's position was tracked on a dual-photodiode system, and the receptor potential was simultaneously measured using a microelectrode. The bundle's resting membrane potential was -47 mV. (b) A plot of the bundle's receptor potential as a function of its displacement reveals a nonlinear relationship between the bundle's response and its position. Each point corresponds to the mean potential and mean displacement over a 2.5 ms time window, beginning 2.5 ms after the onset of mechanical stimulation. Each color represents a set of time series corresponding to the same displacement pulse.

mechanotransduction channels gate, suggesting a mechanical link between channel gating and bundle position (Fig. 1.6). Treatment of a hair bundle with gentamicin, an aminoglycoside antibiotic that blocks the mechanotransduction channel in its open state, abolishes this reduction of stiffness [17]. This result suggests that the reduction in stiffness arises from channel gating, hence its designation as gating compliance. Gating compliance can be understood as the decrease in a bundle's stiffness resulting from the concerted opening of its mechanotransduction channels' gates. This gating non-linearity occurs over a 35-75 nm range of hair-bundle displacements in bullfrog saccular hair cells. Thus if a hair bundle's mechanotransduction channels were to spontaneously open, the bundle would move 35-75 nm towards its tall edge. Motion in the direction of the bundle's axis of sensitivity is related to motion along the tip-link axis through the conversion factor $\gamma = 0.14$ in the bullfrog sacculus. The above 55 nm hair-bundle displacement caused by channel opening thus implies a channel gating distance of $55 \times 0.14 = 8$ nm, assuming channels are arranged in parallel. Though it is unlikely that any portion of the channel swings open by 8 nm, the concept of a swinging door provides an easily visualizable model for gating compliance.

The gating compliance of a hair bundle relies in part on the cooperativity of mechanotransduction channels, which in turn depends on the gating force of each channel. The opening of one mechanotransduction channel causes a redistribution of the force formerly carried by its gating spring onto the other gating springs, increasing their channels' probability of opening. Thus large channel gating forces result in more force redistribution among other channels upon channel opening, and stronger cooperativity. This can lead to gating compliance so extreme that bundle stiffness becomes negative (Fig. 1.6). A bundle displaying negative stiffness does not oppose its stimulus, but instead furthers its stimulus' action. This results in a mechanical instability, because the bundle cannot stably remain in the region of negative stiffness.

Negative stiffness allows large hair-bundle movements to arise from small stimuli, and may thus underlie the hair bundle's activity as an amplifier.

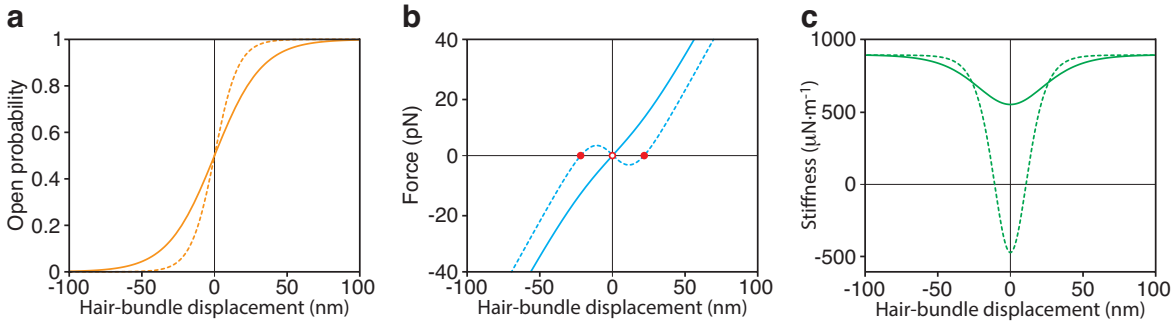

Figure 1.6: Gating compliance. (a) The open probability of a hair bundle's channels is a sigmoidal function of its position. The relation becomes steeper as the gating force for each channel increases (dotted line). (b) The relation between the force applied to a bundle and its ensuing displacement increases monotonically for small gating forces (solid blue line). When the gating force is large, the slope becomes negative in the region where the channels gate. (c) Gating compliance manifests as a reduction in hair-bundle stiffness in the region where channels gate. Large gating forces can give rise to negative hair-bundle stiffness (dotted line). Figures taken from [1].

1.7 Parallel Gating of Mechanotransduction Channels

The mechanically-sensitive elements of a hair bundle appear at first glance to be arranged in series (Fig. 1.7). With such an arrangement, a force applied to the tallest stereocilium would first open mechanotransduction channels in the tallest row of stereocilia, followed by the second, then third, and so on. As transduction channels open and relieve tension, the bundle would reach equilibrium with the stimulus force with the channels on its tall side open and those on the short side closed. This arrangement would result in low sensitivity because each opening event reduces the force felt by the channels that are still closed.

A bundle designed for maximal sensitivity would have a parallel arrangement of mechanosensitive channels (Fig. 1.7a). In such an arrangement, the tension applied to a hair bundle is distributed equally among all tip links. When one channel opens, the tension lost from its tip link is offloaded and equally divided among all remaining tip links, thus increasing the probability of another opening event (Fig. 1.7b). As opening events occur, more and more tension must be carried by the tip links whose channels are still closed, thus triggering a cooperative avalanche of channel opening. A parallel arrangement of channels thus results in high sensitivity over a narrow range of displacements. Evidence for a parallel arrangement of channels comes from an elegant set of experiments in which motion at the tip of the tallest stereocilium was compared to motion at the tip of the shortest stereocilium [18]. The movements at both loci are strongly correlated, revealing that the bundle moves as a unit and stereocilia do not splay. The parallel arrangement of hair cells' mechanically gated channels results in cooperativity and underlies the phenomenon of negative hair-bundle stiffness.

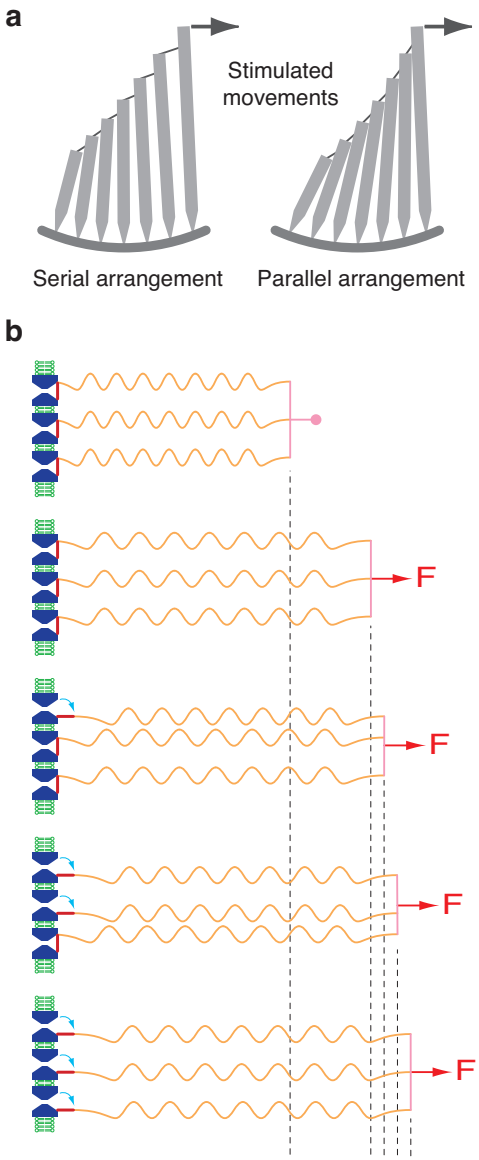

Figure 1.7: Parallel gating. (a) Left: A series arrangement of stereocilia tenses tip links sequentially. Right: A parallel arrangement of stereocilia distributes tension among all tip links, resulting in cooperativity. (b) Three channels are connected in parallel. The application of a force F first stretches the gating springs, moving the bundle towards its tall edge. A single channel then stochastically opens, relieving tension in its gating spring. The relieved tension is distributed among the two remaining closed channels, which are now more likely to open. The second channel opens, further increasing tension on the last channel and increasing its open probability. Images taken from [18, 19].

1.8 Slow Adaptation

The resting open probability of mechanotransduction channels is non-zero and depends upon the external Ca^{2+} concentration. This non-zero open probability stems from the resting tension on tip links, which itself is non-zero. Tip links are attached to molecular motors at their upper insertional points (Fig. 1.4). These molecular motors apply enough tension on tip links to maintain an open probability of approximately 20% in 250 μM $[Ca^{2+}]_o$ and 10% in 2 mM $[Ca^{2+}]_o$ at rest [16]. The resting tension in tip links causes hair bundles to be positioned slightly negative with respect to the equilibrium position of stereociliary pivots. Thus upon rapid rupture of its tip links, a hair bundle snaps forward by several tens of nanometers [14].

The motor molecule responsible for tensioning tip links is myosin 1c, which is likely regulated by Ca^{2+} through interactions with calmodulin [20, 21]. Myosin-1c augments tip-link tension by climbing on the stereociliary actin core. Its climbing rate is diminished as the concentration of Ca^{2+} increases inside stereocilia. Because mechanotransduction channels are calcium-permeable and the endolymphatic fluid bathing saccular hair cells contains 250 μm calcium, the state of mechanotransduction channels regulates myosin-1c activity. This feedback gives rise to slow adaptation, an adaptive mechanism that constantly attempts to place the hair bundle in its most sensitive region. When a hair bundle is pushed and held towards its tall edge, mechanotransduction channels open and pass current, some of which is carried by Ca^{2+}. The resulting increase in $[Ca^{2+}]_i$ weakens the acto-myosin interaction, causing myosin to slip. Myosin slippage reduces tension in the tip link, promoting reclosure of mechanotransduction channels and a slow positive relaxation of the hair bundle (Fig. 1.8a). Conversely, stimulation in the negative direction reduces tip-link tension and closes the mechanotransduction channels that are open at rest. This reduces Ca^{2+} entry and increases myosin activity, thus restoring tip-link tension. When the hair

bundle is moved back to its original position, tension in the tip links is high because myosin motors are now bound higher along the stereociliary actin core. This leads to channel opening and a corresponding inward current at the offset of the pulse (Fig. 1.8a). Myosin-based hair-bundle adaptation therefore serves as a homeostatic mechanism that restores the open probability of a bundle to approximately 20%. This allows a bundle to remain sensitive to displacements even after it has been offset by a constant stimulus (Fig. 1.8b, c). The time constant of myosin-based adaptation in the bullfrog sacculus is 15-20 ms. This value contrasts with that of another adaptation mechanism, termed fast adaptation, that operates with a time constant of approximately 1 ms.

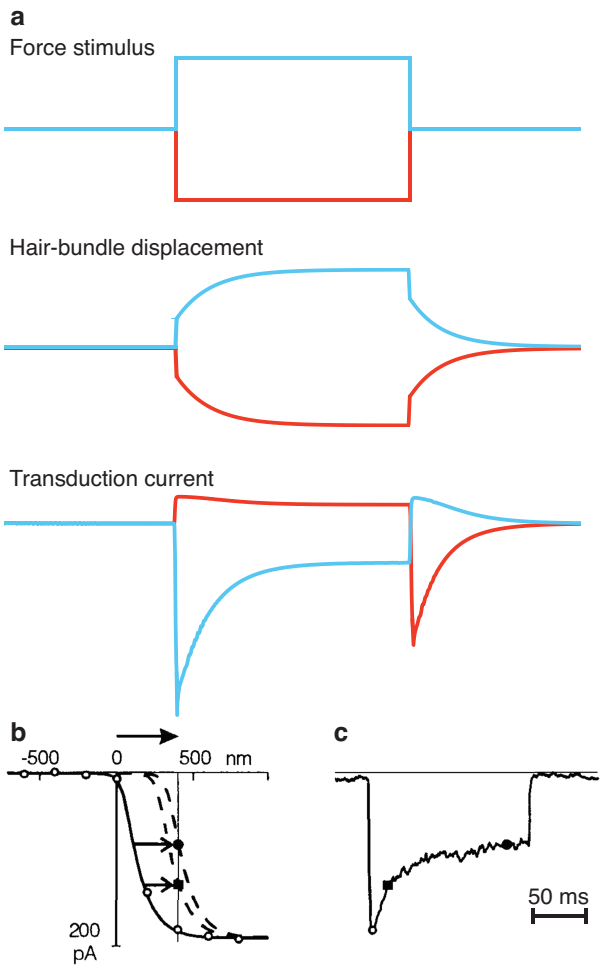

Figure 1.8: Slow adaptation. (a) When a bundle is abruptly forced in the positive direction (blue), it first moves rapidly towards its tall edge and then more slowly relaxes with a time constant of approximately 20 ms. Mechanotransduction channels are opened by the stimulus, resulting in inward current carrying K^+ and Ca^{2+}. Myosin motors respond to the increased intracellular Ca^{2+} by slipping on actin and lowering tip-link tension, resulting in the mechanical relaxation of the bundle and gradual decay in current. When the bundle is forced in the negative direction (red), mechanotransduction channels close, reducing the influx of Ca^{2+}. Myosin motors respond by climbing along actin to re-tension the tip links and restore the steady inward current. When the bundle is returned to its original position, the tension in tip links increased, resulting in an inward current. The plots shown here are model results. (b) Slow adaptation shifts the stimulus-response curve of a hair bundle. The three stimulus-response curves in (b) correspond to the three points in **c**, which shows the current decay during a positive force step. (b) and (c) were taken from [22].

1.9 Spontaneous Oscillations

Hair bundles not only detect sound but also act as active amplifiers. This is most clearly shown by their tendency to spontaneously oscillate (Fig. 1.9a) [23]. Hair bundle oscillations consist of alternating fast and slow phases. The fast phase of oscillation arises from a hair bundle rapidly crossing its region of negative stiffness. Thus fast positively directed jumps stem from concerted channel opening events, and fast, negatively directed jumps represent concerted channel closings. The intervening slow phases stem from the action of myosin motors, which constantly attempt to poise the bundle near an open probability of 20%. As myosin homeostatically alters tip-link tension, it moves the bundle ever closer to its region of negative stiffness. The bundle reaches the region of negative stiffness before reaching its target open probability and overshoots myosin's set point, leading to adaptation in the opposite direction. Now myosin moves the bundle in the opposite direction, towards the open probability set point, only to overshoot it again due to negative stiffness. The repetition of this cycle provides the basis for spontaneous hair-bundle oscillation (Fig. 1.9b).

The molecular underpinnings of the above mechanism were confirmed both pharmacologically and electrophysiologically. First, upon blockage of its mechanotransduction channels with gentamicin, a hair bundle stops oscillating and remains in the positive position [23]. Second, simultaneous recordings of a hair cell's current and its bundle's position reveal that rapid positive bundle motion during spontaneous oscillations is associated with an inward transduction current [24]. The adaptation motor was implicated in spontaneous oscillation with pharmacological evidence. Treatment of an oscillating hair bundle with butanedione monoxime, a putative myosin inhibitor, abolishes spontaneous oscillations [24].

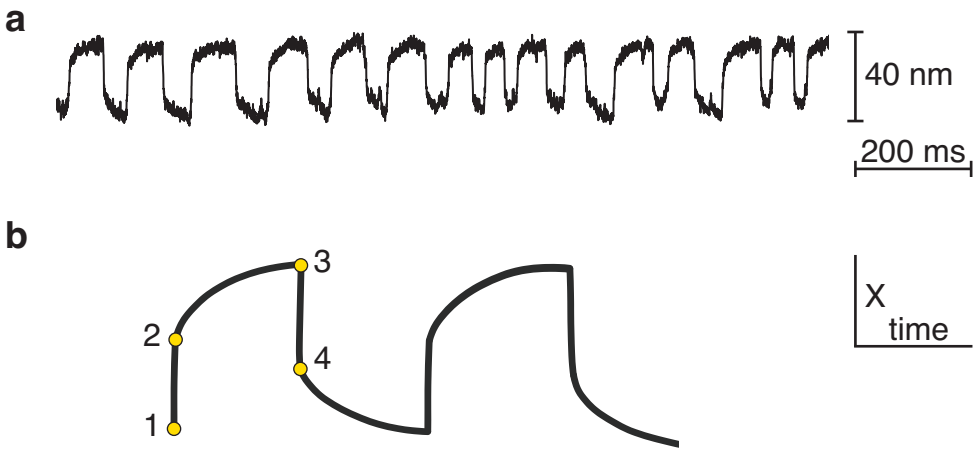

Figure 1.9: Spontaneous oscillations. (a) A hair bundle in a two-chamber preparation oscillates spontaneously. (b) 1, High tip-link tension causes concerted channel opening, rapidly moving the bundle towards its tall edge. 2, Ca^{2+} entry through the open channels leads to myosin slippage, which reduces tip-link tension. This slow reduction allows the bundle to slide further in the positive direction. 3, Tip-link tension drops below a critical point, causing concerted channel closure and rapid movement in the negative direction. 4, With mechanotransduction channels closed, Ca^{2+} pumps in stereocilia reduce the internal Ca^{2+} concentration, allowing myosin motors to climb and restore tip-link tension. Once tip-link tension reaches a critical point required for channel opening, the cycle re-starts at 1.

1.10 Fast Adaptation

When a hair bundle is rapidly forced towards its tall edge, a fraction of the resulting transduction current is abolished within approximately one millisecond. This reduction in current is termed fast adaptation, and is caused by a mechanism distinct from that of slow adaptation. Measurement of a hair bundle's position concurrent with its electrical response reveals a mechanical correlate of fast adaptation: a negatively directed twitch of several tens of nanometers (Fig. 1.10)[17, 25, 26]. The simultaneous reduction in transduction current and negatively directed twitch that characterize fast adaptation suggest that it represents the closure of mechanotransduction channels.

Fast adaptation requires Ca^2+ entry into stereocilia, for neither the mechanical twitch nor adaptation of the transduction current occurs in conditions that reduce Ca^{2+} flux. These conditions include reduction of the external Ca^{2+} concentration, depolarization of a hair cell to reduce the driving force for Ca^{2+} entry, and dialysis of a cell with a Ca^{2+} chelator [17, 27, 28]. The speed of fast adaptation suggests that Ca^{2+} has a direct mechanical effect on a component of the transduction apparatus, which perhaps is the channel itself.

The presence of fast adaptation has long intrigued auditory physiologists because of the possibility that it contributes to force generation and amplification by the hair bundle [29, 30, 31, 32]. The rapid reclosure of mechanotransduction channels might exert a negatively directed force on tip links, which would in turn be transmitted to the hair bundle. This force, if in an appropriate phase with the stimulus, could serve to amplify it. Hair bundles in acoustico-vestibular systems are embedded in an overlying membrane, allowing motion between neighboring hair bundles to be coupled. Thus recoils generated by some cells can amplify the stimulus felt by others. Although the action and potential role of fast adaptation may explain one of the most fundamental actions of hair bundles, there is no consensus on its molecular basis.

Several models for the mechanism of fast adaptation have been proposed, and can be grouped in three categories. In the first model, Ca^{2+} directly binds to the mechanotransduction channel to stabilize its closed state (Fig. 1.11)[29, 31]. In the second model, Ca^{2+} binds to a release element in series with the gating spring and reduces its stiffness, allowing channel reclosure (Fig. 1.11)[33]. The third model postulates that Ca^{2+} acts on the adaptation motor to either reduce its binding probability or to relax its calmodulin-binding neck domain, either of which would reduce gating-spring tension and allow channel reclosure (Fig. 1.11) [34, 35]. It is still unknown which of these three mechanisms underlies fast adaptation.

Because of fast adaptation's potential role in hair bundle-mediated amplification, I set out to study its mechanism as my thesis project. I aimed to use novel tools to study the activity of Ca^{2+} without altering the state of the mechanotransduction channel. Specifically, I intended to rapidly release Ca^{2+} inside hair cells by photolyzing a caged Ca^{2+} compound, nitrophenyl-EGTA (NP-EGTA) [36]. The EGTA component of NP-EGTA chelates Ca^{2+}, serving as a latent pool of releasable Ca^{2+}. The nitrophenyl group of NP-EGTA is a chromophore that triggers lysis of the NP-EGTA backbone upon ultraviolet irradiation, liberating Ca^{2+} in the process. I dialyzed a hair cell with Ca^{2+}-loaded NP-EGTA in the hopes of releasing Ca^{2+} with ultraviolet irradiation. This maneuver seemed promising, for I observed hair bundles move towards their positive direction in response to light. However, in the course of control experiments in which I irradiated undialyzed hair cells, I found that irradiation itself causes hair-bundle motion. After confirming this finding and discovering that the motion requires intact tip links, I decided to seek the basis of light-evoked hair bundle motion.

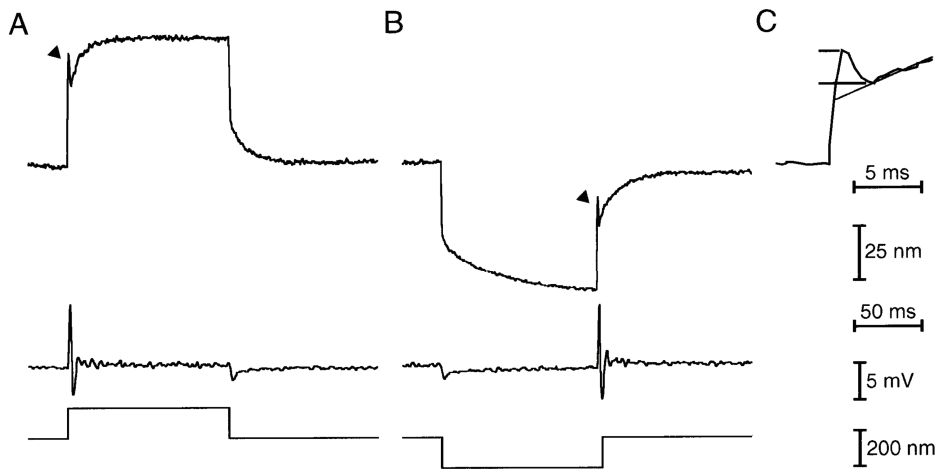

Figure 1.10: (a) A bundle is displaced in the positive direction, generating a receptor potential. Its displacement waveform displays a rapid biphasic twitch, the mechanical correlate of fast adaptation. (b) The same bundle does not exhibit a twitch upon initiation of negative displacement, as this motion closes mechanotransduction channels. Instead, the bundle exhibits a twitch upon its return to the holding position, when mechanotransduction channels are once again opened. (c) Magnified view of the twitch caused by fast adaptation. Figure taken from [25].

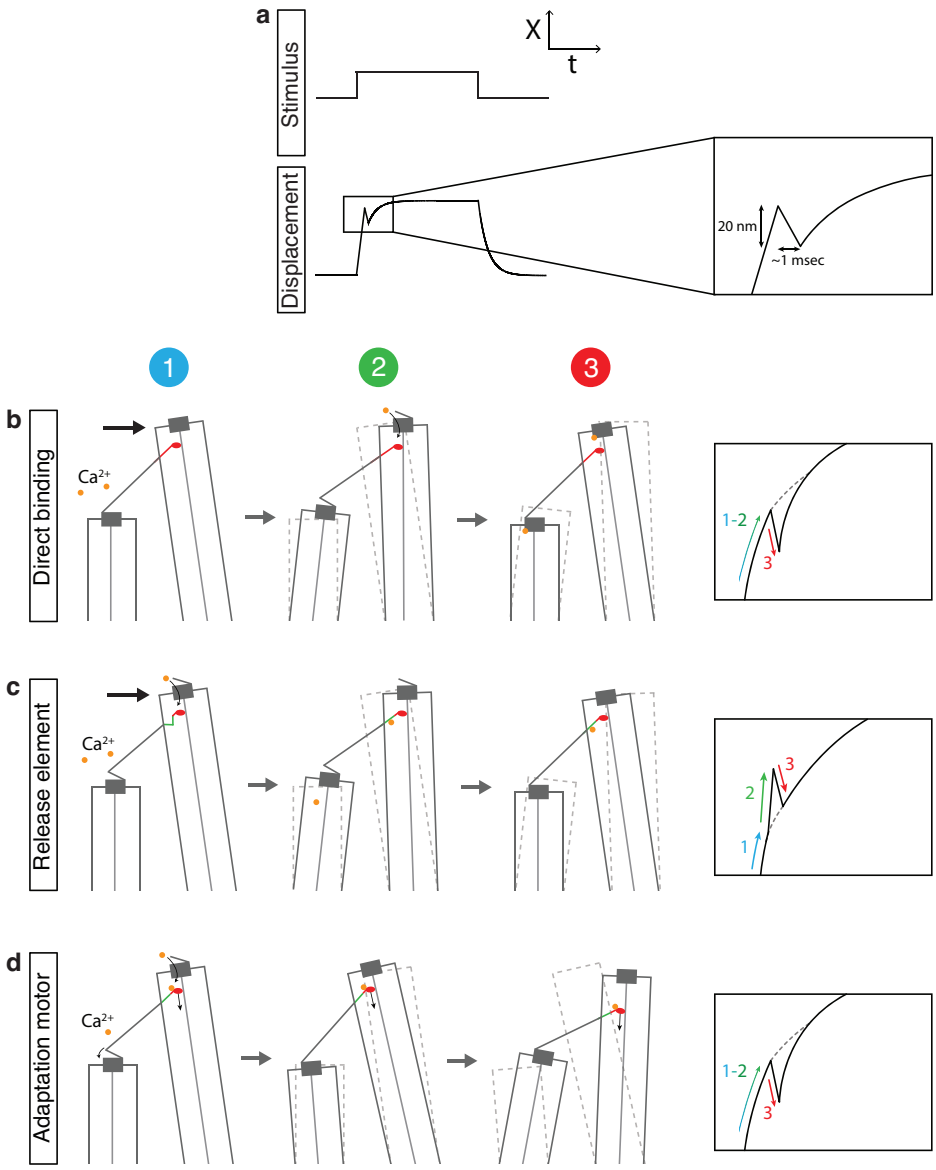

Figure 1.11: Models of fast adaptation. (a) A step displacement stimulus causes a twitch in displacement of a hair bundle (see Fig. 1.10). (b) In the direct binding model, Ca^{2+} binds to the mechanotransduction channel or a neighboring protein and induces its rapid closure. This pulls the tip links taught, leading to a rapid excursion of the bundle in the negative direction. (c) In the release-element model, Ca^{2+} binds to and relaxes a release element in series with the tip link. The transient decrease in tip-link tension caused by this relaxation causes the hair bundle to move positively. The tension release also allows the mechanotransduction channel to close, causing negative hair-bundle motion. (d) In the unified or adaptation motor model, Ca^{2+} binds to the adaptation motor, weakening its interaction with actin. As tension in the tip link is released, mechanotransduction channels rapidly reclose, generating a rapid negative movement. The adaptation motor continues to slip until the Ca^{2+} concentration drops enough to permit climbing.

Chapter 2

Characterization of the Hair-Cell Response to Ultraviolet Light

In this chapter I describe the observations that initially attracted my interest in studying light-evoked hair bundle motion. I review core experiments such as hair-bundle position and electrical recordings in response to light stimulation, as well as the effects of tip-link rupture and mechanotransduction-channel blockage. The chapter concludes with experiments that further characterize the phenomenon of light-evoked hair-bundle motion but do not offer insight into its underlying mechanism. The subsequent chapter deals with the mechanism underlying light-evoked hair-bundle motion.

2.1 Materials and Methods

2.1.1 The Bullfrog Sacculus Preparation

The acousticolateralis organs of mammals possess a complex architecture and lie within an anatomical niche that can be difficult to access. For example, the mammalian cochlea is embedded within the dense temporal bone. Isolation of the cochlea often causes mechanical damage to the sensory cells lying within it and has therefore proven to be a difficult task. Neuroscientists have thus turned to model systems that are more readily extracted from their surroundings.

One of these model systems is the sacculus of the American bullfrog (*Rana catesbeiana*), which for decades has yielded generalizable insight into the function of auditory and vestibular systems. The sacculus is a mixed-function organ with sensory roles in both low-frequency hearing and seismic sensation. It comprises several thousand hair cells embedded in an epithelium. The sacculus appeals to sensory neuroscientists for numerous reasons. Unlike the mammalian cochlea, it lies within the readily accessible otic capsule. Secondly, hair cells within the sacculus remain healthy for several hours under appropriate conditions [37]. This permits experimentation on these cells over long timescales relative to their mammalian counterparts. Third, the organ bears little curvature, permitting easy manipulation. Finally, the bullfrog's sacculus is easily visualized due to the thinness of this organ and large size of its hair cells.

These properties provide great versatility for the study of sensory cells within the bullfrog's sacculus. Depending on the question at hand, one of several experimental preparations can be obtained from the sacculus. The simplest of these is the one-chamber preparation. Here the sacculus is immobilized in a chamber filled with artificial perilymph, a Na^{2+}-rich and high-Ca^{2+} saline. This preparation permits the

study of hair-cell currents and basic hair-bundle mechanics. A second configuration, the two-chamber preparation, can be used to study spontaneous hair-bundle movements [23]. Here the apical side of hair cells is exposed to a K^+-rich and Ca^{2+}-poor saline solution termed artificial endolymph, whereas the basolateral side is bathed in artificial perilymph. These two compartments mimic the *in vivo* arrangement and provide an environment that allows hair bundles to oscillate spontaneously. A third preparation involves the dissociation of hair cells from their epithelial surroundings. Dissociation enables the study of both a cell's hair bundle and soma. Because the rigid apical cuticular plate thwarts the formation of tight seals for the whole-cell recording technique, dissociated hair cells are often used in combination with this technique. Dissociated hair cells also yield the best optical images and are thus useful for imaging studies. Unfortunately, the mechanical disruption required to dissociate hair cells can damage their sensitive hair bundles, making the study of mechanotransduction difficult. To provide access to hair cells' somata without damaging their bundles, I modified the dissociated-cell preparation to develop a configuration in which hair cells gradually extrude from the epithelium. This produces cells with an intact transduction apparatus that rest atop the epithelium.

Saline Solutions

Unless stated otherwise, all dissections and incubations were performed in standard saline composed of (in mM): 110 Na^+, 2 K^+, 2 Ca^{2+}, 118 Cl^-, 5 HEPES, and 3 D-glucose. The high Na^+ and low K^+ of this solution mimic the composition of the perilymphatic compartment of the inner ear, hence this solution is also termed "perilymph." In two-compartment preparations, the top compartment was filled with artificial endolymph, which was composed of (in mM): 2 Na^+, 117.5 K^+, 0.25 Ca^{2+}, 118 Cl^-, 5 HEPES, and 3 D-glucose. The bottom compartment was filled with

standard saline solution. This arrangement mimics the *in vivo* arrangement, resulting in healthy cells that oscillate spontaneously for several hours. The pH was adjusted to 7.2-7.3, and the osmolarity to 230 mOsm kg^{-1}.

For preparations requiring decreased intercellular adhesion, such as the dissociated and extruded preparations, a low-Ca^{2+} version of the standard saline solution was used. This solution is identical to perilymph in all respects other than its Ca^{2+} concentration, which is 100 μM instead of the usual 2 mM. Finally, a zero-Ca^{2+} solution was also needed in these preparations. This solution contained no added Ca^{2+}, and was supplemented with 5 mM EGTA to chelate any residual Ca^{2+} in the water source.

2.1.2 Dissection Procedure

An American bullfrog (*Rana catesbeiana*) was placed in 2.5 g·L^{-1} eugenol solution for 10 minutes to reach anesthesia. The frog was then euthanized by double pithing. After severing the head and splitting the palatal tissue, I opened the otic capsule to reveal the inner ear. The eighth cranial nerve and three semicircular canals were severed to free the inner ear from its surrounding bone. The inner ear was then placed in a dish of ice-cold, oxygenated normal saline for the remainder of the dissection. The perilymphatic cistern was carefully opened, and the sacculus cut away from the remaining inner-ear organs. The viscous mass of otoconia overlying the sacculus was carefully removed from the saccular surface. The sacculus was then digested for 30 minutes in 3 mL of 67 mg·L^{-1} protease XXIV (Sigma). Digestion ruptures the connections between each hair bundle's kinociliary bulb and the overlying otolithic membrane. After digestion, the membrane was gently removed with an eyelash and the sacculus was mounted according to the preparation to be used. Extended descriptions of these steps have been published [10].

Two-Chamber Preparation for Spontaneous Oscillations

Hair bundles oscillate spontaneously when they are placed in an ionic milieu that mimics *in vivo* conditions. This requires bathing their basolateral surfaces with perilymph and apical surfaces with endolymph. To simplify the separation of these two compartments, the sacculus was sealed with cyanoacrylate glue (3M, 1469SB) onto a hole in a 1 cm $\times$ 1 cm square of aluminum foil. The foil extends the edges of the sacculus, giving the experimenter more surface area around which to build the two-chamber apparatus. The foil was placed between a lower chamber containing perilymph, and an upper chamber containing endolymph, and was sealed in place with vacuum grease.

Hair-Cell Dissociation

Hair cells can be dissociated from the saccular epithelium to provide easy access to their somata. The connections between hair cells and the supporting cells that surround them are primarily comprised of cadherins, Ca^{2+}-dependent adhesion proteins. To weaken the interactions between cells, the sacculus was exposed to a solution containing a Ca^{2+} chelator. However, a bundle's tip links are also comprised of calcium-dependent filamentous proteins, so treatment with a chelator would rupture them as well. To prevent tip-link rupture and maintain mechanosensitivity, the incubation in zero-Ca^{2+} saline was performed after removing the perilymphatic cistern and before opening the otoconial sac. This placed the basolateral surface of the sacculus in contact with the chelator-containing solution, while hair bundles protruded into the calcium carbonate-rich otolithic sac. For additional protection, the lumen of the semicircular canal ampullae was glued shut with cyanoacrylate prior to treatment in the chelator. A 12 minute incubation in the chelator sufficed to weaken intercellular adhesions, at which point the sacculus was dissected away from the inner ear and

digested in protease as above.

Once the sacculus had been digested and its otolithic membrane removed, it was gently pinned to an open-chamber experimental dish. The glass surface at the bottom of this dish was acid-cleaned and coated with 20 μ L of 1 mg·mL^{-1} concanavelin A to promote cell adhesion. Hair cells were mechanically dissociated by gentle flicks from a soft eyelash. Fluid flows were created with the eyelash to coax dissociated cells from the sacculus onto the glass surface, where they were allowed to settle.

Hair-Cell Extrusion

Although the dissociation procedure above allows access to hair cells' somata, it can damage the hair bundles through mechanical trauma. When a large fraction of transducing cells was needed, the cells were extruded from the epithelium instead of mechanically isolated. The basis for this procedure was the same as that for dissociation: intercellular linkages were ruptured with a chelator solution to allow cells to be separated from the epithelium. The steps for hair cell extrusion follow those of dissociation until the sacculus was pinned to the experimental chamber. At this point, the sacculus was pinned with two to three pins and placed under tension. After approximately 20 minutes, hair cells spontaneously extruded from the epithelium and lay on top of their neighbors (Fig. 2.1). As time went on, more cells extruded, until eventually the epithelium was covered with extruded hair cells. The optimal time for experimentation was approximately 45 minutes after the tissue was mounted, when one had a good chance of finding extruded hair cells, but the epithelial surface was not yet littered.

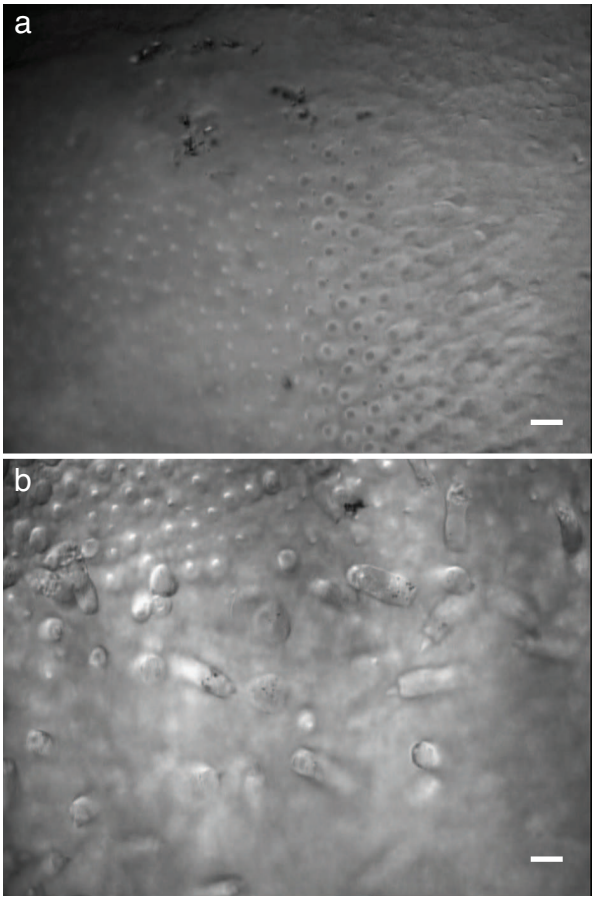

Figure 2.1: Hair-cell extrusion. (a) A top view of the saccular epithelium showing hair cells and their apical hair bundles. (b) Top view of the saccular epithelium after the initiation of cell extrusion. Once extruded, a hair cell tends to lie on its side, with its bundle's axis of sensitivity in the plane of the chamber. Scale bars, 20 μm.

2.1.3 Microscopic Apparatus

Hair cells were visualized with differential-interference-contrast optics at 60x magnification on an upright microscope (BX51WI; Olympus). For recordings of hair-bundle displacement, preparations were illuminated with a 630 nm light-emitting diode (UHP-LED-630; Prizmatix). Images and video were acquired on a CCD camera (OLY-150; Olympus). High-frame-rate videos were acquired with a high-speed CCD camera (MotionScope 2000S; Redlake).

2.1.4 Ultraviolet Stimulation

Both a 375 nm laser diode (LDM-375, Oxxius) and a 405 nm laser diode (DL-405-100, Crystalaser) were used to irradiate hair cells with ultraviolet light. Laser beams were focused on the back focal plane of the objective lens to create a collimated beam exiting the objective lens. The beam of the 375 nm laser consisted of a combination of transverse modes 00 and 01, resulting in an elliptical illumination pattern at the sample plane with minor and major radii of 3 μm and 6 μm. The 405 nm laser consisted of transverse mode 00 and yielded a circular beam of radius 3.5 μm. Beams could easily be localized by irradiating a glass slide painted with permanent marker. A pulse of several tens of milliseconds at several milliwatts of power vaporized the marker, leaving a clear section of glass of the diameter of the beam. Beam dimensions were confirmed with the razor-edge method. A razor edge was advanced by known increments through the field of view while transmitted power was measured by a power meter placed underneath the razor. The beam profile was then calculated from this power-displacement relation.

2.1.5 Photometric Recording

The sample was illuminated with a 630 nm 800 mW light-emitting diode (LED) (UHP-LED-630; Prizmatix). Light piping through stereocilia resulted in a high-contrast image of the hair bundle tip, which was imaged on a dual photodiode at a magnification of 1250×. Output from the photodiode was low-pass filtered at 4 kHz with a Bessel filter (BenchMaster 8; Kemo). The photodiode signal was calibrated by translating a bundle's image by 10 μm steps with a mirror mounted on a piezoelectric actuator (PA 120/14 SG, Piezosystem Jena). This actuator was driven by a 300 mA amplifier and calibrated against a heterodyne interferometer (ENV 300SG; Piezosystem Jena, and OFV 501; Polytec).

2.1.6 Electrophysiology

Hair-cell currents were recorded with whole-cell, tight-seal electrodes filled with potassium gluconate internal solution containing (in mM): 117 K^+, 2 Na^+, 4 Mg^{2+}, 117 gluconate, 1 ATP, 2 Cl^-, 5 EGTA, 5 HEPES at pH 7.2-7.3. Electrodes were pulled to a tip resistance of 3-8 MΩ with an electrode puller (P-2000, Sutter Instruments) and were coated with nail polish to decrease transmural capacitance. Hair cells were held at -70 mV with a voltage-clamp amplifier (Axopatch 200B, Molecular Devices).

Sharp microelectrodes were pulled with an electrode puller (P-80/PC, Sutter Instruments) and their tips were bent through an angle of 60 °to allow vertical insertion into the hair cell apex [38]. When filled with 3M KCl, tip resistances ranged from 100-200 MΩ. Intracellular voltage was recorded by a DC-coupled amplifier set to pass 0-3 kHz (Axoclamp 2B, Axon Instruments).

EGTA and gentamicin were released onto hair bundles by iontophoresis. Iontophoretic electrodes were fabricated from glass capillaries pulled with an electrode puller (P-80/PC, Sutter Instruments). Electrodes were filled with 500 mM EGTA in

1 M NaOH or 500 mM gentamicin sulfate. The tips of iontophoresis electrodes were placed approximately 3 μm from the tip of a hair bundle. An amplifier (Axoclamp 2B; Axon Instruments) was used to pass currents of up to $\pm$ 100 nA through the electrode to elicit release of its contents. A holding current was used to minimize leakage of the electrode's contents onto the hair bundle between iontophoretic episodes.

2.1.7 Video Tracking Hair-Bundle Movement

A camera with a frame rate of 2000 Hz was used to record bundle movements over a wide range of positions in the field of view. In each frame, a hair bundle's center of mass was calculated with a program custom-written in Matlab. Briefly, the center of mass of each row of pixels across a bundle was calculated. These were then averaged to define the bundle's position in a given frame (Fig. 2.2b). Pixel values were converted to micrometers with a ruled microgrid.

2.1.8 Signal Production and Acquisition

All stimuli were controlled and data were acquired with programs written in LabVIEW (version 16.0; National Instruments). Data were digitized by an analog-to-digital converter and sampled at 20 kHz (PCIe-6353; National Instruments). Stimuli were presented through a digital-to-analog converter (PCI-6733; National Instruments).

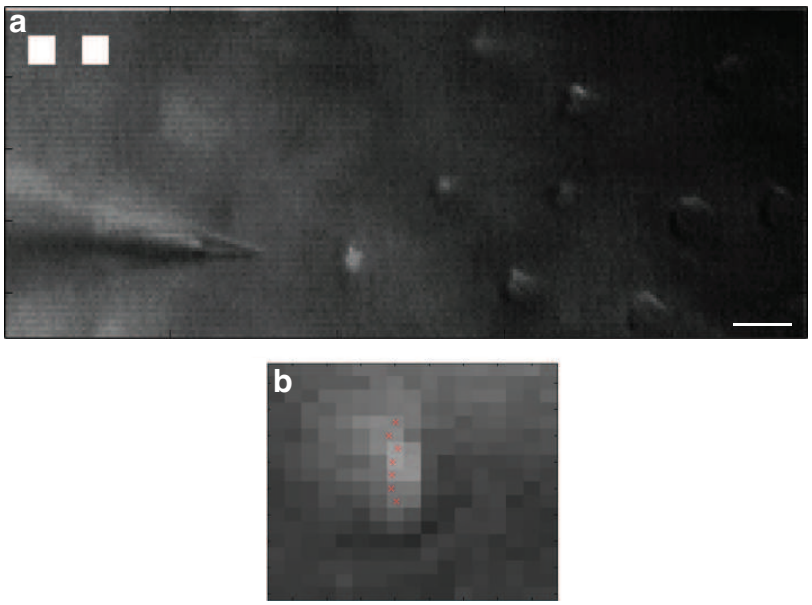

Figure 2.2: Measuring the spatial extent of light-evoked stimulation. (a) Field of view of the 2000 frames-per-second camera used to record hair-bundle motion as a function of distance from the laser beam. The beam, which is absent in the image, is at the lower left corner. A microelectrode demarcates the bundle of interest. White squares at top left were used to synchronize video acquisition and irradiation. Scale bar, 10 μm. (b) Close-up of a hair bundle, with centers of mass for each horizontal line marked with a red cross. The position of each cross was averaged to obtain the position of the bundle in each frame.

2.2 Ultraviolet Light Causes Hair-Bundle Motion

2.2.1 The Light-Evoked Displacement Response

I studied the response of the hair bundle to ultraviolet (UV) irradiation at 375 nm by recording its motion during brief pulses of light. When placed within or directly adjacent to a 6 μm $\times$ 12 μm beam of ultraviolet light, a hair bundle moved rapidly towards its kinocilium for the duration of the light pulse and relaxed to its original position upon light offset (Fig. 2.3a). Bundle motion started within a millisecond after irradiation, and the bundle reached its final offset position within a handful to ten milliseconds. Light-evoked motion was always directed towards the kinocilium, regardless of a bundle's orientation within the epithelium. The waveform of light-evoked hair bundle displacements varied among bundles: whereas some hair bundles exhibited a slow asymptotic displacement, others displayed rapid and biphasic motion (Fig. 2.3a). The amplitude of light-evoked motion varied as well, ranging from 0 nm to 300 nm. However, all hair bundles exhibited a linear power-displacement relation at low power densities. There is no threshold required to elicit hair bundle motion; instead, a bundle's displacement response falls into the noise floor as the power density decreased (Fig. 2.3b). Hair-bundle motion thus likely arises from a continuous rather than a threshold process.

The restriction of light-evoked motion to the direction of a bundle's mechanically sensitive axis intrigued me from the earliest experiments. This constraint meant that when light is shined near the striola, the line of polarity reversal of hair bundles in the sacculus, hair bundles whose tall edges faced each other moved towards each other. One possible explanation for this constraint in the direction of motion is that the geometry or organization of the hair bundle dictates the direction of motion. For example, the stereociliary bevel might decompose downward photonic force into a

horizontal component responsible for kinocilium-directed motion. I tested this by irradiating a hair bundle from a direction orthogonal to its axis of sensitivity. Hair-bundle motion in this configuration was no different from that elicited by apical irradiation, indicating that photonic pressure does not underlie the motion and that the bevel itself is not the source of directional selectivity (Fig. 2.4).

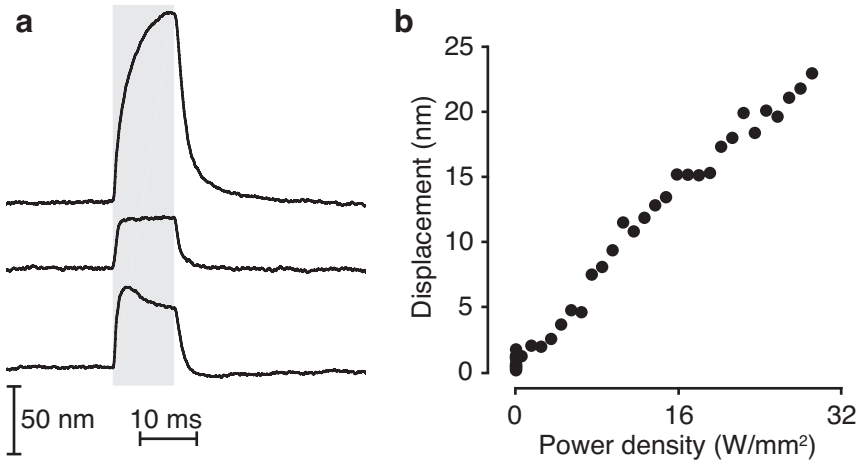

Figure 2.3: Light-evoked hair-bundle motion. (a) Irradiation of three different hair bundles with ultraviolet light evoked hair-bundle movements with differing timecourses. Wavelength, 375 nm; power density, 152 $MW \cdot m^{-2}$. (b) The amplitude of light-evoked hair bundle movement increased linearly with power density.

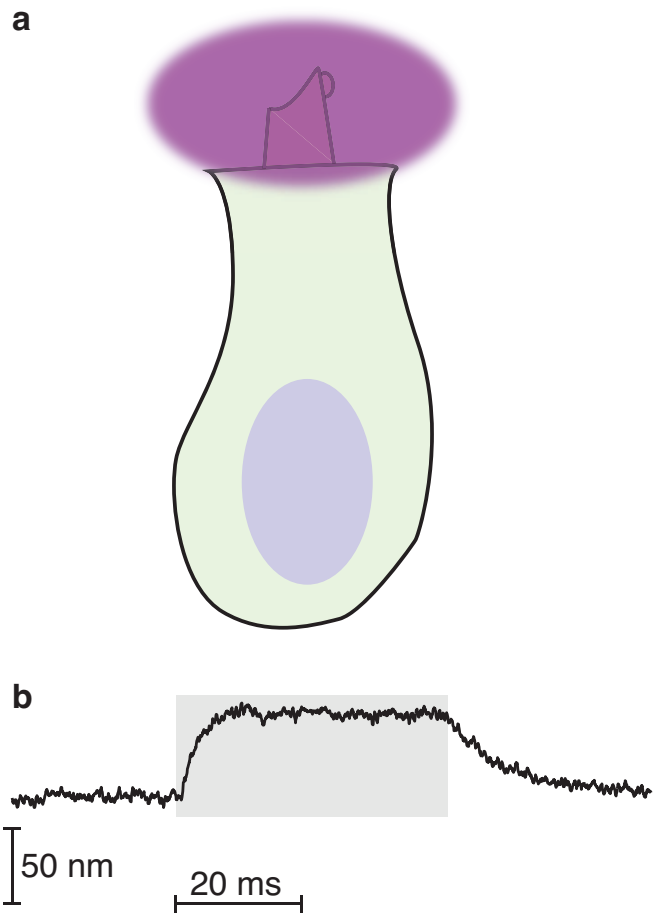

Figure 2.4: Orthogonal irradiation. (a) A hair cell that has been extruded from the epithelium is irradiated orthogonal to its axis of sensitivity. (b) The resulting hair-bundle motion along the direction of sensitivity is recorded on a dual photodiode. Wavelength, 375 nm; Power density, 106 $MW \cdot m^{-2}$.

Although it is clear that a hair bundle moves with respect to the cell's soma in response to light, it is uncertain whether the soma undergoes any motion of its own during irradiation. To determine whether hair-cell somata move as well, I recorded the position of several hair cells' boundaries in response to irradiation. I placed a hair cell's cortex, which is optically denser than its internal contents, on the dual photodiode system. No motion was observed in response to irradiation. However, it is possible that the epithelial tissue constrains light-evoked motion of the soma. Thus this experiment was repeated on extruded cells, whose motion was not constrained by neighbors. Again no cell bodies moved, other than a few cells that had extruded on top of their neighbors' hair bundles and were thus moved by those bundles. In addition to these photometric recordings, I captured high-speed videos of light-evoked hair bundle motion in extruded cells. Subtraction of frames obtained during the laser pulse from those preceding the pulse showed that motion was limited to the hair bundle and maximal at its tip (Fig. 2.5).

Because light-evoked hair-bundle motion was constrained to the direction of mechanosensitivity of a hair bundle, I suspected the involvement of the mechanotransduction apparatus in this response. To test this, I measured a hair bundle's response to light before and after the rupture of tip links by the application of ethylene glycol-bis (β-aminoethyl ether)-N,N,N',N'-tetraacetic acid (EGTA). Rupturing a bundle's tip links decouples the activity of its transduction apparatus from its position. After tip-link rupture, a hair bundle no longer moved in response to ultraviolet irradiation, indicating that the mechanotransduction apparatus is required for response to light (Fig. 2.6). Once tip-links are ruptured, they take several hours to reassemble when the bundle is returned to normal saline solution. Thus a bundle with ruptured tip links does not recover its response to light on the timescale of an experiment.

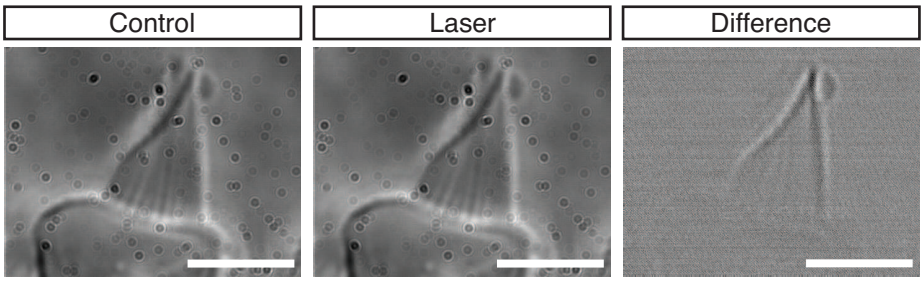

Figure 2.5: Motion is limited to the hair bundle. Subtraction of video frames during laser irradiation of a hair bundle from those before irradiation revealed light-evoked motion that was maximal at the tip of the hair bundle. The soma did not move. Frame rate, 250 Hz. Scale bar, 5 μm. Averaged over 20 presentations. Wavelength, 375 nm; power density, 106 MW$\cdot$m^{-2}.

Figure 2.6: Tip-link rupture. (a) Iontophoresis of the Ca^{2+} chelator EGTA caused tip-link rupture. Top: Current was passed through an iontophoresis electrode to release EGTA onto the hair bundle. EGTA release was maximal with the largest negative current. Bottom: the hair bundle's displacement response decayed as EGTA release increased. Eventually, the Ca^{2+} concentration decreased enough to rupture tip links and eliminate the light-evoked response. (b) Quantification of the displacement response as a function of iontophoretic current. Wavelength, 375 nm; power density, 106 $MW \cdot m^{-2}$. (c) Measurements of hair bundle motion from another cell before (top) and after (bottom) severing tip links with EGTA.

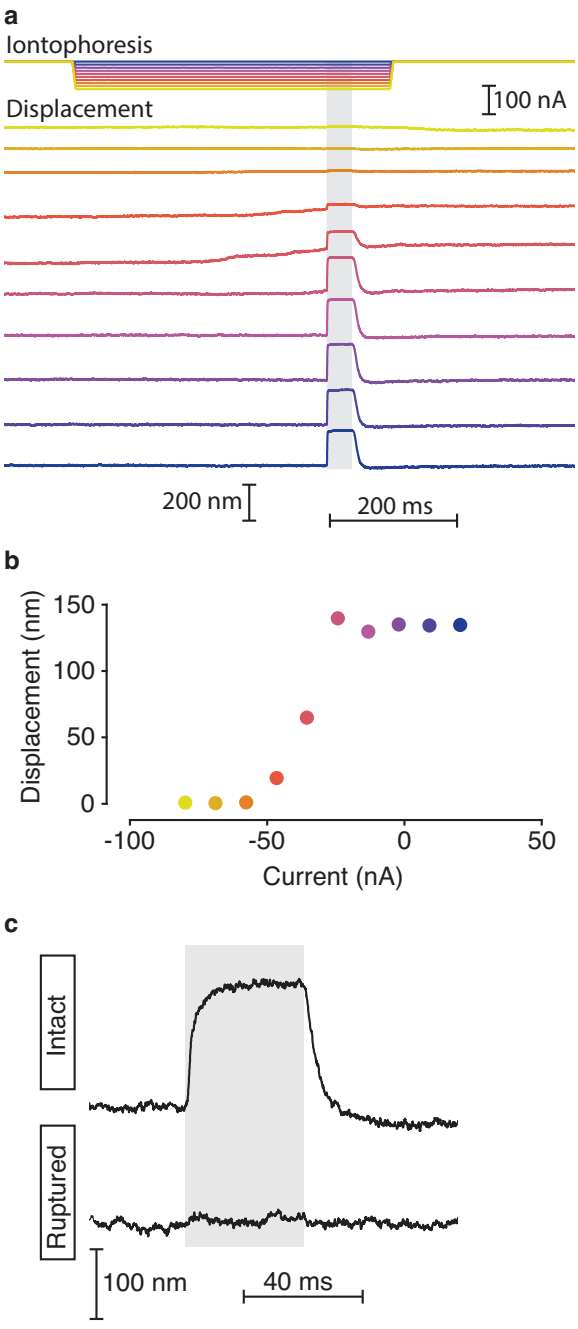
a
Iontophoresis
Displacement
100 nA
200 nm
200 ms
b
Displacement (nm)
150
100
50
0
-100
-50
0
50
Current (nA)
c
Intact
Ruptured
100 nm
40 ms

2.2.2 The Hair-Bundle Response Spreads Beyond the Irradiation Beam

It became apparent in early experiments that light-evoked hair-bundle motion was not spatially restricted to the area directly irradiated by the laser beam. Instead, the response spread some distance around the beam, eventually decaying to zero. I undertook a study of this spatial decay in the hopes of gaining insight into the process underlying light-evoked stimulation. The 375 nm ultraviolet beam spans an ellipse of 6 μm $\times$ 12 μm at the sample plane (see Section 2.1.4). I confirmed these dimensions by imaging the fluorescence pattern of a fluorescein-coated slide (Fig. 2.7). Next I visualized the spatial spread owing to diffraction from the surface of the epithelium by staining a freshly-dissected sacculus with the lipophilic dye DiA, which is incorporated into cell membranes. As expected, light scattering broadened the fluorescent area (Fig. 2.7).

I then measured the spatial decay of hair-bundle motion to compare it to these profiles. Because the photometric recording apparatus can be positioned within only a narrow area of the field of view, however, it could not be used to measure the spread of the laser-evoked response. I thus turned to video recording, which offers a broader field of view at the expense of sampling frequency. Although the sampling rate of the camera was one tenth the typical rate at which the photodiode was sampled, its field of view is considerably larger, enabling me to record motion up to 50 μm from the center of the laser beam (Fig. 2.2a). I recorded the motion of 19 hair bundles at various distances from the laser beam. Each bundle's displacements were normalized to the magnitude of the displacement in the center of the beam and plotted against distance from the beam. The resulting spatial profile for seven bundles is shown in Figure 2.8. Although the hair-bundle response decayed with distance, there was considerable inter-bundle variability in the space constant of this decay. Some hair

bundles even responded best to light when placed several tens of micrometers from the edge of the beam. Overlaying these responses with the fluorescein and DiA emission patterns showed that the spatial decay of hair-bundle responses was not dictated by diffraction at the surface of the epithelium (Fig. 2.8). Instead it appears that something with a distribution broader than that of diffracted light dictates hair-bundle motion. After establishing the mechanism of light-evoked hair-bundle motion I address this observation in Section 3.9.

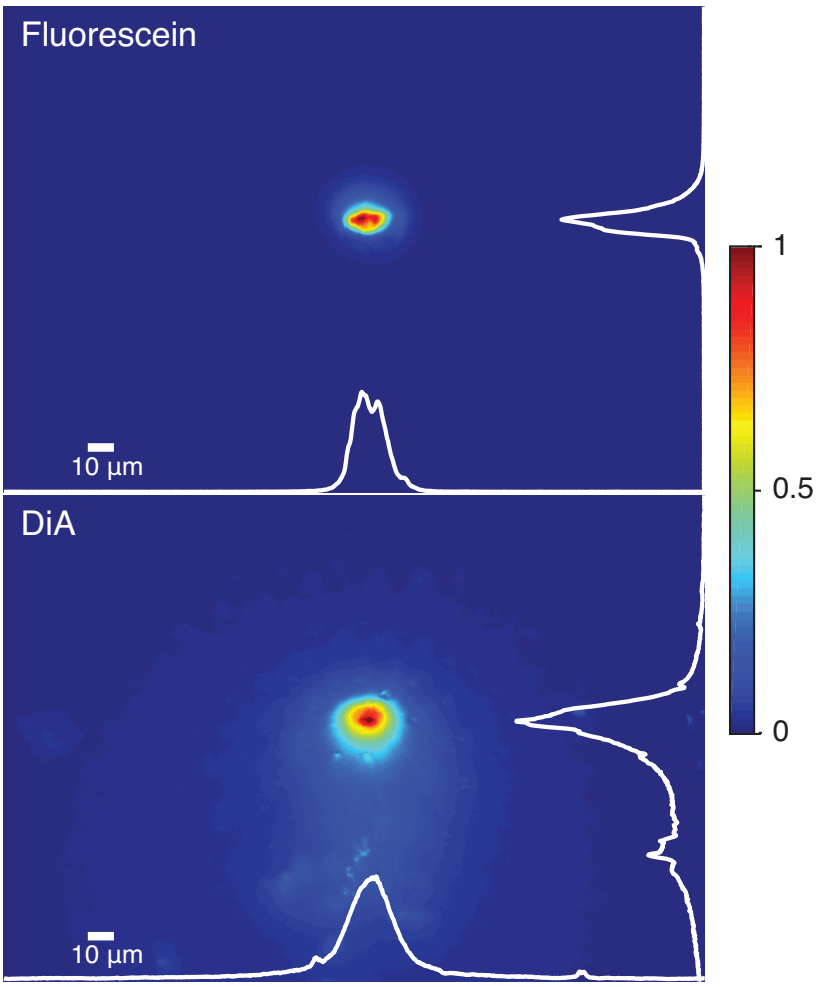

Figure 2.7: The spread of ultraviolet irradiation. Top: Fluorescence profile of a fluorescein-coated glass slide irradiated with a 375 nm laser beam. Bottom: Fluorescence from the surface of a bullfrog sacculus stained with the lipophilic dye DiA. Fluorescence in each image was normalized to the maximum and color-mapped according to the bar on the right. The horizontal and vertical fluorescence profile of lines intersecting in the center of the laser beam are overlaid in white on the images.

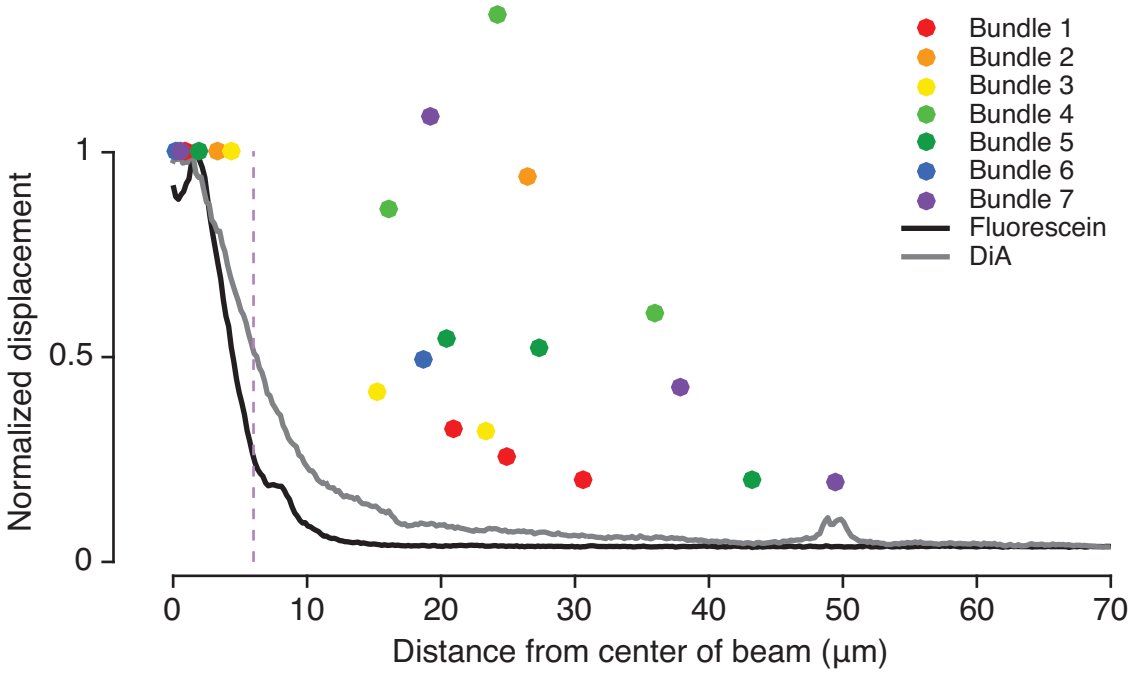

Figure 2.8: The spatial extent of light-evoked stimulation. Hair-bundle responses decayed with distance from the laser beam. Normalized displacement records from seven hair bundles are plotted. Each color represents one bundle, and position along the abscissa marks distance from the center of the laser beam. Height along the ordinate represents laser-evoked displacement, normalized to each bundle's displacement inside the beam. The fluorescence profile of a fluorescein-coated slide and DiA-stained sacculus are plotted for reference. The dashed line demarcates the edge of the laser beam.

2.2.3 Irradiation Opens Mechanotransduction Channels

Light-evoked hair-bundle motion is confined to a bundle's direction of mechanosensitivity and requires intact tip links. These observations suggest that mechanotransduction channels open in response to irradiation. Because the gating swing of mechanotransduction channels alters the tension in tip links, channel gating can produce hair-bundle motion. To determine whether channel gating contributes to light-evoked hair-bundle movement, I irradiated spontaneously oscillating hair bundles with ultraviolet light. The mechanotransduction channels of a spontaneously oscillating hair bundle alternate between the closed and open configurations, (Section 1.9), providing an opportunity to compare hair-bundle responses in each state [23].

The light-evoked displacement of an oscillating hair bundle in its open-channel phase was smaller than its displacement in the closed-channel phase (Fig. 2.9). This result is consistent with the theory that the gating spring contributes to light-evoked displacement. A confounding factor is the state of the adaptation motors: the adaptation motors slip down their actin tracks when transduction channels are open and climb up the tracks when channels are closed. It is thus possible that the difference in responses between the two phases of oscillation arose from a difference in the state of the adaptation motor.

To more conclusively determine whether channel gating contributes to light-evoked hair bundle motion, I blocked mechanotransduction channels with the aminoglycoside antibiotic gentamicin. Aminoglycoside antibiotics are positively charged molecules that reversibly plug the pores of mechanotransduction channels and stabilize their open state [39]. When a hair bundle is exposed to gentamicin, it first jerks rapidly towards its tall edge as its channels are stabilized in their open state by gentamicin. Because gentamicin blocks the channel pore and abolishes the resting influx of Ca^{2+} through these channels, the intracellular Ca^{2+} concentration subsequently drops, ac-

tivating the adaptation motors. The motors climb on their actin track, increasing tip-link tension and moving the bundle towards its negative edge.

Treatment with gentamicin decreased the amplitude of light-evoked hair-bundle motion but did not abolish it (Fig. 2.10). Channel gating thus likely contributes to the light-evoked displacement response, but does not underlie it entirely. Although we do not know the exact concentration of gentamicin released by iontophoresis, the asymptotic shape of the displacement-iontophoresis curve in Figure 2.10b suggests that the drug concentration was sufficient to block nearly all channels. Additional experiments were performed with gentamicin present in the bath at a concentration several times its dissociation constant with the transduction channel. These confirmed that there is residual hair-bundle motion in the presence of gentamicin.

The gentamicin experiments above allow us to dissociate the contributions of the transduction channel and the adaptation motor to light-evoked hair bundle motion. In the presence of gentamicin, adaptation motors are able to climb and tip-link tension increases. The light-evoked displacement in this state is smaller than it is without application of the drug. We may now compare this amplitude to another condition in which motors are climbing, the negative phase of spontaneous oscillation. Although motors are climbing and increasing tip-link tension during the negative phase of oscillation, the light-evoked response is larger in this phase than in the positive. The difference between a gentamicin-blocked bundle and a bundle in its negative oscillating phase lies in the state of its channels. In the former the transduction channels are open, whereas in the latter they are closed. Thus the reason that a gentamicin-blocked bundle has a smaller response is that its transduction channels are pre-opened by gentamicin and cannot be further opened by irradiation. In an oscillating bundle, however, the response was largest in the negative phase because that is when most channels were closed and thus available to be opened. This conclusion is supported

by the observation that spontaneously oscillating hair bundles always restart their oscillations in the negative phase after the offset of irradiation. Light opens channels, causing an influx of Ca^{2+} that places the adaptation motor in the slipping state. The adaptation motor must wait for Ca^{2+} to be pumped out of stereocilia before it can climb again and restart the oscillations.

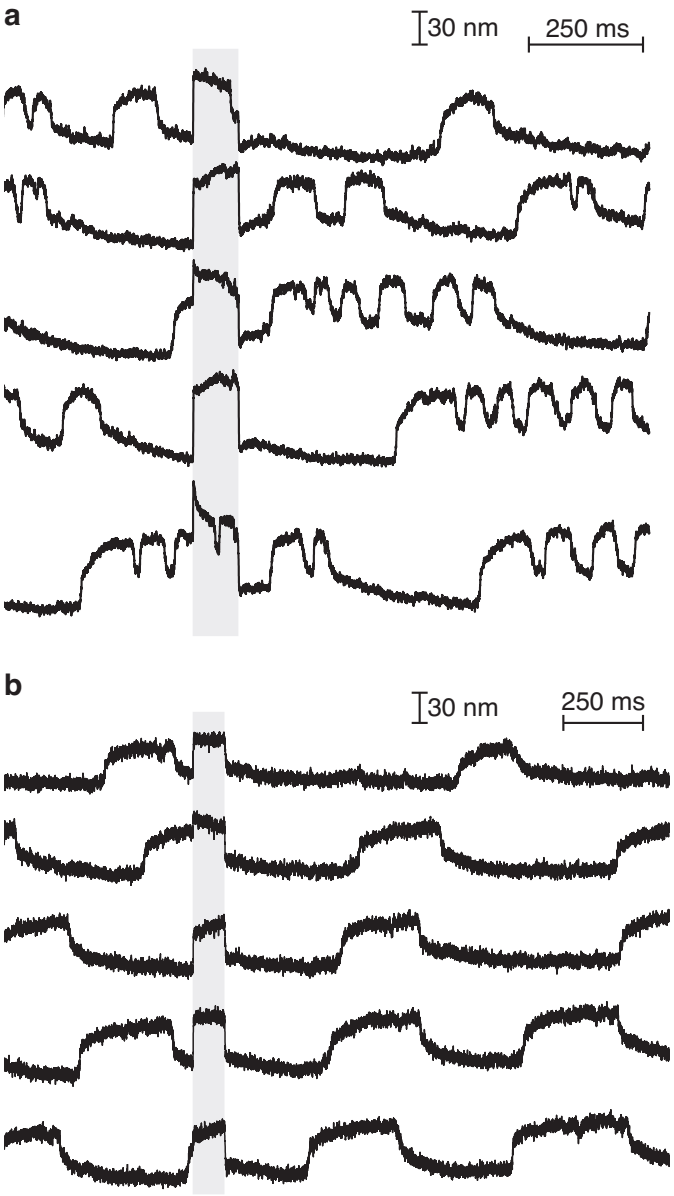

Figure 2.9: Irradiating spontaneously oscillating hair bundles. (a) A spontaneously oscillating hair bundle was irradiated with ultraviolet light at various phases of its oscillatory cycle. Irradiation during the positive phase of the cycle resulted in a smaller displacement response. (b) The same experiment as (a) was performed on second oscillatory hair bundle. Wavelength, 375 nm; power density 106 $\mathrm{MW{\cdot}m^{-2}}$.

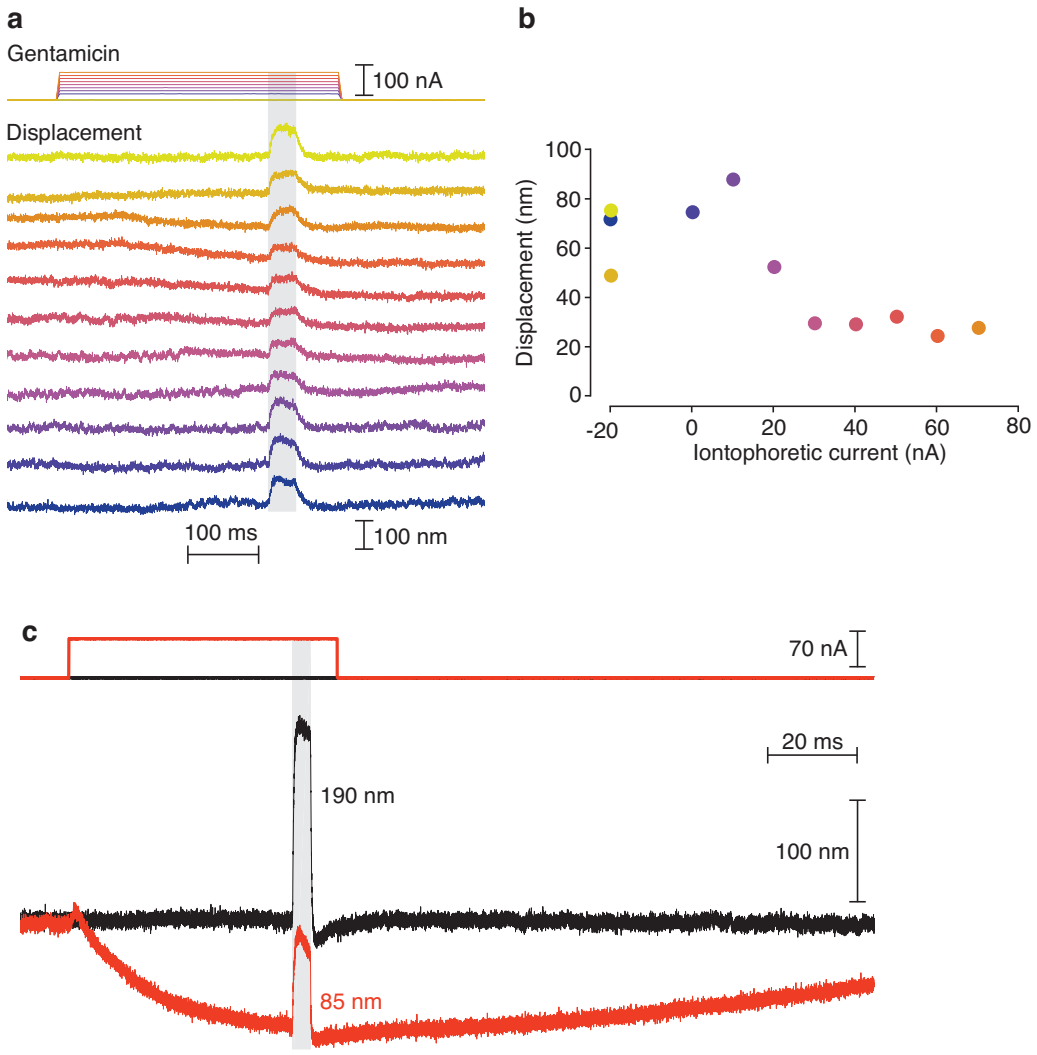

Figure 2.10: Blockage of the mechanotransduction channel. (a) Gentamicin was iontophoresed onto a bundle while its laser-evoked displacement was recorded. Gentamicin release increases with large positive current. After a ramp in gentamicin release, the current was returned to a holding value of -20 nA to recover the original response. (b) Displacement as a function of gentamicin iontophoresis. Wavelength, 375 nm; power density, 106 MW·m^{-2}. (c) The light-evoked displacement response of another hair bundle before and during a saturating release of gentamicin. The response was reduced by 105 nm. Wavelength, 405 nm; power density, 168 MW·m^{-2}.

If mechanotransduction channels do indeed open in response to irradiation, they are expected to pass an inward current and depolarize the hair cell. Using the whole-cell, tight-seal method, I recorded inward currents in response to ultraviolet irradiation of hair bundles (Fig. 2.11a). The amplitude of the inward current varied between cells, with most cells passing 50-100 pA of current. This reflects the opening of about a third of the mechanotransduction channels, which have a conductance of approximately 100 pS [27]. The largest current recorded was 190 pA. The light-evoked current through mechanotransduction channels adapted during stimulation. The rate of adaptation was similar to that seen with mechanical stimulation (Fig. 2.11b). Although adaptation during traditional displacement stimuli stems from the action of myosin motors, it is unclear what underlies adaptation to light-evoked stimulation. To confirm that the current originates from the mechanotransduction channels, I blocked channels with gentamicin while stimulating a bundle with light. The light-evoked inward current diminished with gentamicin iontophoresis, confirming that it was passed by the mechanotransduction channels (Fig. 2.11c, d).

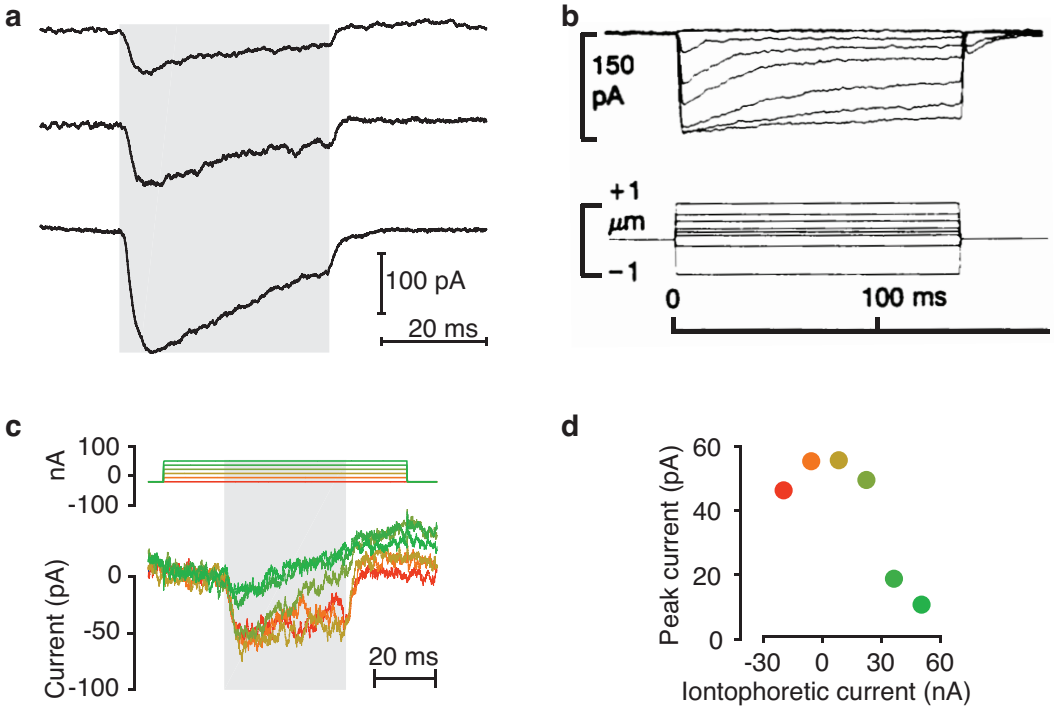

Figure 2.11: Irradiation opens mechanotransduction channels. (a) Light-evoked transduction currents from three different hair cells. Wavelength, 375 nm; power density, 106 MW·m^{-2}; holding potential, -70 mV. (b) Mechanically evoked transduction currents show adaptation. From Figure 1c in Assad et al., 1989 [40]. (c) Iontophoresis of gentamicin reduced the light-evoked transduction current in a dose-dependent manner. Absolute current is shown. (d) The peak current as a function of iontophoretic current.

The current that passes through mechanotransduction channels depolarizes the hair cell and leads to synaptic release. Using sharp microelectrodes, I measured this voltage change and found that hair cells depolarized in response to stimulation with light (Fig. 2.12a). Light-evoked depolarization was often followed by voltage oscillations of decaying amplitude, a feature also seen with mechanical stimulation of hair cells (Fig. 2.12b). This response arises from the interplay of a voltage-gated somatic Ca^{2+} current with a delayed Ca^{2+}-gated K^+ current, and is thought to tune the hair cell response [41]. To determine whether light-mediated channel opening requires intact tip links, I ruptured tip links by exposing cells to saline solution containing 10 mM EGTA before irradiation. No electrical activity was seen in response to irradiation once tip links were ruptured (Fig. 2.12a, and Table 2.1). The reduction in Ca^{2+} concentration required to rupture tip links disrupts the electrical seal between a recording electrode and the cell membrane. Thus after tip links were ruptured the Ca^{2+} concentration was returned to its normal value of 2 mM to make electrical recordings. I performed the voltage recordings in intact cells and cells with ruptured tip links, and report the statistics in Table 2.1. The voltage response was blocked by gentamicin, confirming that it stems from current passed by mechanotransduction channels (Fig. 2.12c, d)

Table 2.1: Voltage response as a function of tip-link integrity. Summary statistics of the voltage responses of hair cells with intact or ruptured tip links. All records were obtained with sharp microelectrodes.

	Intact tip links	Ruptured tip links
Number of cells recorded	31	18
Mean resting V_m [Std Dev]	-53.5 mV [11.6 mV]	-52.8 mV [4.6 mV]
Number cells depolarized [Avg]	25 [2.3 mV]	0 [0 mV]
Number cells hyperpolarized [Avg]	5 [-1.9 mV]	0 [0 mV]
Number cells with no response	1	18

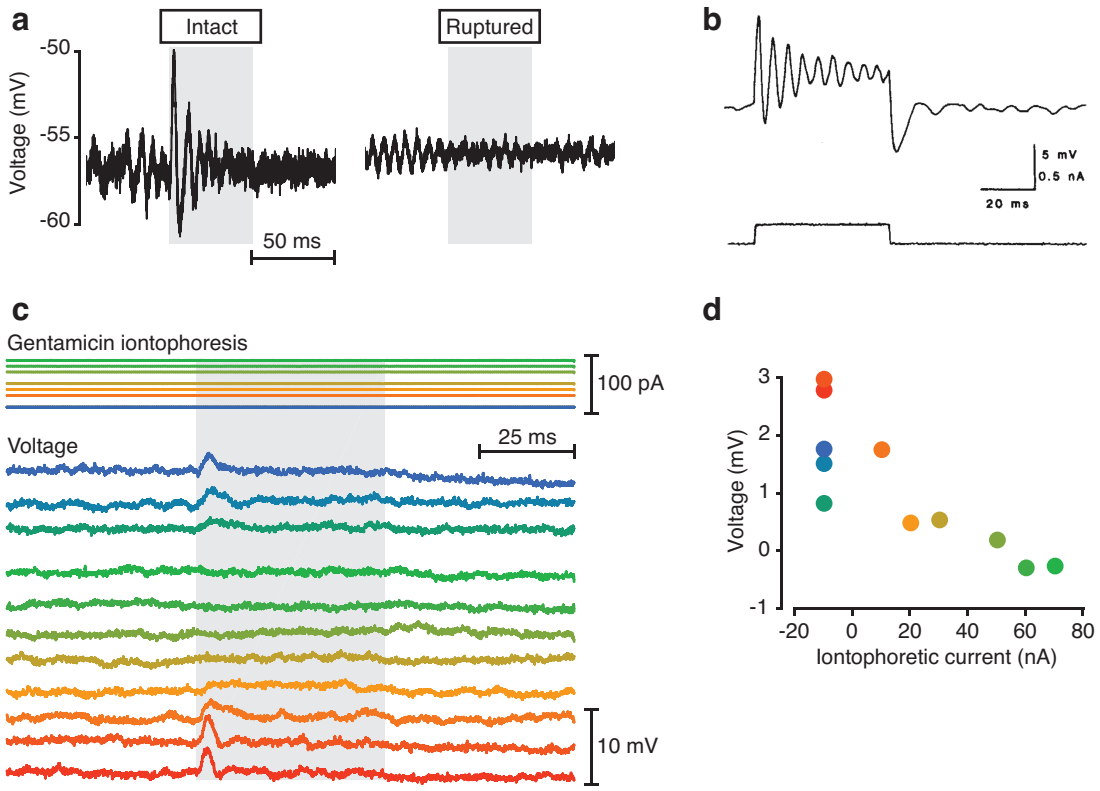

Figure 2.12: Irradiation depolarizes hair cells. (a) Microelectrode recordings of receptor potentials obtained in hair cells with intact (left) and ruptured (right) tip links. Wavelength, 375 nm; power density, 106 MW·m^{-2}. (b) Voltage oscillations in a hair cell whose bundle is mechanically stimulated. Taken from Figure 2 in Lewis and Hudspeth, 1983 [42]. (c) A hair cell's voltage response to irradiation completely abolished with gentamicin treatment, and recovered upon drug washout. Positive iontophoretic current releases gentamicin. (d) The voltage response as a function of iontophoretic current.

2.2.4 Protracted Stimulation

The irradiation stimuli presented thus far have been on the order of several tens of milliseconds long. To determine whether the hair-bundle displacement response to light fatigues or adapts with longer stimuli, I irradiated cells for several hundreds of milliseconds. Of five irradiated cells, two did not adapt and three did. In adapting hair bundles, the decay in position was incomplete. Instead, during irradiation hair bundles gradually moved towards their negative edge and stabilized at a position positive to their resting position (Fig. 2.13). Hair bundles returned to their original position once the light stimulus was turned off. Figure 2.13a shows that hair-bundle oscillations can continue during protracted stimulation. This bundle's initial response to irradiation was large. It was then followed by a gradual decay to a new stable position around which the bundle continued oscillating. The oscillations during irradiation were of smaller amplitude and higher frequency than before irradiation, a change consistent with increased intracellular Ca^{2+} concentration [23]. Irradiation likely increased the open probability of transduction channels significantly at the onset of the pulse, causing the large, positive hair-bundle movement. The adaptation motors were presumably able to neutralize this change, eventually bringing the bundle back to an oscillatory state. Irradiation seems to have caused an increase in the baseline open probability of channels, leading to faster and smaller oscillations. Myosin motors are thus able to function in the presence of irradiation.

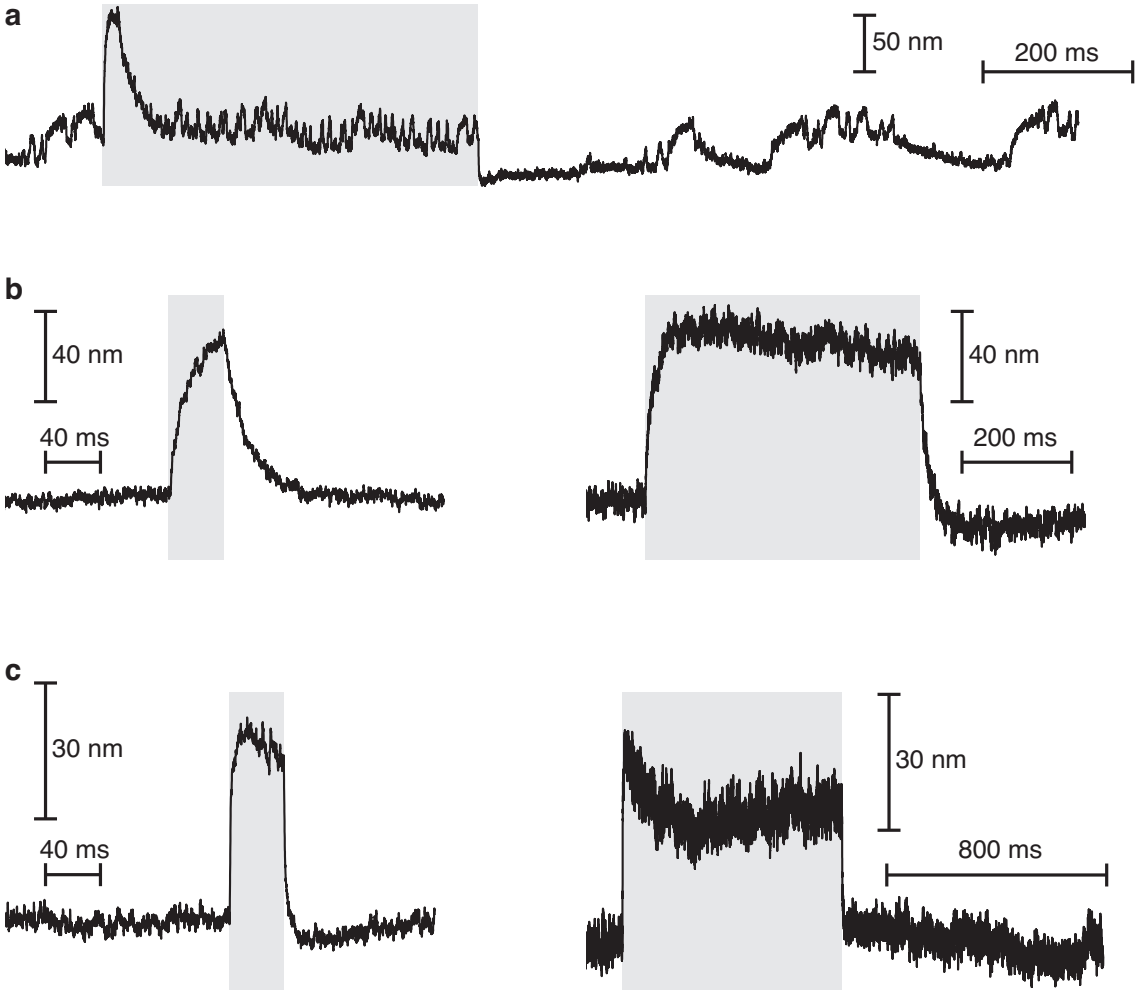

Figure 2.13: Protracted stimulation. (a) An oscillating hair bundle was irradiated with 375 nm light for 500 ms. Power density, 85 MW·m^{-2} (b) A different hair bundle was irradiated first for 40 ms (left) and then for 500 ms (right). Wavelength, 375 nm; power density, 106 MW·m^{-2}. (c) A third hair bundle was irradiated for 40 ms (left) and 800 ms (right). Wavelength, 375 nm; power density, 106 MW·m^{-2}.

2.3 Discussion of Results

The results presented here uncover a new means of stimulating hair cells. Ultraviolet irradiation of hair cells causes positively directed hair-bundle motion, a response typically associated with mechanical stimulation. The hair-bundle response appears to be caused by an intracellular change, for the rupture of tip links abolishes it entirely. If the light-mediated action was external, hair-bundle motion would not be limited to the axis of sensitivity and would not disappear upon tip-link rupture. Although tip links may appear to contribute significantly to the cohesion of a hair bundle, they in fact do not [18]. A bundle with ruptured tip links displays coordinated and coherent Brownian motion equal to that of an intact bundle. Thus the requirement for intact tip links does not imply a requirement for cohesion of the bundle, rather it signifies the requirement for an intact transduction apparatus.

Hair-bundle motion is reduced upon exposure to gentamicin, suggesting that the mechanotransduction channel's gating swing might contribute to hair-bundle motion. The gating swing is expected to contribute up to approximately 60 nm of positively directed motion. This value stems from an estimated 8 nm channel gating swing [43]. A swing of 8 nm along the length of the tip link generates $\frac{d}{\gamma} = \frac{8\,nm}{0.14} = 57$ nm of motion at the tip of the hair bundle. Our records are generally in line with this value: gentamicin never reduces light-evoked hair-bundle motion by more than 105 nm. The concerted opening of transduction channels can generate motion through means other than the channel gating swing itself. Ca^{2+} entry through open channels leads to myosin slippage and positive hair-bundle motion. Thus gentamicin might block light-mediated hair-bundle motion not only by locking channels in their open state but also by preventing Ca^{2+} entry and myosin slippage, potentially explaining the slight discrepancy above.

Hair bundles show great variability in the amplitude and kinetics of their light-

evoked displacements (Fig. 2.3). Some of this variability likely stems from inter-hair-bundle differences in parameters such as tip-link stiffness, resting open probability, and adaptation motor sensitivity. Hair bundles of the frog sacculus display some variability in their dimensions, as shown in Table 1 of Jacobs and Hudspeth, and likely differ in other ways as well [11]. This variability may be particularly important if it alters a bundle's position within a state space of key parameters such as stiffness and offset force [44]. Specific combinations of these parameter values can give rise to qualitatively different responses to stimulation [45]. We do not know how wide the constellation of hair-bundle state-space positions is among the cells of a given sacculus, but it may be wide enough to explain the variability in our present results. Finally, the variability in our results could also be explained by differences in the way each hair bundle is stimulated. The stimulation mechanism is not yet understood, thus we do not know the key parameters regulating a hair-bundle's response.

Chapter 3

The Mechanism of Hair-Cell Stimulation by Ultraviolet Light

In the previous chapter I described the observation that ultraviolet light leads to hair-bundle motion and hair cell stimulation. Light stimulation leads to mechanotransduction channel opening and requires intact tip links. However, the mechanism underlying this observation was not established. The current chapter describes experiments designed to identify the absorber and its mechanism of action in stimulating hair cells.

3.1 Materials and Methods

3.1.1 Folded Epithelial Preparation

The folded epithelial preparation allows visualization of hair cells that are embedded in the sensory epithelium from a direction orthogonal to their axis of sensitivity. In order to achieve this configuration, the saccular epithelium is folded along its axis of symmetry so that hair bundles are observed orthogonally from their axis of sensitivity. Prior to folding, the epithelial layer of the sacculus is separated from its underlying connective tissue with a soft eyelash. The flexible epithelial layer is folded and placed under a gold electron microscopy grid to stabilize it. Hair bundles then protrude radially away from the crease (Fig. 3.1a).

Because the cells remain embedded in the epithelium, no low-Ca^{2+} treatment is needed to loosen inter-cellular junctions, and all hair bundles remain intact. Additionally, hair cells in this configuration are stable because they are held in place by neighboring cells and the electron microscopy grid. This preparation was first performed by Kozlov et al. [18].

3.1.2 Holding a Single Hair Cell

It is sometimes necessary to visualize and study a single hair cell from the side while maintaining its mechanotransduction apparatus intact. Because hair-cell dissociation often leads to cells with disrupted tip links that cannot be distinguished from intact cells, I used a new method to reliably obtain intact single hair cells. The cells were first extruded from the epithelium with the technique discussed in Section 2.1.2. I then gently suctioned a single cell into a polished glass electrode (Fig. 3.1b, c). Once the cell had been positioned in the electrode, I moved it away from the epithelium, where the light path for photometric recordings was unobstructed. Although tedious,

this method guaranteed that a cell would have intact tip links. It also stabilized the cell in the glass holder so that it could not move, unlike extruded hair cells on the epithelial surface.

The glass cell-holder is made by first pulling a glass capillary into two sharp microelectrodes. One electrode is then used to etch the shank of the other at a position where its inner diameter is approximately 10 μm. The etched electrode is then pushed to snap off its tip and heat-polished smooth. Because cell membranes tend to stick tightly to clean glass and rupture with suction, it is advisable to suction and rupture a few cells in order to coat the inside of the electrode with cellular material before attempting to hold a cell for an experiment.

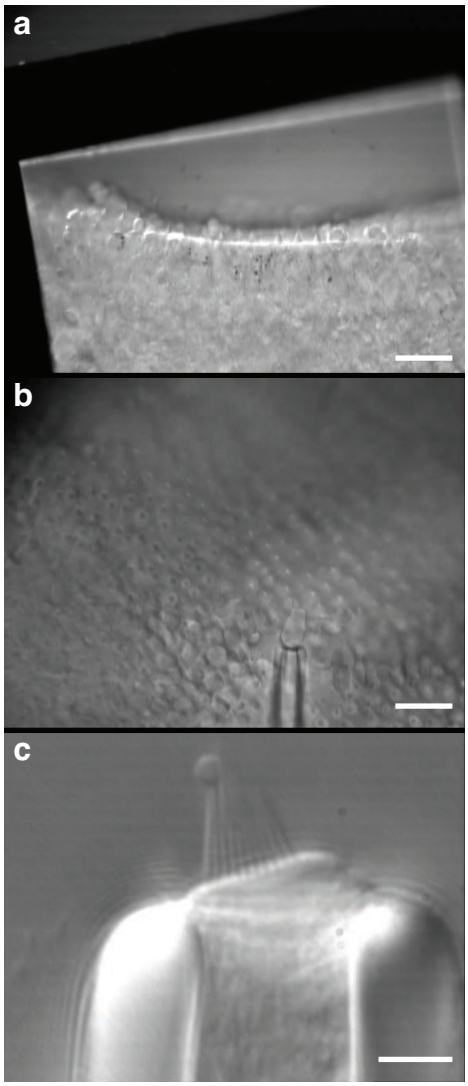

Figure 3.1: Tissue preparations for patterned illumination. (a) A folded saccular epithelium placed under an electron-microscopic grid. Hair bundles are seen radiating from the crease in the epithelium. Scale bar, 40 μm. (b) An extruded hair cell is coaxed into a glass cell holder with gentle negative pressure. Scale bar, 40 μm.(c) Once inside the holder, a cell is stable and its hair-bundle motion can be recorded. Scale bar, 5 μm.

3.1.3 Kinociliary Dissection

The kinocilium is the only true cilium in the hair bundle. It is comprised of microtubules and topped by a globoid structure of 1 μm diameter termed the kinociliary bulb. In the bullfrog, the kinociliary bulb is attached to the otolithic membrane and conveys force from it to the rest of the hair bundle. Because the links between the kinociliary bulb and the tallest row of stereocilia are not cleaved by the protease digestion used to cleave the links to the otolithic membrane, they must be cleaved mechanically in order to detach the kinocilium from the hair bundle.

I separated the kinocilium from a hair bundle by severing the links attaching it to the tallest stereocilia and forcing it away from the bundle. The kinociliary links were severed by sliding a pipette tip between the kinocilium and the tallest stereocilia at a height of 2 μm from the apical cellular surface and then moving upwards, through the kinociliary links.

3.1.4 Optical Masks

Opaque masks were made of either carbon fiber or silver-coated glass. Glass masks were made by first pulling a capillary into two fine-tipped pipettes. One pipette was used to score the other's shank at a location where its width is 2 - 5 μm. The cleaved pipette tip was then primed with tin and chemically plated with silver (Pouring Silver Kit, Angel Gilding). Masks were inspected and discarded if they showed significant irregularity in the silver coat.

Carbon masks were made by isolating a single 4.8 μm carbon fiber from a multifilament tow. A tow of several hundred filaments was cut and threaded through a glass capillary. The capillary was then pulled on an electrode puller (P-80/PC, Sutter Instruments) and the tow was cleaved between the two pipette tapers. The tuft of carbon fibers emanating from each pipette tip was epoxied in place. Once the epoxy

had cured, all carbon fibers but one were trimmed with iris scissors. The remaining fiber was used as a photodense mask.

Both the glass-based and carbon fiber-based masks were photodense and could block light from reaching certain areas of a hair bundle (Fig. 3.2a). We confirmed their opacity to ultraviolet light by placing them over a permanent marker-coated slide during laser irradiation (Fig. 3.2b). Both mask types protected the permanent marker below them from vaporization. A typical mask is shown next to a hair bundle in Figure 3.2c.

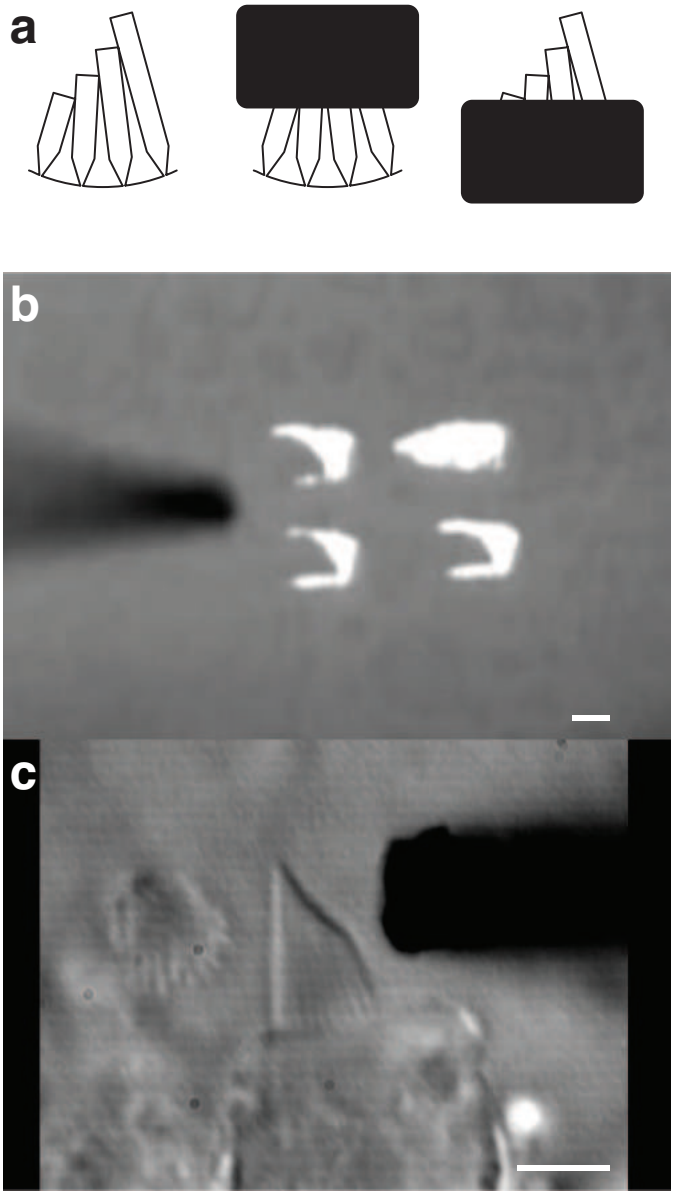

Figure 3.2: Light-blocking masks. (a) Opaque masks are used to block light from various regions of a hair bundle. (b) A silver-coated mask is used to block ultraviolet light-mediated vaporization of permanent marker coated on a glass slide. At the top right, the slide was irradiated without masking. The marker was vaporized in an area outlining the shape of the beam. At the bottom right, the mask was placed on the surface of the glass to protect it. At the bottom left, the mask was placed 3 μm from the surface, and at the top left it was 6 μm from the surface. Scale bar, 5 μm. (c) A silver-coated mask is positioned next to a hair bundle. Scale bar, 5 μm.

3.1.5 Patterned Illumination

We irradiated hair cells with custom spatial patterns by building an optical system based on a digital micromirror device (DLP2010, Texas Instruments). This device consists of an array of mirrors whose orientation can be toggled between two positions. Each mirror rests upon a memory cell that is programmed into one of the two states, resulting in either a positive or negative 12° tilt of the mirror (Fig. 3.3a). The mirrors are several micrometers in size and densely packed on the array, which is several millimeters wide (Fig. 3.3b). We combined a miniature micromirror device with a 405 nm laser diode (DL-405-100, Crystalaser) to stimulate hair cells in certain spatial patterns. Light reflected from micromirrors in the "on" position was collected behind the epifluorescence port of the microscope by a lens (XLFluor4x, Olympus) to form an image of the digital micromirror device surface (dashed line in Fig. 3.3c). This image was relayed and demagnified onto the sample plane through an aspheric lens (ASL-10142-A, Thorlabs) and the objective lens (LumPlanFLN60x, Olympus). Micromirror patterns were loaded on a digital controller (DLPC3435, Texas Instruments) with LabVIEW software (version 16.0, National Instruments).

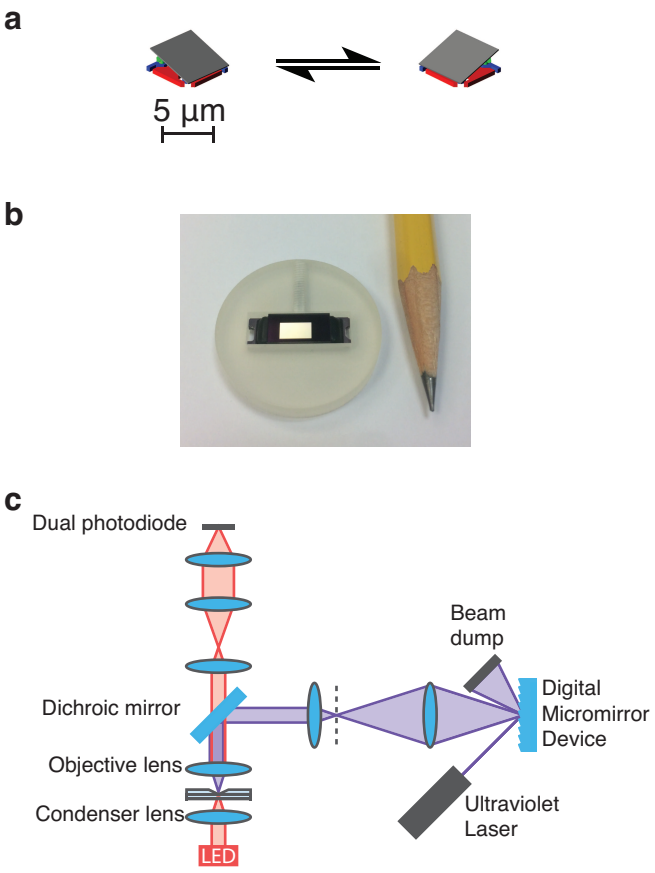

Figure 3.3: Patterned illumination optics. (a) Diagram of a single micromirror from a digital micromirror device alternating between its two tilt positions. Images are from Texas Instruments. (b) We used a DLP2010 micromirror device fixed in a 3D-printed mount. A pencil tip is shown for scale. (c) Optical path for patterned illumination and photometric recording.

3.1.6 Mechanical Stimulation

Mechanical stimuli were delivered by flexible or stiff glass probes fabricated with borosilicate capillaries (1B120F-3, World Precision Instruments). A flexible probe is made by first thinning a capillary with an electrode puller (P-2000, Sutter Instruments) and subsequently pulling its tip laterally with a 120-V solenoid to form a 90° angle with the capillary shaft. Probes were no longer than 100 μm in length, and between 0.5-0.8 μm in diameter. To increase optical contrast, probes were sputter-coated with gold-palladium (Hummer 6.2, Anatech). Flexible probes were calibrated by imaging their Brownian motion on the dual photodiode. A Lorentzian fit to the power spectrum of this motion yielded the probe's stiffness and drag coefficients [46, 45].

Stiff probes were made by pulling borosilicate capillaries to a tip diameter of 1-2 μm. The tip was fire polished to a diameter of 1 μm and attached directly to a kinociliary bulb with light suction. All probes were displaced by a piezoelectric actuator (PA 4/12, Piezosystem Jena) driven by an 800-mA amplifier (ENV 800, Piezosystem Jena). The actuator was mounted on a micromanipulator (MP-285, Sutter Instruments) to control probe position. The control signal sent to the amplifier was digitally filtered at 2 kHz.

3.1.7 Action Spectra

Action spectra were elicited with six illumination bands filtered from the emission of a mercury lamp (X-Cite exacte, Excelitas technologies). The mercury lamp was mounted in the epifluorescence port of the microscope and focused with a lens (AC254-250, ThorLABS) placed 250 mm from the objective lens. Broadband light was filtered and reflected into the sample with six filter and dichroic mirror sets to give rise to the following wavelength bands (in nm): 350-390, 395-415, 426-446, 480-520, 543-557,

and 568-590. The filters and dichroic mirrors used in each band are given in Table 3.1. All filters and mirrors were obtained from Chroma technology, except FF01-370/36-25, which was from Semrock. The intensity at each wavelength band was attenuated to output 5.9 mW of light. Figure 3.4 shows the emission spectrum of the mercury lamp, as well as the wavelength bands used for the action spectrum.

Table 3.1: Filters used to obtain action spectrum.

Wavelength band	Excitation filter	Dichroic mirror	Emission filter
350-390 nm	FF01-370/36-25	T425lpxr	ET425lp
395-415 nm	ET405/20x	T425lpxr	ET430lp
426-446 nm	ET436/20x	T470lpxr	ET460lp
480-520 nm	ET500/40x	T525lpxr	ET542lp
543-557 nm	ET550/15x	T570lpxr	ET570lp
568-590 nm	ET580/25x	T605lpxr	ET610lp

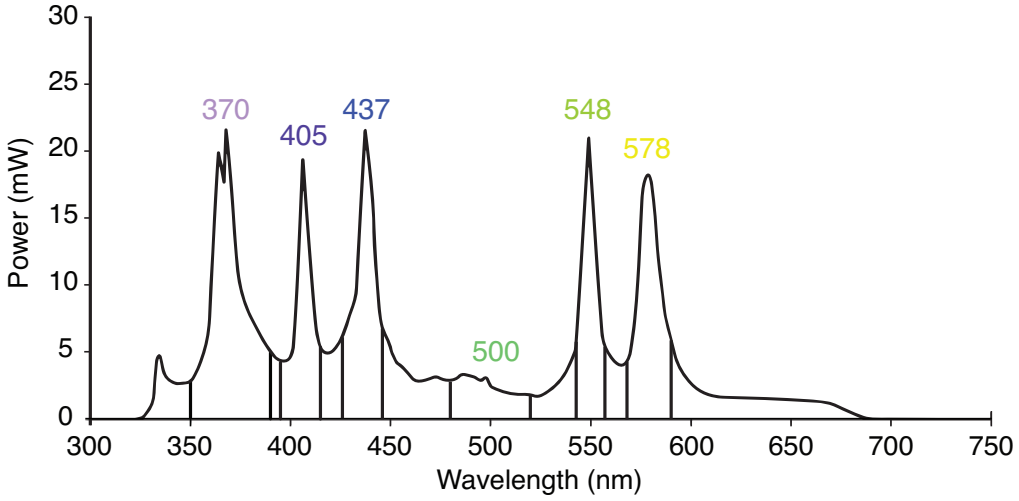

Figure 3.4: Light source for action spectrum. The emission spectrum of the Xcite *exacte* lamp has several peaks. We filtered these peaks, as well as a broad region near 500 nm, to obtain an action spectrum of the hair-cell response to light.

3.1.8 Fluorescence Imaging

Intracellular chromophores were imaged by epifluorescence using a mercury lamp with several emission peaks (X-Cite exacte, Excelitas Technologies). Nicotinamide adenine dinucleotide (NADH) was excited between 350-390 nm (FF01-370/36-25, Semrock) and imaged between 425-475 nm (ET450/50m, Chroma Technology). Flavins and hemoproteins were excited between 426-446 nm (ET436/20x, Chroma Technology) and imaged between 510-560 nm (ET550/50m, Chroma Technology). Images were captured with a CCD camera (ORCA-R2, Hamamatsu).

3.1.9 Temperature Measurement

The calibrated resistance of an electrode was used to measure temperature [47]. Electrodes were pulled with an electrode puller (P-2000; Sutter Instruments) and filled with saline solution identical to that being used in the experiment. Tip resistances ranged from 4-10 MΩ and were determined by measuring the current required to elicit a 5 mV voltage drop across the pipette tip with a voltage-clamp amplifier (Axopatch 200B; Molecular Devices). Each electrode was calibrated by recording its resistance at several temperatures. The electrode tip was placed in approximately 2 mL of saline solution whose temperature was controlled with a chilling and heating dry bath (Echotherm IC20XT; Torrey Pines). A linear fit to the relation of the logarithm of resistance with the reciprocal of temperature yielded the relation between temperature and resistance (Fig. 3.5).

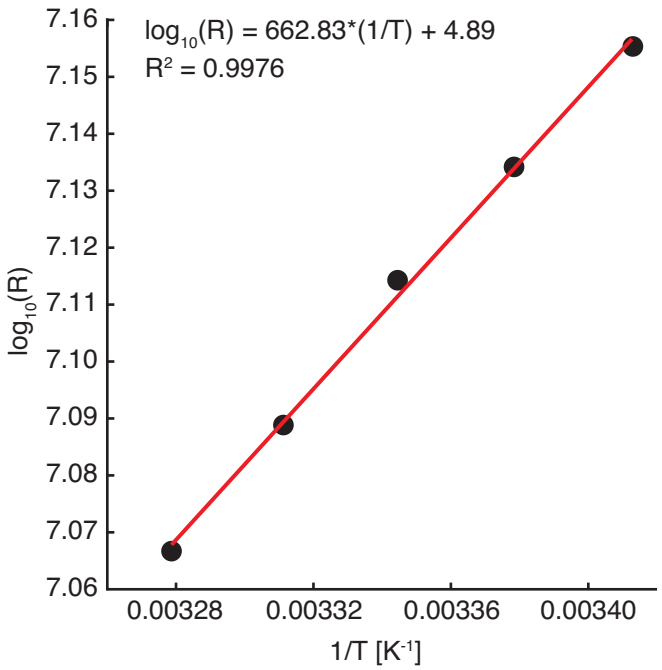

Figure 3.5: Temperature-resistance calibration. The relation between the logarithm of the resistance and the reciprocal of temperature was fit with a line and used to calibrate the temperature-sensitive electrode.

3.1.10 Delay Calculation

To measure the delay between the onset of a laser pulse and the initiation of hair-bundle movement, the motion of a hair bundle was recorded with a photodiode at a sampling rate of 100 kHz. Light production by the laser was detected with a biased silicon photodetector (ET-2020, Electro-Optics Technology) and sampled at the same frequency. A line was fit to the hair-bundle position trace from 500 to 800 μs after the laser trigger. The x-intercept was extrapolated from this line and subtracted from the time at which the laser power reached its half-maximal value, which was typically 200 μs. The subtracted time is the delay until initiation of hair-bundle motion. A similar procedure was carried out to find the delay until initiation of temperature increase after irradiation.

3.1.11 Infrared-Light Stimulation

Cells were irradiated with infrared light from a 1470 nm laser diode (MDL-III 1470, Changchun New Industries Optoelectronics Technology Company). Light was delivered from a 105 μm diameter optical fiber with a flat-cleaved tip (FG105LCA, Thorlabs). The fiber tip was positioned between 100 - 200 μm from the cells studied.

3.2 Candidates for Motion: The Transduction Channel and the Kinocilium

We found in Section 2.2.3 that blockage of the transduction channel with gentamicin diminishes but does not abolish light-evoked hair-bundle displacement. We reasoned that the channel's gating swing contributes to light-evoked hair-bundle motion but does not account for it entirely. Here we repeat this experiment while recording cellular voltage and hair-bundle position simultaneously. The electrical record provides a readout of the state of the mechanotransduction channel, and thus a readout of the degree of gentamicin block. We see in Figure 3.6 that the light-evoked voltage response vanishes with increasing gentamicin release, but the corresponding hair-bundle displacement does not decay to zero. Both the electrical response's disappearance and the displacement response's saturation with increasing gentamicin release confirmed that the majority of channels were blocked. This result confirms that an element other than the channel's gating swing contributes to hair-bundle movement.

The fraction of hair-bundle motion that is not attributed to the gating swing does not depend on the channel being in a particular state. Indeed, this component of hair-bundle motion was evoked even with the channels' pores fully blocked. This result rules out mechanisms for this component such as slippage of myosin motors due to Ca^{2+} influx through the transduction channel.

One possible source of light-evoked motion is the kinocilium. It is not known whether the kinocilium serves a function other than anchoring the hair bundle to the overlying otolithic membrane. However, as implied by its name, the kinocilium is a true cilium comprising microtubules, and thus may be motile. We tested whether the kinocilium plays a role in light-evoked hair-bundle motion by micro-dissecting it from a bundle. There was no significant change in a bundle's response to light after

kinociliary dissection (Fig. 3.7).

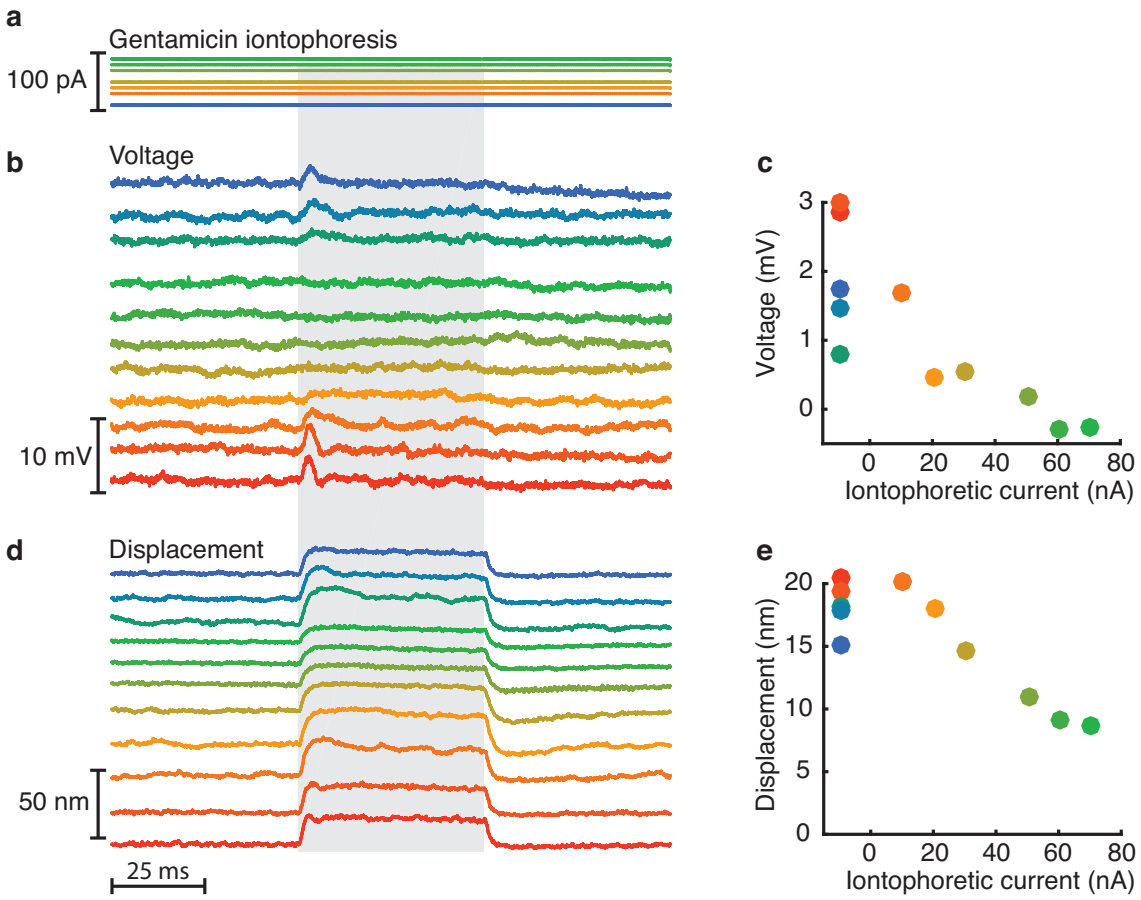

Figure 3.6: The gating swing contributes to light-evoked hair-bundle motion. (a) Gentamicin iontophoresis current. Larger positive currents release more gentamicin. (b) Voltage records for an irradiated hair cell that is exposed to increasing amounts of gentamicin. Resting membrane potential, -52 mV. (c) Receptor-potential records as a function of gentamicin iontophoresis. (d) Position record of the hair bundle obtained simultaneously with (b). (e) Displacements as a function of gentamicin iontophoresis. Wavelength, 375 nm; power density, 106 $MW \cdot m^{-2}$. Although the receptor potential is eliminated at the highest gentamicin concentration, some hair-bundle motion remains.

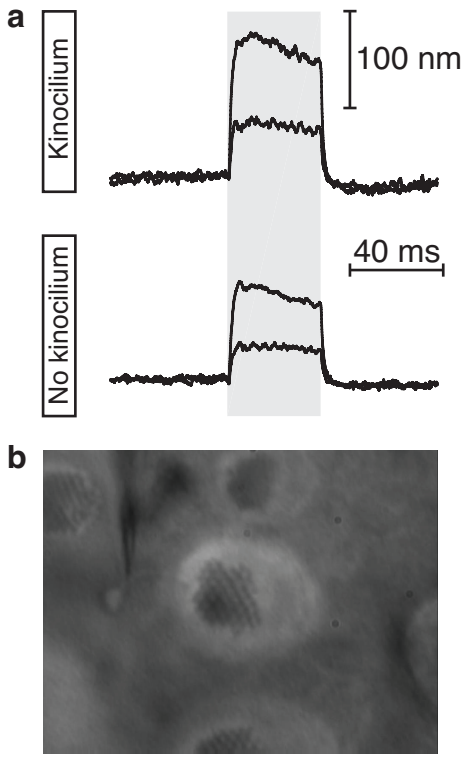

Figure 3.7: An attached kinocilium is not required for light-evoked motion. (a) Top: Hair-bundle motion in an intact bundle was recorded in response to pulses of two power densities, 35 MW·m^{-2} and 71 MW·m^{-2}. Bottom: The same bundle's kinocilium was carefully dissected and held with a sharp glass fiber and the measurement was repeated. Wavelength, 375 nm. (b) Image of a bundle with its kinocilium immobilized.

3.3 Using a Mask to Localize the Light-Responsive Element

In the previous section we demonstrated that light-evoked motion does not depend on the kinocilium and includes a component that is independent of channel gating. I sought to identify this component by localizing the effect of light within the hair bundle. To do this, I irradiated each individual extruded hair cell with ultraviolet light while protecting certain apical areas with an opaque mask. I hoped to see a drastic reduction in the light-evoked response when a mask was placed over the sensitive region of the cell. Surprisingly, I found that hair bundle responses changed in the presence of a mask, but that this change was independent of the mask's location. Masking any portion of a hair bundle led to biphasic displacement responses with a rapid peak after laser onset and a decay to a stable position (Fig. 3.8). The mask also caused a significant undershoot in the bundle's position after laser offset. Because these effects appeared to be independent of the location of the mask, I repeated these experiments with a mask placed next to a hair bundle. In this configuration, the "mask" does not protect any part of the bundle from irradiation. The presence of a mask next to a hair bundle led to similar changes in a hair bundle's displacement response (Fig. 3.9).

All mask experiments discussed so far were performed with silver-coated glass fibers. To control for any effects of irradiating silver, the experiments were repeated with a mask made of carbon fiber. The response of a hair bundle next to a carbon fiber was similar to the response near a silver-coated fiber (data not shown). Thus the effect of opaque fibers seems unrelated to masking. Instead, another property of these opaque fibers seems to modulate the hair bundle response to light. In the next section, we consider the possibility that these fibers release heat when irradiated with

ultraviolet light.

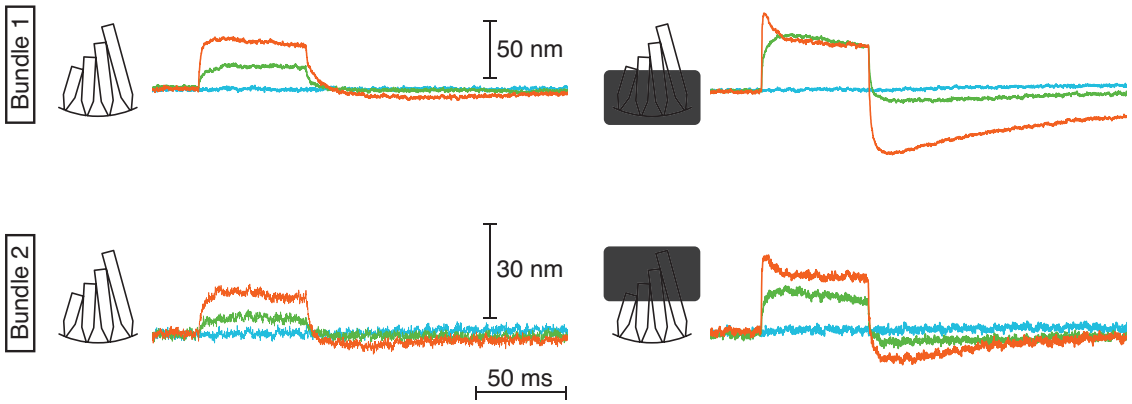

Figure 3.8: Displacement responses of masked hair bundles. Bundle 1, left: The displacement response of a bundle when irradiated with ultraviolet light. Bundle 1, right: The same hair bundle's response with a silver-coated mask over the base of its hair bundle. Bundle 2, left: Displacement response of another hair bundle. Bundle 2, right: The same hair bundle's response when a mask is placed over the tip of the hair bundle. Wavelength, 375 nm. Power densities by color: blue, 0 $MW \cdot m^{-2}$; green, 35 $MW \cdot m^{-2}$; orange, 106 $MW \cdot m^{-2}$.

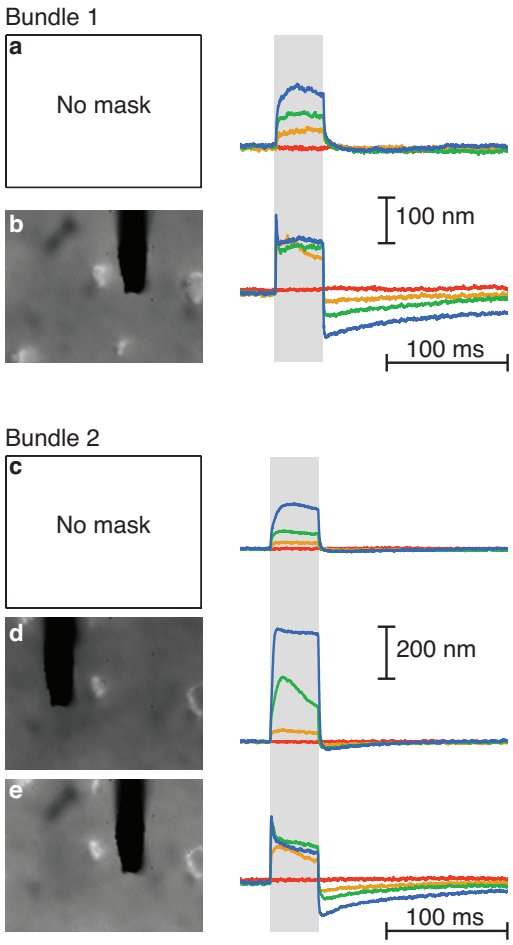

Figure 3.9: Displacement responses of hair bundles next to a mask. (a) A hair bundle's position is recorded in response to irradiation at four power densities: red, 0 MW·m^{-2}; orange, 35 MW·m^{-2}; green, 71 MW·m^{-2}; blue, 106 MW·m^{-2}. (b) The same bundle's response is recorded, with a silver-coated mask adjacent to its tall edge. (c) The response of a second bundle to the same four power densities. (d) The second bundle's response is modified by the presence of a silver-coated fiber on its short edge. (e) The bundle's response is also altered by presence of the fiber on its tall edge. Wavelength, 375 nm.

3.3.1 The Hair-Bundle Mask Generates Heat

In the previous section we found that opaque masks transform the hair bundle's response to light into a biphasic motion with an undershoot, regardless of the composition or position of the mask. Here we explore the possibility that irradiation of masks generates heat that underlies the observed changes in hair-bundle response. The opacity of both mask types stems from their absorption and reflection of light. Some absorbed light must necessarily be emitted as heat. To quantify the amount of heat generated by irradiating opaque masks, we recorded the temperature near a mask by measuring the resistance of a calibrated electrode. As temperature rises, electrode resistance drops.

Irradiation of a silver-coated mask caused a large temperature increase in its vicinity (Fig. 3.10). This increase appears to be responsible for the alterations observed in a hair bundle's response to light in the presence of a mask. I compared the heating profiles of solid and hollow silver-coated masks and found that solid masks generate much larger temperature increases. The presence of water in the core must significantly accelerate cooling.

Irradiation of light-absorbing fibers may be useful as a method to deliver heat stimuli in a spatially and temporally controlled manner. To better understand the spread of heat around an irradiated fiber, I measured the temperature change at several distances from a carbon fiber placed under an ultraviolet beam (Fig. 3.11a). The temperature profile was broad, decaying to half-maximum over a distance of approximately 15 μm from the fiber. A fiber could also be used to conduct heat at a distance from the light source (Fig. 3.11b). This was demonstrated by placing a fiber under a laser beam with its tip extending beyond the edge of the beam.

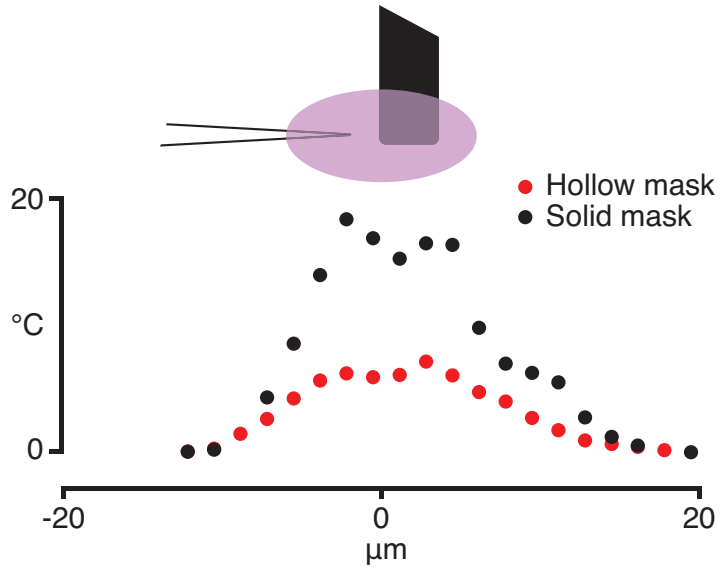

Figure 3.10: Irradiation of a mask generates heat. Irradiation of a silver-coated glass fiber generates a temperature increase. Temperature was measured with an electrode at a distance of 1.7 μm from the lateral edge of the fiber. The fiber and electrode were translated together through the laser beam, which had a diameter of 12 μm. The position of the center of the fiber is plotted on the abscissa. The solid-glass fiber (black) generated larger heat pulses than the hollow fiber (red). Wavelength, 375 nm; power density, 106 MW·m^{-2}.

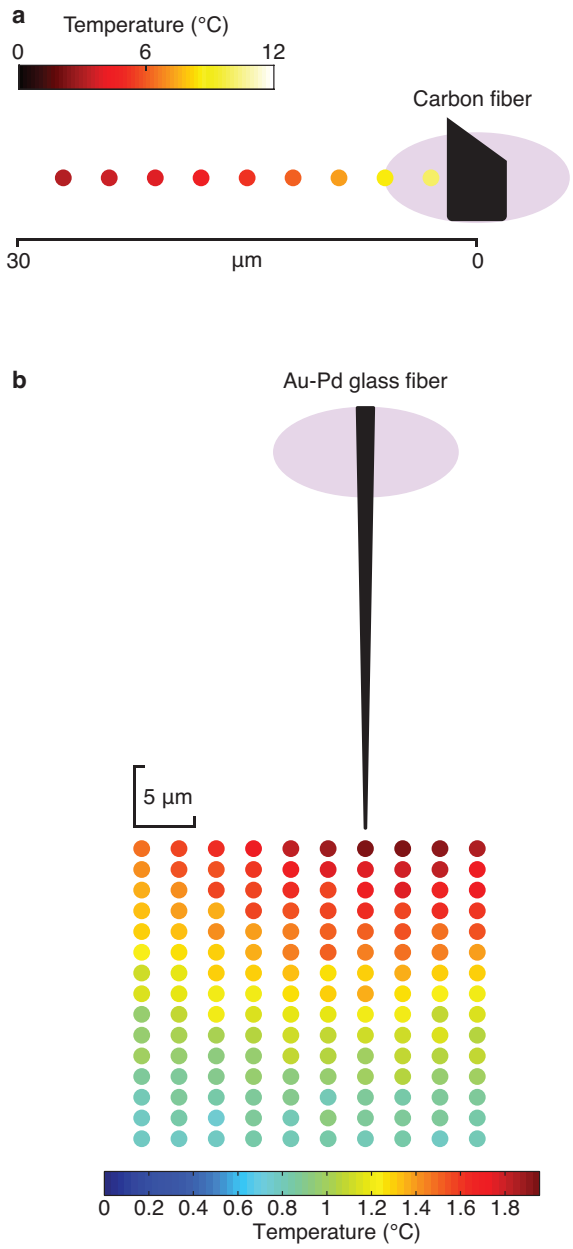

Figure 3.11: Masks as sources of heat. (a) Temperature change as a function of distance from an irradiated carbon fiber. The carbon fiber is schematized on the right. A color map representing temperature change is given at the top. Colored dots represent loci of temperature measurement. The distance to the center of the carbon fiber is given by the scale bar on the bottom. (b) A gold-palladium-coated glass fiber was placed underneath the laser beam with its tip extending 25 μm from the beam center. The resulting light-evoked temperature change was recorded in a 10 $\times$ 15 grid of positions. Temperature changes are given by the color bar below. Wavelength, 375 nm; power density, 106 MW$\cdot$m^{-2}.

3.4 Localization of the Light-Responsive Element in Hair Cells

The attempt to localize the light-responsive element in the hair cell using an opaque mask did not succeed due to the heat-generating properties of the masks used. I therefore decided instead to localize the responsive element by irradiating spatially distinct areas of a hair cell while measuring the displacement response of its hair bundle. To do so, I confined ultraviolet irradiation to sub-cellular regions with a custom-built patterned-illumination system based on a digital micromirror device (Fig. 3.3). Each hair cell was positioned with its axis of sensitivity orthogonal to the beam of light, allowing irradiation of cellular regions at various distances from the bundle. The experiment was conducted both in extruded cells and cells individually held in a micropipette.

The results of patterned illumination were surprising. A cell responded maximally to light directly below its hair bundle (Fig. 3.12). Indeed, the response was minimal when irradiation was confined to the hair bundle. The absorbers responsible for hair-bundle motion therefore lie in the region beneath the hair bundle.

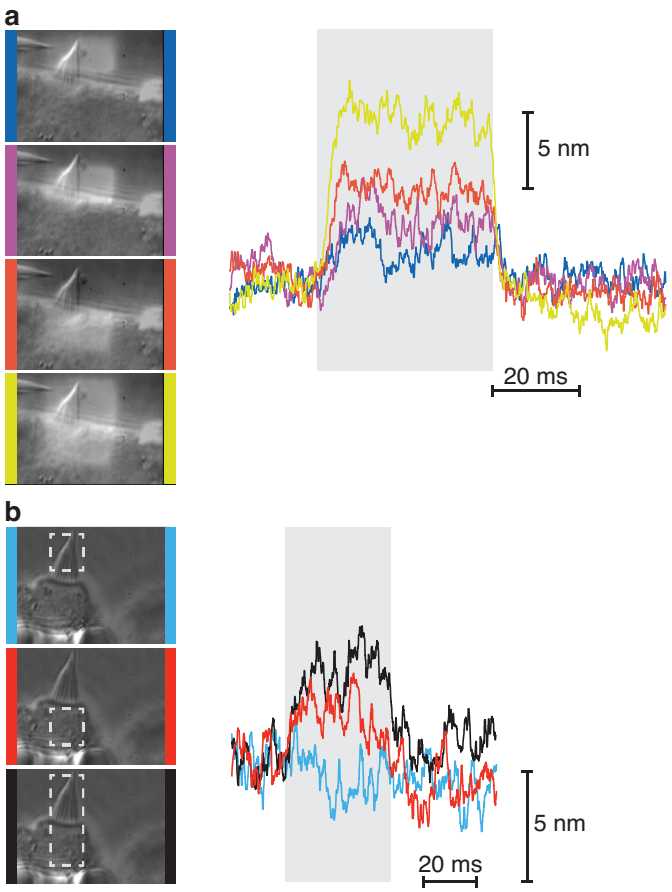

Figure 3.12: The light-responsive element resides below the hair bundle. (a) A digital micromirror device projects light patterns onto a laterally-imaged hair cell in a folded preparation. Images of the light patterns are overlaid on an image of the cell, and each of the four patterns is assigned a color. The hair bundle's displacement in response to each pattern is shown on the right. The yellow pattern is a positive control that encompasses all other patterns. Wavelength, 405 nm; power density by color: blue, 2.52 ; violet, 2.60; orange, 2.35; yellow, 2.37 $MW \cdot m^{-2}$. (b) A hair cell is held in a polished micropipette and irradiated with the patterns outlined in dashed white boxes. Hair bundle displacement was maximal when the largest area was illuminated (bottom image, black trace). Irradiation of the hair bundle alone did not evoke motion (top image, blue trace), while irradiation of the area below it resulted in near-maximal motion (middle image, red trace). Power densities from top to bottom, 4.8, 4.3, 4.7 $MW \cdot m^{-2}$.

3.5 Action Spectrum

To characterize the cellular absorbers underlying photostimulation of hair cells, I obtained a coarse action spectrum of hair bundle displacement. The motion of hair bundles was recorded in response to light in six different wavelength ranges, each encompassing the same stimulus power. Because there is variability in hair cells' response to light, I normalized a cell's displacement in each wavelength band to its largest displacement. The results from all eleven cells were then averaged together. The resulting action spectrum revealed that photostimulation was most efficient near a wavelength of 400 nm (Fig. 3.13a). This sensitivity resembles the absorption spectra of NADH, flavoproteins, and hemoproteins, the principal absorbers of ultraviolet light (Fig. 3.13b) [48, 49, 50]. Because these molecules are principally redox mediators in cells, it is not immediately obvious how they might give rise to light-mediated hair-bundle displacement.

To better understand the potential role of intracellular ultraviolet absorbers, I localized them within the cell. Because these molecules fluoresce, I was able to visualize them in hair cells by fluorescence microscopy. As shown in Figure 3.14, the chromophores were present primarily at the apices of hair cells near the cuticular plate, and at their bases. No chromophores were observed in the hair bundle. The two regions of strong fluorescence are dense with mitochondria and peroxisomes, organelles filled with NADH, flavins, and cytochromes (Fig. 3.15). This distribution of organelles likely reflects the metabolic demands placed upon these two areas, which abut the energetically costly hair bundle and synaptic machinery.

The localization of intracellular ultraviolet-light absorbers matches the locus of a hair bundle's maximal sensitivity to light (see Figure 3.12). This evidence, along with the action spectrum of the response, strongly suggests that mitochondrial and peroxisomal absorbers underlie the response to light. Apical mitochondria abut the

cuticular plate, a rigid, actin-based organelle thought to anchor the hair bundle. The close apposition of mitochondria to the cuticular plate suggests a possible interaction between the organelles. Indeed, mitochondrial cristae are more densely packed on the side abutting the cuticular plate than on the opposite side (personal communication, Dr. Anna Lysakowsky, University of Illinois at Chicago). This specialization and the close apposition are likely optimizations for efficient energy delivery, but could play another role as well. For example, mitochondria regulate the intracellular Ca^{2+} concentration, an ability that may be significant near an organelle — such as the hair bundle — with two Ca^{2+}-dependent adaptation processes [51, 52]. Ca^{2+} regulation by mitochondria could also alter the mechanical properties of the cuticular plate. Although the molecular architecture of the cuticular plate is not fully elucidated, it is known to contain tropomyosin and myosin VI, two constituents whose activity is likely altered by Ca^{2+} [53, 54, 55]. One can imagine a role for the cuticular plate in long-term adaptation. When a hair bundle is vigorously stimulated for a long period of time, its Ca^{2+} concentration may rise enough to reach the cuticular plate, which might soften and thus protect the hair bundle from damage. Perhaps light alters mitochondrial Ca^{2+} regulation and thus cuticular plate structure. Because of the exquisite sensitivity of a hair bundle, a minute mechanical change in the cuticular plate could trigger cooperative gating of transduction channels and cause hair-bundle motion.

To determine whether the cuticular plate displays mechanical motion in response to light, we recorded 250 Hz videos of hair bundles irradiated with ultraviolet light. No motion was seen in the cuticular plate after image subtraction (data not shown). Nevertheless we describe in the next section a test of a potential mechanism for mitochondrial stimulation of the hair bundle.

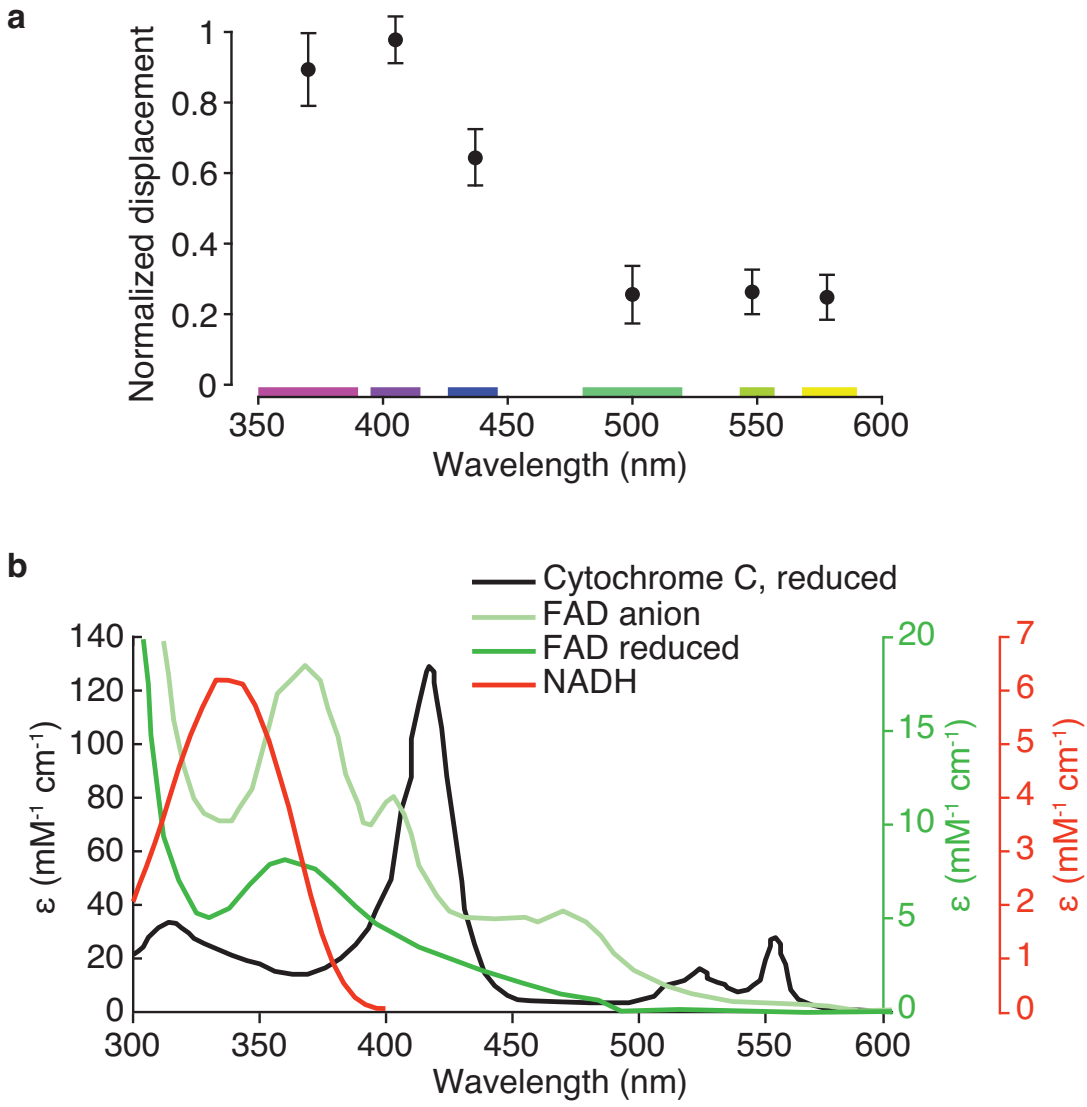

Figure 3.13: Action spectrum of hair-bundle motion. (a) The action spectrum of light-evoked hair-bundle motion for 11 cells shows a peak response in the 400 nm wavelength band. Means and standard deviations are plotted. The width of each wavelength band is drawn in its corresponding color along the abscissa. (b) The absorption spectra for cytochrome c, flavin adenine dinucleotide (a flavoprotein), and NADH are plotted. Data were obtained from Butt and Keilin, Bin Liu et al., and Siegel and Montgomery [48, 49, 50]. Data were digitized with DigitizeIt and converted to extinction coefficients using values in the publications when given in other units.

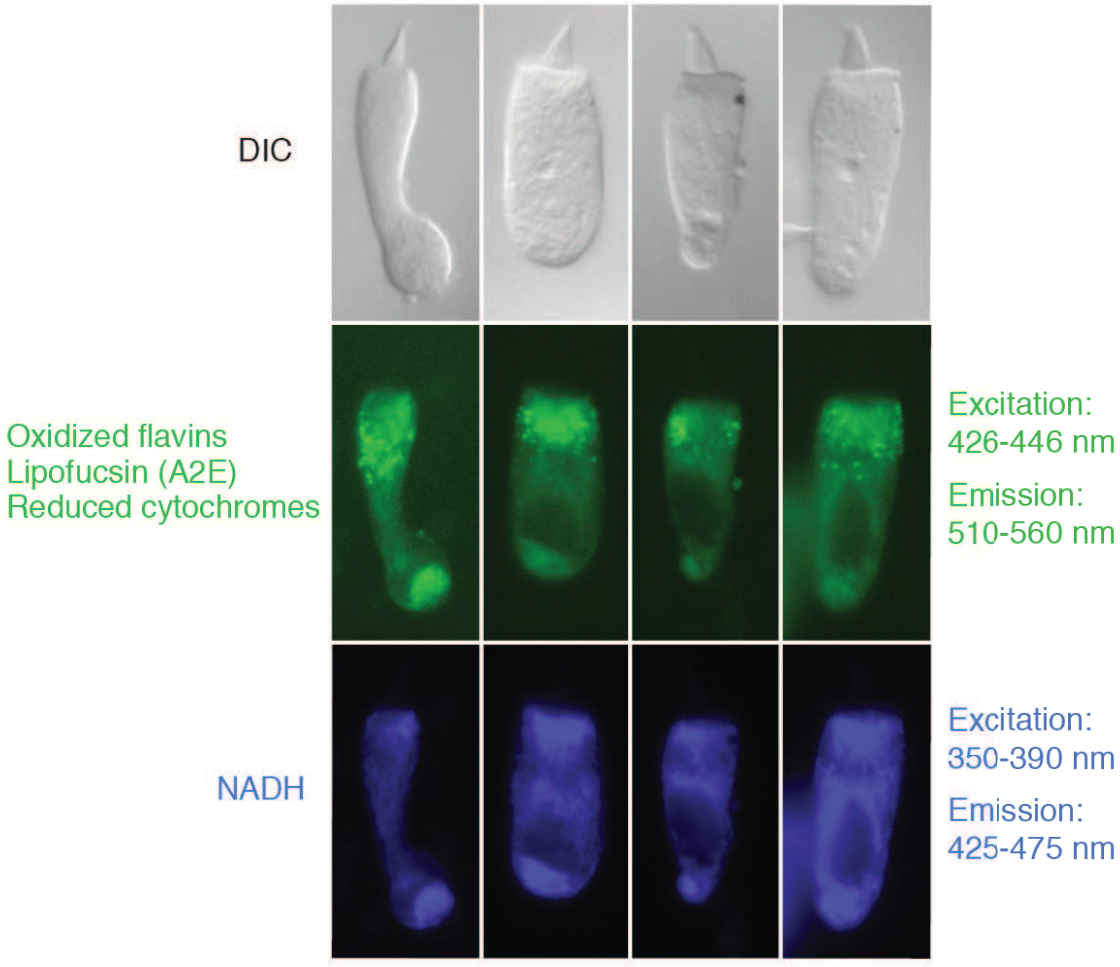

Figure 3.14: Fluorescence localization of intracellular absorbers. Top: Differential-interference-contrast image of four dissociated hair cells. Middle: Autofluorescence of cytochrome c and oxidized flavins. Bottom: Autofluorescence of intracellular NADH.

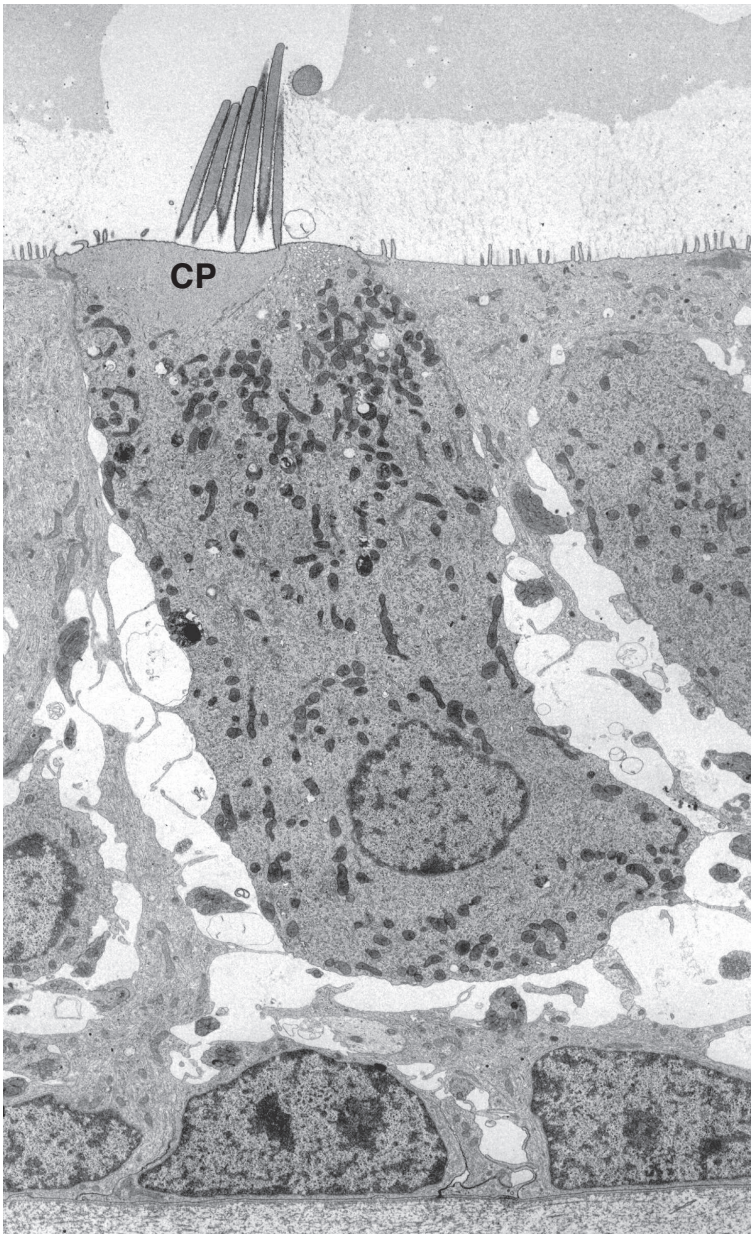

Figure 3.15: Electron micrograph of a bullfrog hair cell. A transmission electron micrograph shows the high density of mitochondria near the cuticular plate (marked CP). Mitochondria are the dark striated oganelles. Image taken from Jacobs and Hudspeth [11].

3.6 Investigation of the Role of Mitochondria

In the previous section we found that ultraviolet absorbers in peri-cuticular mitochondria underlie the hair bundle's response to light. Here we test a potential mitochondrion-based mechanism of hair-bundle stimulation. Because mitochondria are important regulators of Ca^{2+}, altering their state could lead to Ca^{2+}-mediated changes in the hair bundle and other Ca^{2+}-sensitive elements of the hair cell. Mitochondria primarily uptake Ca^{2+} through the mitochondrial calcium uniporter (mCU), a transporter on the inner mitochondrial membrane that is inhibited by ruthenium red. Ca^{2+} efflux is mediated by the mitochondrial sodium-calcium exchanger (mNCX) and mitochondrial proton-calcium exchanger (mHCX). Both of these are also localized on the inner mitochondrial membrane, and mNCX is inhibited by CGP-37157. No inhibitor has been found for mHCX, whose function is the least well understood. The outer mitochondrial membrane is permeable to molecules under 5 kDa, allowing Ca^{2+} to cross freely [51].

Irradiation could cause mitochondrial Ca^{2+} release by generating a thermal pulse. Dittami et al. showed that a brief infrared (IR) laser pulse is able to trigger mitochondrial Ca^{2+} release in rat cardiomyocytes [56]. The Ca^{2+} release was initiated by stimulation of the mitochondrial calcium uniporter, initially increasing the mitochondrial Ca^{2+} concentration. The imported Ca^{2+} then increases the activity of the mitochondrial sodium-calcium exchanger, which releases mitochondrial Ca^{2+} stores into the cytoplasm (see Fig. 3.16 for mitochondrial Ca^{2+}-transport mechanisms). When mCU was inhibited with ruthenium red for 10-15 minutes, the IR-evoked response disappeared entirely (Fig. 5, Dittami et. al, 2011 [56]). However when mNCX was inhibited, IR activation of mCU caused a slight decreases in cytoplasmic Ca^{2+} as mCU transported Ca^{2+} into mitochondria. This Ca^{2+} influx was unable to trigger the inhibited mNCX, causing the slight decrease in cytosolic Ca^{2+} concentration. The

mechanism of infrared activation of mCU is unknown, however IR light is strongly absorbed by water and frequently used to deliver thermal stimuli [57]. Thus mCU activity may have been triggered by a thermal pulse.

Ca^{2+} release from mitochondria can also occur through the permeability transition pore (PTP). However, this large-conductance pore typically opens in response to mitochondrial oxidative stress or Ca^{2+} overload and has not been associated with cellular excitation [52]. Because we did not investigate its role in the hair cell's response to ultraviolet light, it remains a candidate for future work.

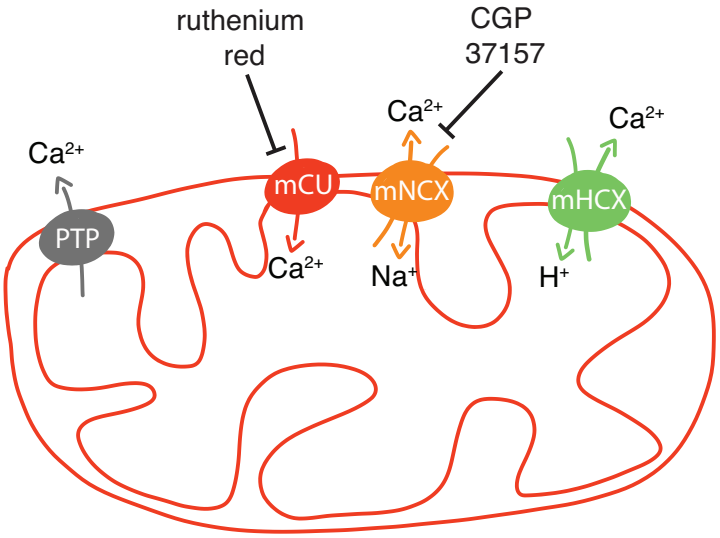

Figure 3.16: Mitochondrial calcium transport Mitochondrial Ca^{2+} influx is mediated by the mitochondrial calcium uniporter (mCU). The mitochondrial sodium-calcium exchanger (mNCX) and mitochondrial proton-calcium exchanger (mHCX) make use of the Na^+ and H^+ gradients respectively to export Ca^{2+} from mitochondria. The permeability transition pore (PTP) can also pass Ca^{2+} into the cytosol. Ruthenium Red inhibits the mCU, and CGP-37157 inhibits mNCX. Although drawn across both the inner and outer mitochondrial membranes, mCU, mNCX, and mHCX occur on the inner membrane. They are drawn over both by convention, because ions can diffuse freely across the outer membrane.

3.6.1 Irradiation Produces Heat

Absorption of ultraviolet light by peri-cuticular mitochondria could conceivably generate heat and lead to mitochondrial Ca^{2+} release through the mCU-mNCX pathway as infrared irradiation does. To determine whether light absorbed by mitochondria generates a significant thermal pulse in hair cells, I recorded the temperature next to a hair cell while irradiating it with ultraviolet light. Ultraviolet irradiation of a hair cell generated a local temperature increase of one to several degrees (Fig. 3.17a). Irradiation of saline solution conversely did not lead to an increase in temperature. An action spectrum of the temperature increase near a cell revealed a relation matching that of the displacement action spectrum, suggesting that the same molecular source underlies both hair-bundle displacement and heat production (Fig. 3.17b). In support of this, measurements of light-evoked heating along the side of a dissociated hair cell revealed that heat production is maximal near the cuticular plate (Fig. 3.18a).

To verify our understanding of the diffusion of heat from mitochondria, we compared measurements of the steady-state temperature achieved above a hair bundle after irradiation to the results of a model. The model calculates the steady-state temperature near a hair bundle as a result of power dissipation by a ring of mitochondria lying below the cell's apex. The ring of mitochondria consists of n individual elements, each of which produces $\frac{1}{n}^{th}$ of the total power flux of the ring. At any point in space, the steady-state temperature increase owing to a single power source is given by

$$\Delta T = \frac{(J/n)}{4\pi\kappa r}\,, \tag{3.1}$$

in which J is the power flux, n the number of power sources, κ the thermal conductivity of water, and r the distance from the source to the relevant point in space. Because superposition holds in the linear equations of diffusion, the contributions of

all sources can be summed to determine the total temperature change at the measurement point [58]. An 8 μm-diameter cell has a cross-sectional area of 50 μm^2. If this cell is irradiated with a power density of 60 $MW \cdot m^{-2}$, a quarter of which impinges on mitochondria, 75 μW of thermal power will be emitted by the mitochondrial ring assuming a 10% rate of absorption and conversion of light to heat. The steady-state temperature around such a hair bundle is calculated in Figure 3.18c. A 4° temperature drop is observed between the apical surface of the cell and a location 10 μm above it. This gradient is consistent with temperature measurements made at several heights above a saccular hair bundle (Fig. 3.18b).

Enough ultraviolet light is absorbed by apical organelles to generate a significant temperature increase in a hair cell. Although Dittami et al. did not record the temperature change evoked by their IR stimulation, similar pulses in another study evoked temperature changes of a few (less than ten) degrees Celsius [56, 57]. Thus the temperature increases I recorded may suffice to trigger Ca^{2+} release from mitochondria through the mCA-mNCX pathway.

The glass electrode used to measure temperature might have a high enough heat capacity to blunt the measured temperature increase. To assess this effect, I recorded and compared light-evoked temperature pulses in the presence of a second glass pipette to pulses in the absence of the second pipette. The presence of a second glass pipette did not significantly alter the temperature measurement (Fig. 3.19). The measurements in Figure 3.19 exhibit a gradual decay in light-evoked temperature. This may be due to progressive photoreduction of cytochrome c with repeated ultraviolet stimulation. The oxidized form of cytochrome c has a lower extinction coefficient in the ultraviolet wavelength range [48].

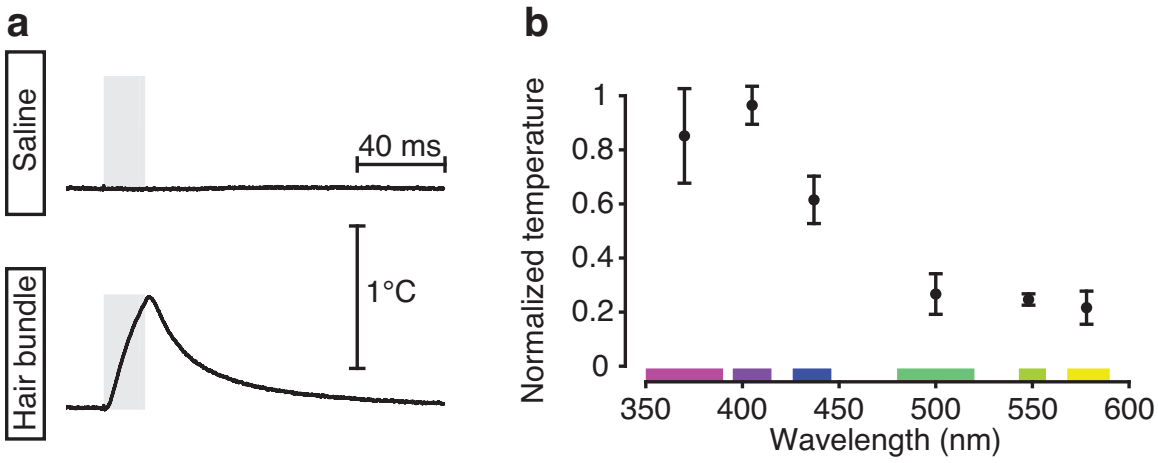

Figure 3.17: Temperature measurement next to a hair cell. (a) Ultraviolet irradiation of a hair cell leads to heat generation (bottom), whereas irradiation of saline solution does not (top). The calibrated resistance of an electrode was used to record temperature at a distance of 2 μm from the hair bundle. Wavelength, 375 nm; power density, 106 MW·m^{-2}. (b) A temperature action spectrum of four hair cells reveals peak heat production in the 400 nm wavelength band. Means and standard deviations are plotted.

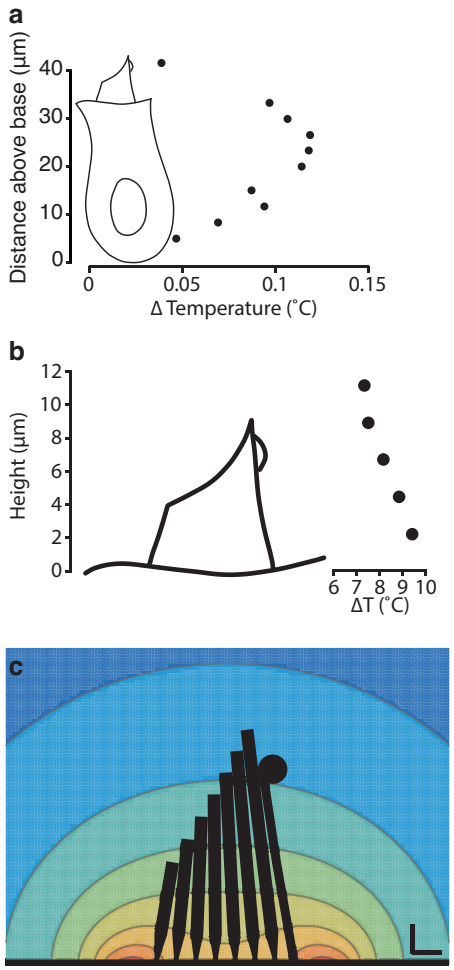

Figure 3.18: Heat production is maximal near mitochondria. (a) Temperature measurements along the side of a dissociated hair cell revealed that the largest temperature increase occurs in the top half of the soma. The cell was irradiated diffusely with light between 350-390 nm. (b) We measured the temperature increase evoked by ultraviolet irradiation of a hair bundle at various heights above the cell surface, at a distance of 2 μm from the kinociliary bulb. The outline of a hair bundle is drawn to scale to guide the viewer's eye. Wavelength, 405 nm. (c) The steady-state profile of temperature increases resulting from a model of the dissipation of 75 μW by a ring of emitters around the hair bundle. Each contour line demarcates a 0.5˚ step in temperature. The temperature changes in the red shaded region are $>$ 4.5 ˚C, and those in the dark blue region $<$ 1.5 ˚C. Scale bars, 1 μm.

Figure 3.19: Control for the heat capacity of a glass microelectrode. I measured irradiation-evoked temperature increases in the vicinity of a hair bundle with and without a second glass micropipette. (a) Several recording configurations are drawn. The temperature-measuring electrode is on the left. The second electrode was either placed opposite the first, or beside the hair bundle. (b) Dark blue: A minimal temperature increase was recorded when the temperature-measuring electrode was positioned away from the irradiated cell. Red: A similarly small increase was recorded 30 μm above the bundle. Yellow: Positioning the electrode 2 μm from the bundle led to a large temperature increase. Violet: The temperature increase with a glass pipette on the opposite side was similar to the record without it. Green: Placing the second glass pipette beside the bundle also resulted in a similar temperature increase. Light blue: A repeat of the recording done in the absence of the second pipette shows gradual decay in the temperature elicited by irradiation.

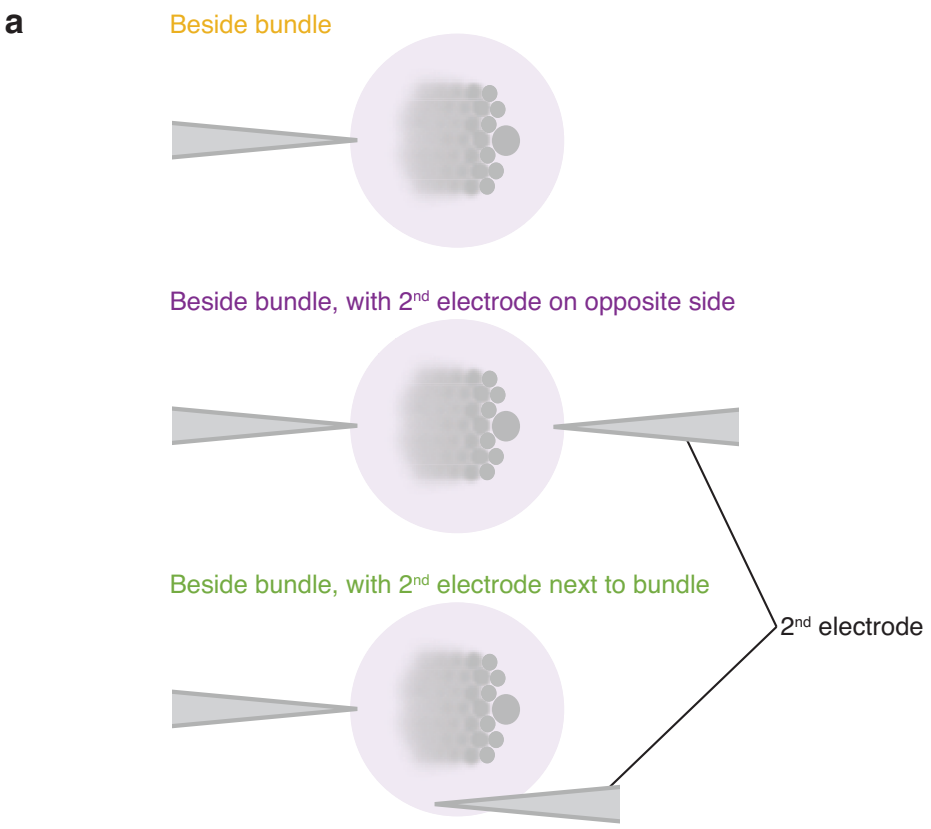
a
Beside bundle
Beside bundle, with 2nd electrode on opposite side
Beside bundle, with 2nd electrode next to bundle
2nd electrode
b
Location of temperature-measuring electrode
Outside beam, 30 µm away
In beam, 30 µm above bundle
Beside bundle
Beside bundle, with 2nd electrode on opposite side
Beside bundle, with 2nd electrode next to bundle
Beside bundle
2 ˚C
40 ms

3.6.2 Heat Production by Irradiated Cells is Ubiquitous

Having determined that irradiation of hair cells generates heat in mitochondria, we reasoned that other cell types may also produce heat upon irradiation. We found that irradiation of other cells, such as red blood cells and saccular supporting cells, also results in local heating (Fig. 3.20a). The magnitude of heating appears to depend on each cell type's concentration of absorbers. The large concentration in red blood cells of hemoglobin, a hemoprotein with a strong absorption peak in the ultraviolet, accounts for those cells' extraordinarily large production of heat. Although the amount of heat produced by irradiation varies among cell types, the action spectrum of heat production is similar among all cells, supporting the conclusion that the major absorbers responsible for light-evoked heating in the visible spectrum are ubiquitous (Fig. 3.20b).

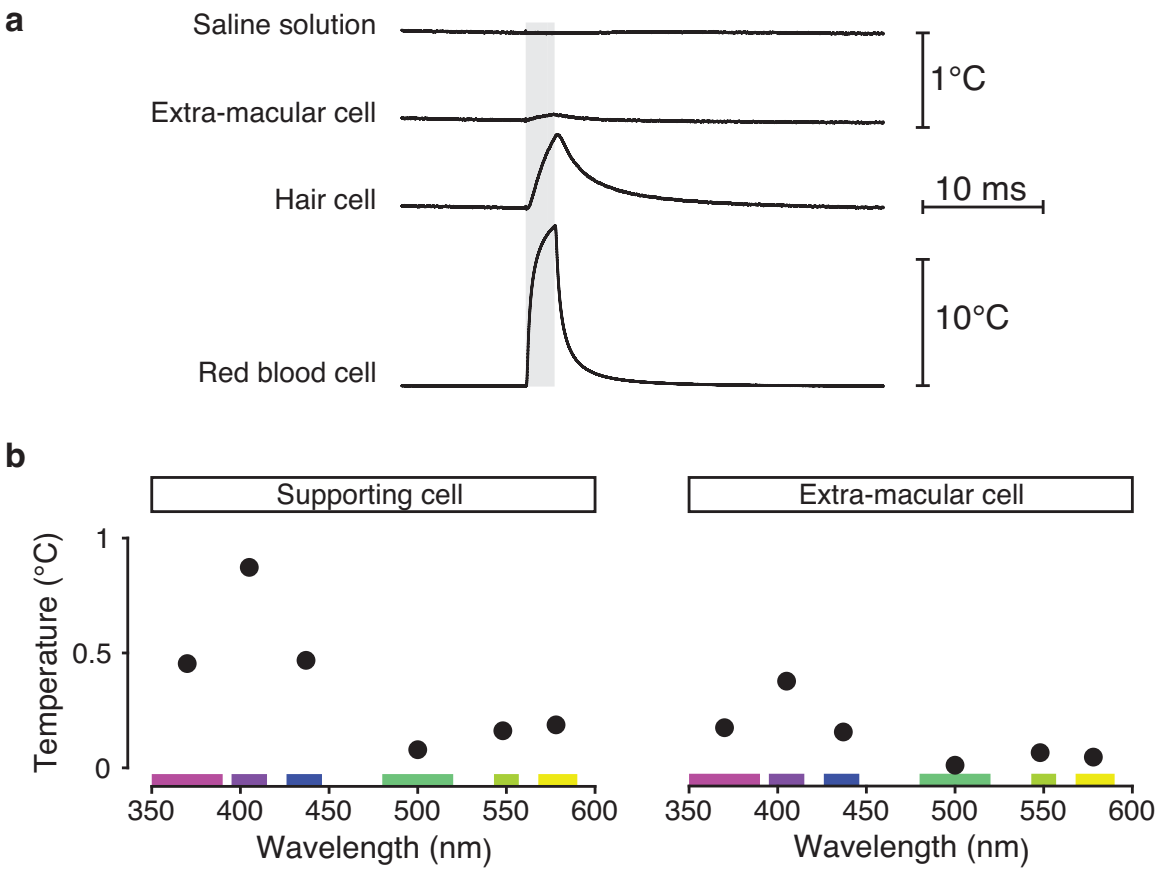

Figure 3.20: Ultraviolet irradiation leads to heat generation in all cell types. (a) Irradiation of saline solution does not lead to an increase in temperature. However, irradiation of extra-macular cells, hair cells, or red blood cells does. Temperature was measured using a calibrated electrode held 2 μm from the cell membrane. Wavelength, 375 nm; power density, 106 MW·m^{-2}. (b) Thermal action spectra above a supporting cell and an extra-macular cell are similar in shape to the thermal action spectrum of a hair cell (Fig. 3.17b).

3.6.3 Mitochondrial Ca^{2+} Release

If mitochondrial Ca^{2+} release evoked by ultraviolet irradiation causes hair-bundle motion, the hair cell response to light should disappear upon inhibition of the mitochondrial Ca^{2+} release machinery. We inhibited the mCU and mNCX transporters with ruthenium red and CGP-37157, respectively, and did not observe any changes in hair-bundle motion (Fig. 3.21). The lack of a response could be due to several factors. First, the blockers might not have reached the mitochondria. Although we used concentrations and solutions similar to those published in the study by Dittami et al., hair cells may be less permeable than cardiomyocytes to these pharmacological agents. Second, it is possible that ultraviolet light does not cause Ca^{2+} release from mitochondria. Perhaps the temperature increase evoked by ultraviolet irradiation is slower than that generated by infrared radiation. Finally, it is possible that mitochondrial Ca^{2+} release does occur with ultraviolet irradiation, but that it is not linked to hair-bundle displacement.

Further exploration of mitochondrial Ca^{2+} release may provide more insight into its occurrence in hair cells. For example, Ca^{2+} imaging during irradiation would allow the visualization and localization of Ca^{2+} events. A preliminary experiment of this type was performed by Dr. Marcotti at the University of Sheffield. He observed pulses of cytosolic Ca^{2+} in mouse hair cell somata after attempting to photolyze Ca^{2+} with ultraviolet light (Personal communication, February 2017). The Ca^{2+} pulses persisted even when the caged Ca^{2+} compound was not loaded. Because of the dense mobile Ca^{2+} buffers and pumps present in the hair bundle [59], it is unlikely that Ca^{2+} entry through the hair bundle would lead to somatic flares of Ca^{2+}, suggesting that mitochondria could be the source of Dr. Marcotti's observations . However, the results are preliminary, and until a conclusive test of mitochondrial Ca^{2+} release in hair cells is performed we will assume it is unproven. Conclusive proof of Ca^{2+} release

from an internal source would come in the form of an ultraviolet-light-evoked Ca^{2+} flare in a cell with ruptured tip links that is bathed in low-Ca^{2+} solution.

Figure 3.21: Blocking mitochondrial calcium efflux. (a) The ultraviolet-evoked displacement response of hair bundles does not change upon exposure to 40 μM ruthenium red. Top row: Baseline displacement records for 4 cells at two power levels (red: 113 MW·m^{-2}, black: 227 MW·m^{-2}). Middle row: Displacement records for the same 4 cells after 5, 7, 8, and 9 minutes in ruthenium red, from left to right. Bottom row: Displacement records after 23, 24, 26, and 27 minutes in ruthenium red. (b) A similar experiment was performed with four cells exposed to 40 μM CGP-37157 in 0.1% DMSO. Second row: Responses after 11, 13, 14, and 16 minutes in CGP-37157. Bottom row: Responses after 36, 38, 40, and 40 minutes in CGP-37157.

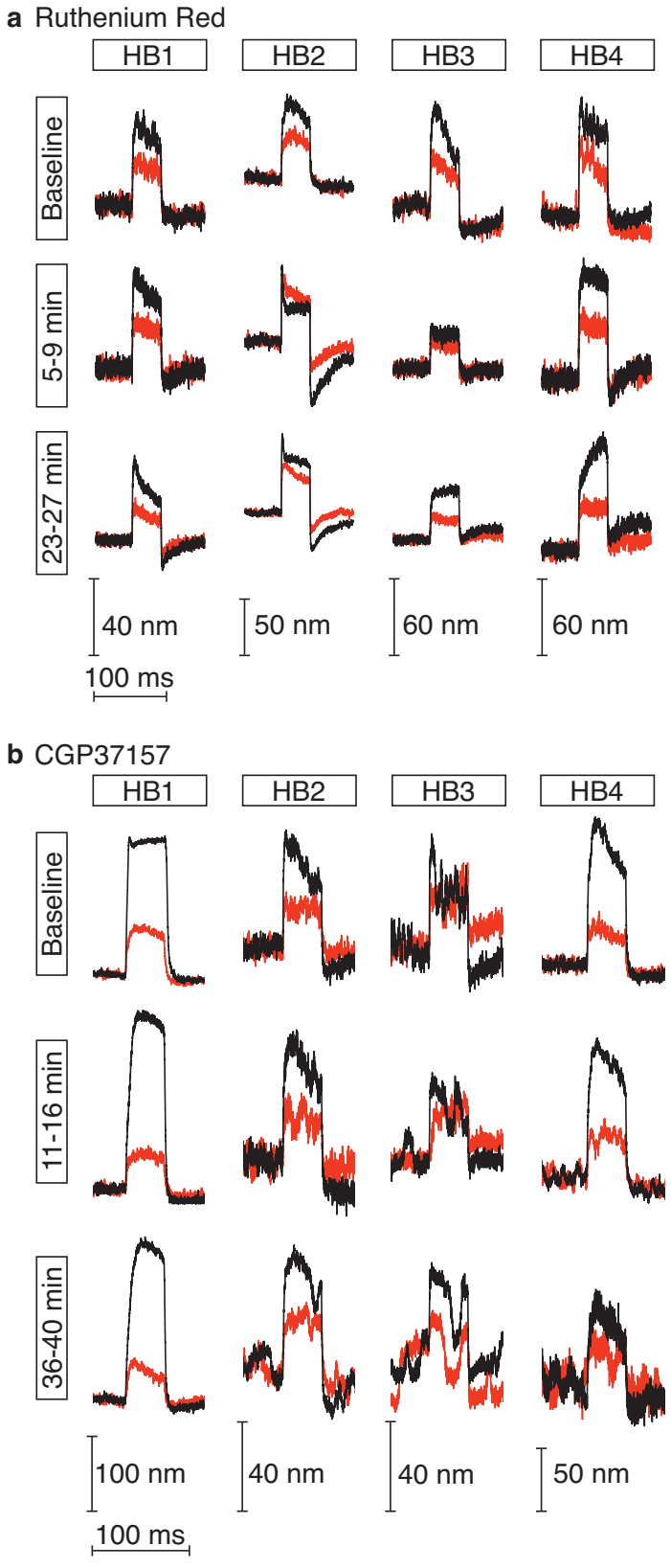
a Ruthenium Red
HB1
HB2
HB3
HB4
Baseline
5-9 min
23-27 min
40 nm
50 nm
60 nm
60 nm
100 ms
b CGP37157
HB1
HB2
HB3
HB4
Baseline
11-16 min
36-40 min
100 nm
40 nm
40 nm
50 nm
100 ms

3.6.4 Time Delay to Hair-Bundle Motion

The hypothesis that Ca^{2+} can mechanically alter the structure of the cuticular plate is a conjecture based upon the cuticular plate's composition. Only one study to date has described a potential Ca^{2+}-dependent motion of the cuticular plate, and it took place over a span of 20 minutes [60]. Here we examine the possibility that laser-evoked Ca^{2+} release at the base of the bundle could affect bundle mechanics by acting on known calcium-sensitive elements at the stereociliary tip, such as the mechanotransduction channel and adaptation motors. Frog saccular hair bundles' stereocilia are of height 3 μm to 7 μm. By adding 2 μm to this value for the thickness of the cuticular plate, we come to an average distance of 7 μm between the base of the cuticular plate and the tip of stereocilia. The average time for a Ca^{2+} ion to diffuse this distance in one dimension is $t = \frac{x^2}{2D} = \frac{(7\times10^{-6}\,m)^2}{2\times(8\times10^{-10}\,m^2\cdot s^{-1})} = 30$ ms, in which D is the diffusion coefficient of Ca^{2+}, 8×10^{-10} m^2 $\cdot$s^{-1}. This time is much longer than the observed time until initiation of hair-bundle motion, which is 1 ms or less. For comparison, we calculate the time required for heat to diffuse to the tip of a bundle. The temperature at time t and distance x from a source in a homogeneous semi-infinite medium is given by

$$\mathrm{T}(x,t) = \frac{2F_o}{K}\left\{\sqrt{\frac{\kappa t}{\pi}}e^{-x^2/4\kappa t} - \frac{x}{2}\,\mathrm{erfc}\left(\frac{x}{2\sqrt{\kappa t}}\right)\right\}, \tag{3.2}$$

in which F_o is the power flux per unit area and time, K the thermal conductivity of water, and κ the thermal diffusivity of water (p. 75, Carslaw and Jaeger [61]). It takes approximately 40 μs for temperature to rise by 1 °C at a distance of 7 μm from a flux density of 10 MW$\cdot$m^2. Although Ca^{2+} diffuses too slowly to reach the stereociliary tips in time to generate motion, heat might spread fast enough to do so.

To gain a better understanding of the process underlying light-evoked hair-bundle motion, we calculated the delay between the laser onset and hair-bundle motion, as

well as between laser onset and temperature increase [1]. Although the delay before hair-bundle motion can be calculated from a bundle's position trace, finding the delay before temperature increases in the hair bundle requires more effort. Because the temperature electrode can not be placed inside the hair bundle, I resorted to extrapolation to estimate the time required for the temperature to increase inside a hair bundle. Temperature was recorded at several distances from a hair bundle, and the latency of temperature increase was calculated at each of these positions. A line was fit through these points and extrapolated to the position of the hair bundle. Results indicated that hair-bundle motion starts after a delay of approximately 150 μs, whereas temperature starts to rise in the hair bundle after approximately 60 μs (Fig. 3.22). The temperature increase thus leads hair-bundle displacement, raising the possibility that heat itself leads to hair-bundle stimulation. I address this possibility in next section. Importantly, hair-bundle motion is not caused by the action of a molecule diffusing from the hair-bundle base to the stereociliary tips.

The possibility that Ca^{2+} might act at the cuticular plate is unchanged by the above results. However the mCU-mNCX Ca^{2+} efflux mechanism is mediated by transporters, and therefore slow. The alternative Ca^{2+} release mechanism, through the mitochondrial permeability transition pore (PTP) is unlikely as well, for it only releases Ca^{2+} in conditions of oxidative stress or Ca^{2+} overload [52].

[1] See Section 3.1.10 for the method by which delay was calculated.

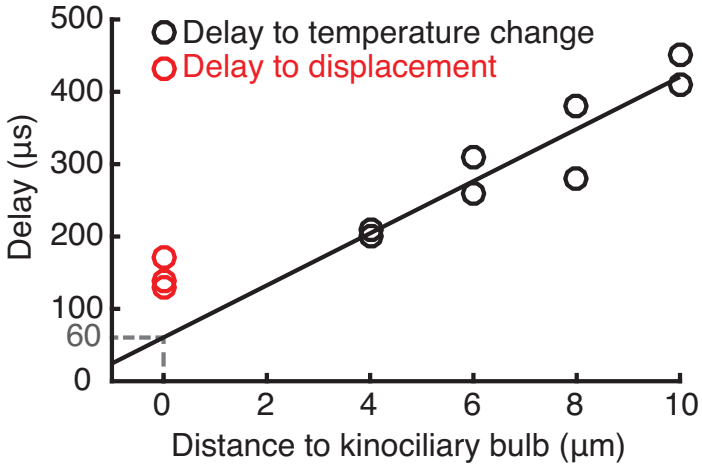

Figure 3.22: The delay to hair-bundle motion. The delay between laser irradiation and hair-bundle displacement for three hair bundles is plotted in red. The delay between laser irradiation and temperature increase, measured at four distances from a hair bundle, is plotted in black. Temperature delays were obtained twice at each position. A linear extrapolation of the relation between delay and distance estimates a temperature delay of 60 μs at the hair bundle. The measurements shown were obtained from a single hair bundle.

3.7 Heat Pulses Underlie the Hair-Bundle Response to Light

In this section we consider the possibility that the temperature change evoked by hair-cell irradiation underlies hair-bundle motion. To test this hypothesis I generated a temperature pulse by heating water with infrared radiation. A hair cell was placed in the path of both an ultraviolet beam passing through the objective lens and an infrared beam emanating from a 100 μm-diameter optical fiber (Fig. 3.23a). I simultaneously recorded hair-bundle movement and temperature at a distance of 2 μm from the hair bundle in response to ultraviolet and infrared irradiation. With the infrared power set to generate a similar temperature increase to the ultraviolet pulse at the hair bundle, I observed nearly identical hair-bundle displacements in both configurations (Fig. 3.23b). This result suggests that heat causes hair-bundle motion. Owing to water's efficient absorption of infrared light, an infrared power density of 0.13 MW$\cdot$m^{-2} was sufficient to elicit this response, whereas 71 MW$\cdot$m^{-2} was required for ultraviolet irradiation.

I confirmed that heat underlies hair-bundle motion by exchanging H_2O, the primary absorber of infrared light in the system, with D_2O, whose absorption coefficient is approximately 0.5% that of water at 1470 nm [62]. In D_2O-based solution, more infrared radiation reaches the hair bundle, but a smaller temperature increase occurs. We measured a 60 percent decrease in the infrared-evoked temperature increase in D_2O-based saline solution, and a corresponding reduction of 63 percent in hair-bundle displacement (Fig. 3.23b). The temperature and displacement response to ultraviolet light were not changed in D_2O, confirming the intracellular location of ultraviolet absorbers.

To further illustrate that a heat pulse is sufficient to evoke hair-bundle motion, I

generated a local pulse of heat. The tip of a 5 μm-diameter carbon fiber was placed next to a dissociated hair cell, and its shaft was irradiated with ultraviolet light to heat it. This direct thermal stimulus resulted in hair-bundle motion that disappeared upon retraction of the carbon fiber (Fig. 3.24).

Figure 3.23: Infrared and ultraviolet stimulation of a hair bundle. (a) A 100 μm-diameter optical fiber passing 1470 nm infrared light is placed 100 μm from a hair bundle. The bundle is also underneath a beam of 405 nm ultraviolet light, allowing for stimulation with either wavelength. (b) Black: Simultaneous temperature and displacement records of a bundle irradiated with 71 MW$\cdot$m^{-2} ultraviolet or 0.13 MW$\cdot$m^{-2} infrared light. Power densities were chosen to evoke the same temperature increase with either wavelength. Red: Records from the same cell after several exchanges with D_2O-based saline show a 60% decrease in temperature and 63% decrease in displacement with infrared stimulation, indicating that the temperature increase underlies hair-bundle motion. Temperature records are taken 2 μm from the side of the bundle, at a height of 7 μm from the apical cell surface.

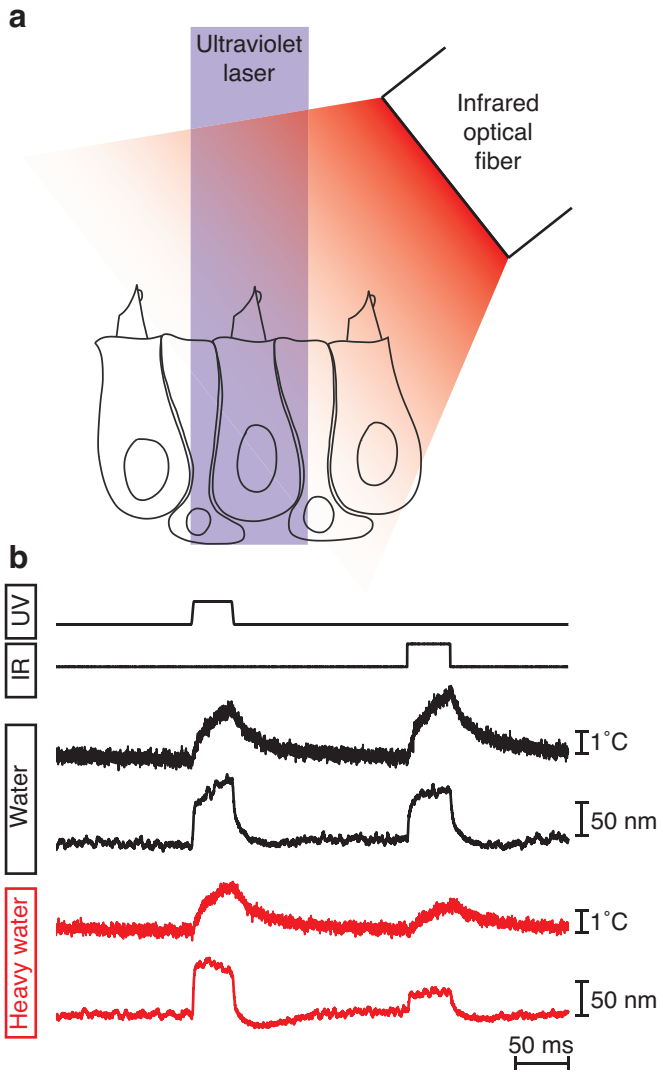
a
Ultraviolet
laser
Infrared
optical
fiber
b
UV
IR
Water
Heavy water
1˚C
50 nm
1˚C
50 nm
50 ms

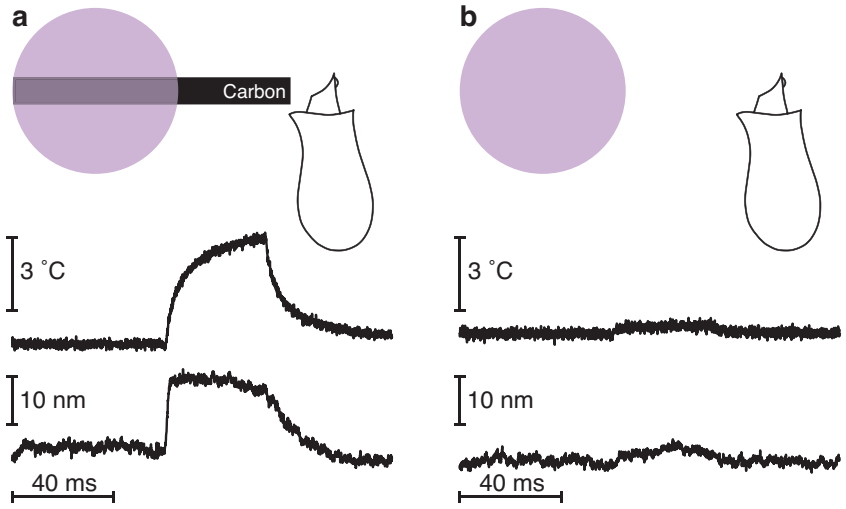

Figure 3.24: Heat from a carbon probe stimulates a hair bundle. (a) A 5 μm diameter carbon fiber was positioned within a laser beam with its tip extending beyond the beam. The fiber tip was 3 μm away from the hair bundle of a dissociated hair cell. Temperature was measured with a calibrated electrode 2 μm from the kinociliary bulb. When irradiated, the carbon fiber radiated heat and caused hair-bundle motion. (b) Upon retraction of the carbon fiber, both temperature increase and hair-bundle motion were reduced. Same cell as (a). Wavelength, 405 nm.

3.8 A Simple Model for Heat-Evoked Hair Bundle Motion

Heat pulses have a variety of effects on excitable biological tissue. Because it requires intact tip links, heat-evoked stimulation of hair cells is not mediated by thermally gated channels, changes in membrane capacitance, or any other process that is independent from the hair bundle. I therefore investigated whether heat pulses stimulate hair bundles by mechanically altering their components. The hair bundle can be viewed as a structure whose position is determined by forces in two sets of opposing elastic elements, tip links and stereociliary pivots (Fig. 3.25a). Given this arrangement, positively-directed motion can be elicited either by a stiffening of stereociliary pivots or by a loosening of tip links (Fig. 3.25b). This is shown by summing the forces on tip links and stereociliary pivots:

$$F_{sp} + F_{tl} = 0 \tag{3.3}$$

$$k_{sp}(X_{sp} - X) + k_{tl}(X_{tl} - X) = 0 \tag{3.4}$$

$$X = \frac{k_{sp}X_{sp} + k_{tl}X_{tl}}{k_{sp} + k_{tl}}\,. \tag{3.5}$$

Here F_{sp} is the force on the stereociliary pivot, k_{sp} the stereociliary pivot stiffness, X_{sp} the stereociliary pivot reference position, F_{tl} the force on tip links, k_{tl} the tip link stiffness, X_{tl} the reference position for tip links, and X the position of the hair bundle. Figure 3.25 was generated with the following unitless parameter values: K_{sp} = 100, K_{tl} = 100, X_{sp} = 1, X_{tl} = -1, ΔK_{tl} = 0.5, ΔK_{sp} = 1.0.

The two alternative ways to elicit positive motion can be differentiated with the help of offsets from an external probe. The position of the hair bundle after sustaining

force offsets from an external probe is given by:

$$F_{sp} + F_{tl} = F_{probe} \tag{3.6}$$

$$k_{sp}(X_{sp} - X) + k_{tl}(X_{tl} - X) = k_{probe}(X - X_c) \tag{3.7}$$

$$X = \frac{k_{sp}X_{sp} + k_{tl}X_{tl} + k_{probe}X_c}{k_{sp} + k_{tl} + k_{probe}} \tag{3.8}$$

in which F_{probe} is the force applied by the probe, k_{probe} the probe stiffness, X_{probe} the probe's reference position, and all other variables retain their previous assignments. Using Equation 3.8, two predictions of temperature-evoked hair bundle motion were made. If a heat pulse causes hair-bundle motion by decreasing tip-link stiffness, then positive offsets would increase the amplitude of motion evoked by heat, and negative offsets would reduce it (Fig. 3.26). If hair-bundle motion is caused by an increase in stereociliary pivot stiffness, the opposite result is expected. These two predictions are shown in Figure 3.26a. Although both options result in positive hair bundle motion, the difference in the pattern evoked with offsets can be used to differentiate them. Figure 3.26 was generated with the same parameter values as Figure 3.25 and K_{probe} = 100. Offset commands were: -2, -1, 0, 1, 2. To determine which elastic element most likely underlies heat-mediated hair bundle motion, we performed the offset experiment on a frog hair bundle. The hair bundle was offset with a flexible glass fiber and then irradiated. We found that the amplitude of light-evoked motion increased with positive offsets (Fig. 3.26b). Thus heat likely softens tip links or other elements in series with them, such as the insertional plaques or adaptation motors.

To verify that heat does not alter the stiffness of the stereociliary pivots, I severed the tip links and measured the stiffness of stereociliary pivots before and after irradiation (Fig. 3.27). No change in stiffness was detected. I next reasoned that if tip links or other elements in series with them do indeed relax upon irradiation,

the mechanotransduction channels that are open at rest should close if a bundle is prevented from moving towards its tall edge. Upon blocking a bundle's motion with a stiff probe, we found that the light-evoked response changes from depolarization to hyperpolarization, confirming that heat softens an element in series with the tip link (Fig. 3.28). A similar experiment was performed with mechanical stimulation by a flexible probe. A bundle was first stimulated with a flexible probe, giving rise to a receptor potential (Fig. 3.29). The bundle was then stimulated again while simultaneously irradiated with ultraviolet light for the duration of the mechanical pulse. The bundle was less sensitive to mechanical stimulation during irradiation. Additionally, irradiation of the bundle while the flexible probe was attached but not applying any force resulted in hyperpolarization of the cell. Taken together, these observations suggest that heat softens tip links, causing channel reclosure if the bundle faces resistance to forward motion.

Although the results above suggest that ultraviolet irradiation stimulates hair cells by softening their tip links, it is not immediately clear how tip-link softening can open mechanotransduction channels. The solution may lie in the parallel arrangement of tip links within the hair bundle. We recall from Section 1.7 that when one tip link suddenly carries less tension, the relieved load is redistributed among the remaining tip links. If the relieved load increases the tension on some tip links beyond their channel's gating force, those mechanotransduction channels will open. This mechanism could underlie heat-evoked hair-bundle motion. Heat originates in mitochondria and reaches short stereocilia several tens of microseconds before tall ones. As the tip links of short stereocilia soften, those of tall stereocilia carry the excess load and eventually open their associated mechanotransduction channels. Thus it is possible to open mechanotransduction channels through a reduction in tip-link tension.

The precise mechanism of tension reduction in the tip link is a mystery. Although

it is easiest to think of heat as softening the tip link itself, any number of actions could result in a reduction of tip-link tension. For example, the hypothesized release element that may underlie fast adaptation could undergo a conformational change to release tension upon heating [33]. Alternatively, a heat-dependent conformational change in the adaptation motor could slacken tip links.

Our previous experimental results are consistent with the mechanism proposed above. When tip links are ruptured, changes in gating spring stiffness are no longer coupled to hair bundle position, thus the response to light disappears. When mechanotransduction channels are blocked with gentamicin, softening of the tip-link chain reduces the force it applies to the hair bundle, causing the bundle to move forward. The short delay between the onset of the laser pulse and the initiation of hair-bundle movement is also explained by the direct mechanical action of a light-evoked heat pulse.

Hair-bundle structure is conserved across species and sensory organs. Thus the mechanism described here may be widespread among hair cells. I tested this hypothesis by irradiating hair cells from the mouse's utricle and the tokay gecko's basilar papilla with ultraviolet light. In support of this hypothesis, rapid, positively directed hair bundle movements were observed in both cases (data not shown).

The data presented here demonstrate that rapid temperature changes lead to hair-bundle motion. To investigate whether hair-bundle motion is caused by temperature per se or by a rapid change in temperature, I generated temperature pulses around hair bundles while changing the temperature of their environment. Hair bundles responded equally well to temperature pulses evoked in cold solution or in room-temperature solution (data not shown).

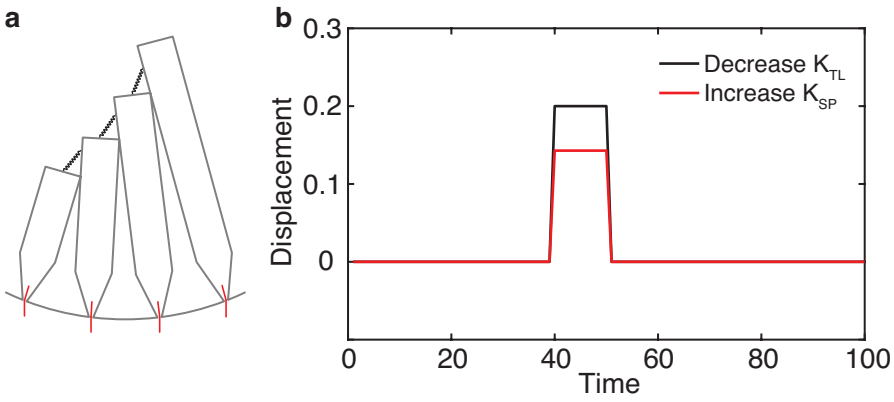

Figure 3.25: Changes in tip link or stereociliary pivot stiffness can cause forward bundle motion. (a) Schematic of a minimal hair-bundle model consisting of tip links (black) and stereociliary pivots (red). The bundle's resting position is a function of the stiffness of each these elements. (b) Forward bundle motion arises at time 40 from either a reduction in tip-link stiffness (K_{tl}) or an increase in stereociliary pivot stiffness (K_{sp}).

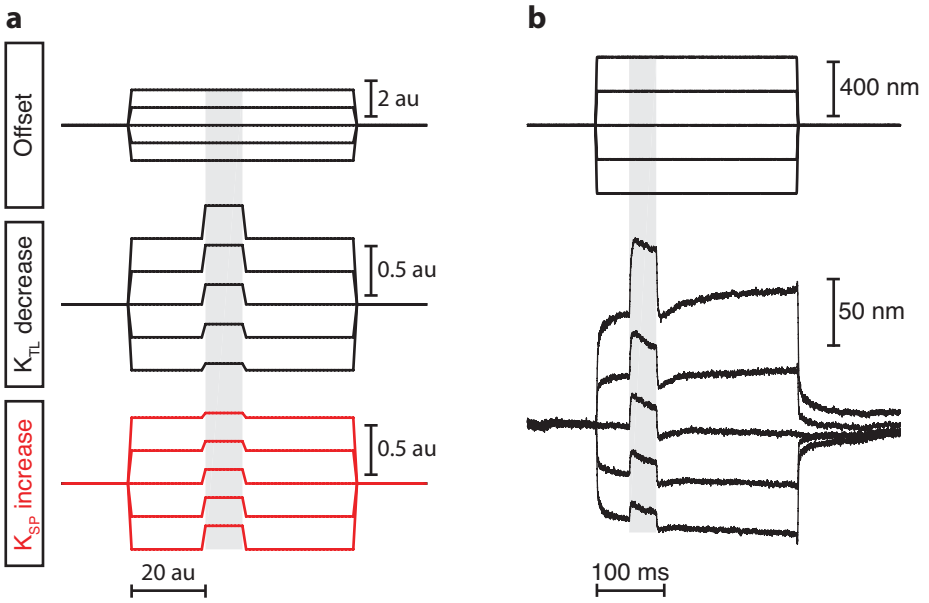

Figure 3.26: Distinguishing between a change in pivot stiffness and tip-link stiffness. (a) The two stiffness alterations that lead to positive hair-bundle motion are differentiated by their opposite responses to offsets imposed by a probe. (b) A bullfrog saccular hair bundle is offset in both positive and negative directions with a flexible glass fiber while iontophoretically exposed to gentamicin. 50 ms after the initiation of the fiber-mediated offset, the bundle is exposed to 83 MW·m^{-2} of 405 nm light for 40 ms to elicit motion. Fiber stiffness, 280 μN·m^{-1}.

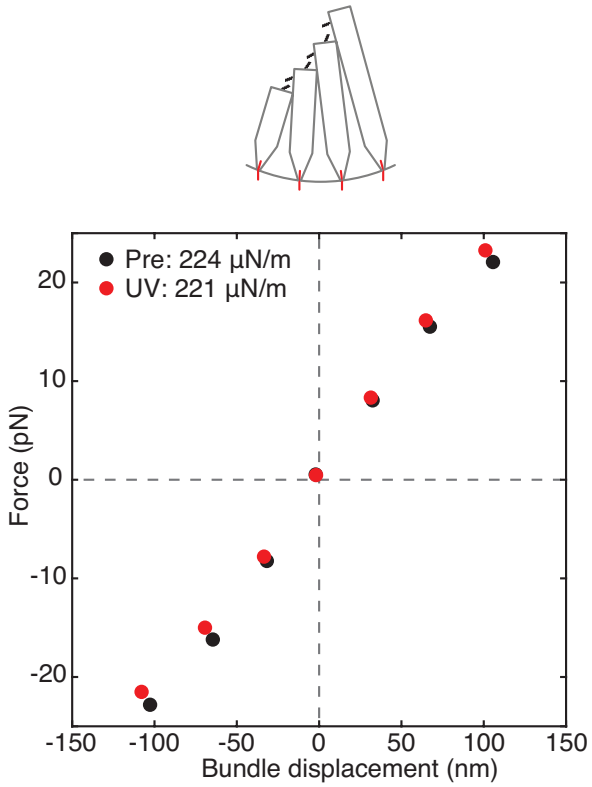

Figure 3.27: Ultraviolet irradiation does not change stereociliary pivot stiffness. A bundle whose tip links were ruptured with EGTA was displaced with a calibrated glass fiber. The force experienced by the bundle is plotted against its displacement. The stereociliary pivot stiffness was 224 μN·m^{-1} without irradiation and 221 μN·m^{-1} with ultraviolet irradiation. Wavelength, 405 nm.

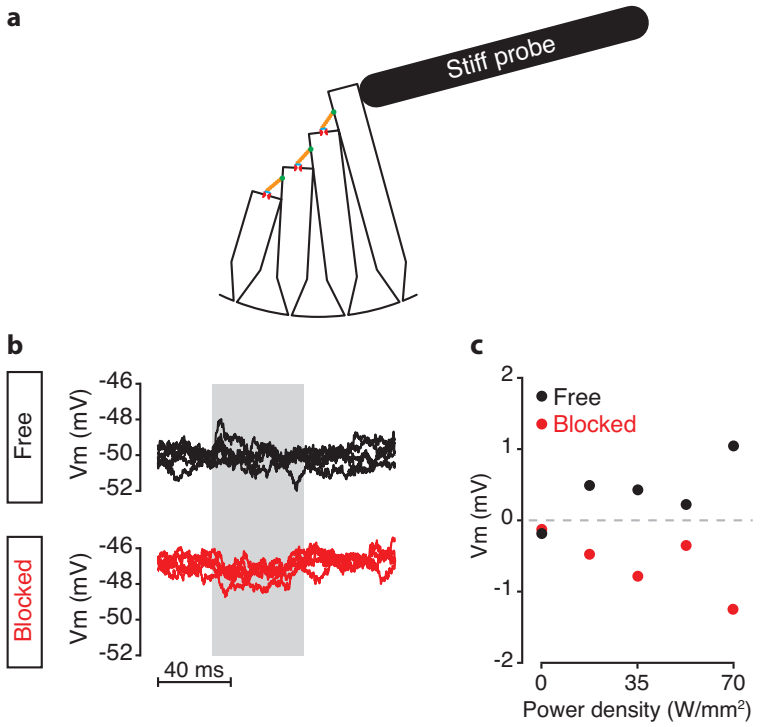

Figure 3.28: Light stimulation while blocking bundle motion. (a) A stiff probe is used to prevent hair-bundle motion. (b) A hair cell depolarizes in response to irradiation with ultraviolet light of increasing power density (black). When the same cell's hair bundle is held stationary with a stiff probe, irradiation leads to hyperpolarization. (c) The peak voltage response is plotted against power density.

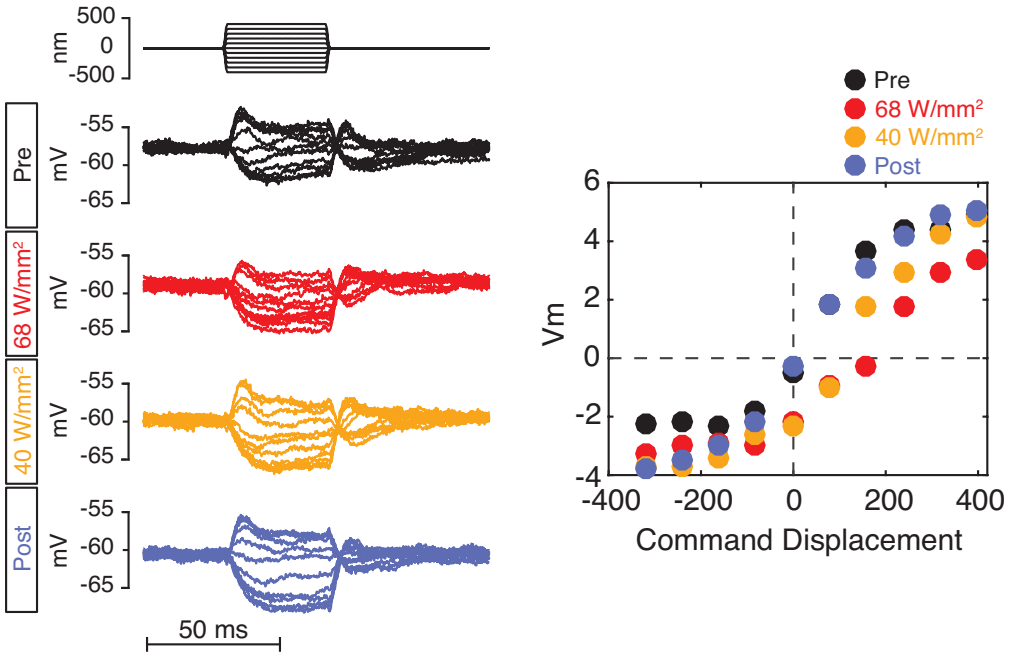

Figure 3.29: Light modulates the mechanical sensitivity of a hair bundle. (Left) Mechanical stimuli were applied to a hair bundle with a flexible probe. The resulting voltage response is shown in black. The stimulus train was repeated with simultaneous light irradiation at 40 MW·m^{-2} and 68 MW·m^{-2}, and finally once more without irradiation. (Right) The peak voltage in each condition is plotted against the commanded probe displacement.

3.9 Discussion of Results

The results presented here demonstrate that ultraviolet light is absorbed and converted to heat by chromophores in mitochondria. Heat then leads to a mechanical change in the hair bundle, opening mechanotransduction channels and displacing it towards its tall edge. This mechanism clarifies some of our early and puzzling results. Specifically, we found that hair bundles located outside of the laser beam moved in response to light. This response decayed with distance from the beam, but the rate of decay with distance varied among bundles. It now seems likely that different temperature pulses were evoked as a bundle was moved further away from the beam. As the microscope stage was translated to displace a bundle, the beam impinged on tissue of varying composition. When the beam irradiated a mitochondrial-rich area, a large temperature change arose. Conversely, when an area with few mitochondria was irradiated, such as a supporting cell, the temperature change was likely minimal. This variation likely contributed to the large range of spatial decay profiles between different bundles (Fig. 2.8). The spread of heat likely contributed to a response perimeter that was larger than the beam's extent. Variations in the precise positioning of hair cells under the beam, as well as the geometrical arrangement of each cell's mitochondria, likely underlay much of the variation in kinetics and amplitude of hair-bundle movements.

Chapter 4

Conclusion

The present results demonstrate that heat pulses evoked by ultraviolet or infrared irradiation stimulate hair bundles. Heat is generated by the ultraviolet excitation of intracellular chromophores, the preponderance of which reside in mitochondria [63, 64]. The transformation of light into thermal energy is a ubiquitous property of cells that depends on their concentration of chromophores. Hair cells may be particularly prone to photothermal stimulation owing to their high concentration of mitochondria. We anticipate that the function of other mitochondrion-rich cells, such as myocytes, hepatocytes, and neurons, could similarly be altered by irradiation-evoked heating, especially if these cells contain highly temperature-dependent molecules.

This work may be the first report of thermal stimulation of excitable cells by mechanical modulation. Prior studies have found that transient heating stimulates cells through photocapacitive depolarization, gating of thermally sensitive channels, or mitochondrial Ca^{2+} release [56, 57, 65, 66]. The ability of a hair cell to detect thermal pulses hinges upon the high sensitivity of its mechanical antenna, the hair bundle. A hair bundle's channels are connected in parallel, an arrangement that equally divides tension among all of its tip links. When a fraction of the bundle's tip links relaxes,

that tension is redistributed among the remaining links, increasing their channels' open probability. The tension release is not obliged to occur in the tip link itself, but may arise in any of the elements in series with it. For example, the release element hypothesized to underlie fast adaptation could undergo a conformational change to release tension upon heating [33]. Alternatively, a heat-dependent conformational change in the adaptation motor might slacken tip links.

The present results are unlikely to be explained by any process that results in an increase in tip-link tension. Such processes might include stereociliary lenghthening, thermal expansion of the stereociliary core, or an increase in tip-link stiffness. Although a heat-evoked increase in tip-link tension would open mechanotransduction channels and cause positively-directed hair-bundle motion, the polarity of movement would reverse upon blockage of channels with gentamicin. Additionaly, blocking hair-bundle motion with a stiff probe would not lead to reclosure of the channels open at rest, but would open closed channels. This is the opposite of the observations made in Figure 3.28, thus it is unlikely that heat increases tip-link tension.

An alternative mechanism of action for heat-evoked hair-bundle motion is calcium release from intracellular stores such as mitochondria and endoplasmic reticulum. Calcium released from intracellular stores might have several actions on a hair cell. First, it would likely open calcium-gated potassium channels on the basolateral cell membrane. This would result in hyperpolarization in a tip-link independent manner. Hyperpolarization could in turn cause hair-bundle motion [40]. Although we did not observe heat-evoked hyperpolarization in cells with ruptured tip links, five cells with intact tip links were hyperpolarized by ultraviolet irradiation (Table 2.1). It is unclear whether this stems from a calcium-dependent potassium conductance, or from reclosure of mechanotransduction channels through another mechanism. It is possible that heat-mediated reduction in tip-link tension can cause channel reclosure in some

instances, perhaps when the stiffness decrease is not enough to induce other channels to open. Calcium might also act on the cuticular plate, although any mechanism involving this organelle is speculative because its function is poorly understood. Motion at the cuticular plate could cause mechanotransduction channel gating, however, any motion evoked by the cuticular plate is not expected to be tip-link dependent. Because the stereocilia of a hair bundle remain coherent even without their tip links, hair-bundle motion caused by cuticular plate movement should be observed even with ruptured tip links. It is possible, however, that heat generates an increase in stereociliary pivot tension. Such an effect would cause hair-bundle motion when tip links are intact, as the increased stiffness would cause channel gating. Several lines of evidence argue against this possibility however. First, the pattern of light-evoked motion observed with hair-bundle offsets does not match that expected for a change in stereociliary pivots (Figure 3.26). Second, we did not observe a change in stereociliary pivot stiffness when a hair bundle was irradiated with ultraviolet light (Fig. 3.27). Finally, blockage of a hair bundle with a stiff probe would not alter the open probability of transduction channels if the mechanism of motion was an increase in stereociliary pivot stiffness. Taken together these observations suggest that the cuticular plate is unlikely to underlie heat-evoked hair-bundle stimulation.

It is unlikely that a temperature step would significantly alter the equilibrium open probability of the transduction channel. The channel's open probability at rest, P_o , is a function of the free energy difference between its open and closed states given by

$$P_o = \frac{1}{1 + e^{-\Delta G/kT}} = \frac{1}{1 + e^{\Delta S/k} \cdot e^{-\Delta H/kT}}\,, \tag{4.1}$$

in which ΔG is the free energy difference, ΔS and ΔH are, respectively, the entropic and enthalpic contributions to the free energy, k is the Boltzmann constant, and

T is the absolute temperature. The temperature dependence of the open probability is found by differentiating P_o with respect to T:

$$\frac{dP_o}{dT} = -\frac{1}{(1 + e^{\Delta S/k} \cdot e^{-\Delta H/kT})^2} \cdot \left(e^{\Delta S/k} e^{-\Delta H/kT}\right) \cdot \left(\frac{\Delta H}{kT^2}\right) = -P_o(1 - P_o)\left(\frac{\Delta H}{kT^2}\right). \tag{4.2}$$

The free energy difference between closed and open states is primarily enthalpic, and estimated to be 1 kT per molecule [67]. Assuming that this value is entirely enthalpic, and for an open probability of 0.5, the rate of change of the open probability is only 8.5×10^{-4} K^{-1} . A 10 K temperature increase, on the high end of the values observed in this study, would increase the open probability by only 8.5×10^{-3}. This value is several orders of magnitude smaller than needed to explain our present results. The above calculation, however, does not take into account the intrinsic energy difference between the closed and open states, the energy difference when each state is disconnected from the transduction apparatus. That value, ΔG^0, is estimated to be on the order of 10 kT per molecule [68]. Though no estimate of the enthalpic contribution to this energy exists, a calculation of the change in P_o under the assumption that ΔG^0 is entirely enthalpic gives a tenfold increase in the ΔP_o cited above. If the transition from closed to open involves an increase in entropy, the intrinsic enthalpic difference could be larger than the difference in free energy. However, the opening of an ion channel is expected to decrease entropy due to increased ordering of water molecules along the pore, making this scenario unlikely.

One alternative mechanism for light-evoked hair-bundle movement is photocapacitive hair-cell depolarization. The total capacitance of a cell membrane has contributions from both the lipid bilayer and the double ion bilayers lying to either side of it [69]. Upon rapid heating of the cell membrane, the diffusion rate of the ions form-

ing the bilayers increases, causing a change in capacitance. This capacitance change generates a current and depolarizes the cell by several millivolts [70, 65]. Because photocapacitive current is proportional to the rate of temperature increase, brief heat pulses most efficiently depolarize cells. Because the nature of photocapacitive depolarization is general, we expect it to occur in hair cells. Indeed, transient heat pulses generate excitatory photocapacitive currents in mammalian vestibular hair cells [57]. Because hair-cell voltage changes are known to cause hair-bundle motion, photocapacitive depolarization could underlie our current results. Hair-cell depolarization, however, displaces hair bundles away from the kinociliary bulb [40, 33]. This rapid motion is thought to stem from retensioning of the gating springs upon expulsion of intracellular Ca^{2+} by cellular depolarization.

The strongest evidence against a photocapacitive mechanism in the present results is the lack of an electrical response in bundles with severed tip links. Our stimuli did not generate temperature changes fast enough to alter the membrane capacitance. Had the rate of heating been higher, we would likely have seen a contribution by depolarization-evoked hair-bundle movement. The interaction of depolarization-evoked hair-bundle motion with motion stemming from mechanical changes of the sort seen in this study may result in biphasic displacement timecourses.

Another alternative mechanism for light-evoked stimulation of hair cells is optoacoustic stimulation. When light energy is deposited in a volume faster than heat can diffuse away from it, a pressure - or optoacoustic - wave develops. This wave might stimulate hair bundles, resulting in hair-cell activation. *In vivo* studies have shown that optoacoustic stimulation can occur in the cochlea and relies primarily on the absorption of light by hemoglobin and water [71]. The present results, however, cannot be explained by optoacoustic stimulation. Optoacoustic waves are generated under conditions of thermal confinement, the regime in which heat is deposited in a

region faster than it is carried away by diffusion [72]. The longest irradiation pulse permissible for thermal confinement, τ_{th} is given by

$$\tau_{th} = \frac{\delta^2}{4\kappa}\,, \tag{4.3}$$

in which δ is the beam radius or the optical penetration depth of the irradiating light, whichever is smaller, and κ is the thermal diffusivity of water, 1.43×10^{-7} $\mathrm{m}^2 \cdot \mathrm{s}^{-1}$ [72]. The primary mitochondrial absorber is cytochrome c, with a molar absorption coefficient of 0.06 $\mathrm{M}^{-1} \cdot \mathrm{cm}^{-1}$ at 405 nm [48]. Assuming a cytochrome c concentration of 100 μM in mitochondria, the absorption coefficient is 6×10^{-6} cm^{-1} [73]. For a cylinder of mitochondria of diameter 10 μm and height 5 μm at the apex of a hair cell, δ is 5 μm. τ_{th} is therefore 43 μs, or one thousandth shorter our typical pulse duration of 40 ms. Thermal confinement is not present, and no optoacoustic wave is generated. Water's absorption coefficient at a wavelength of 405 nm is so low that an optoacoustic pulse owing to water is also impossible. This analysis is supported by our observation that hair bundles do not respond to light after their tip links are ruptured. If hair-bundle motion arose from optoacoustic stimulation, the response would be expected to persist.

The mechanism described here permits remote stimulation of hair cells. The ability to stimulate hair cells without genetic manipulation or mechanical implements may allow novel and previously impossible studies. For example, I anticipate that irradiation can be used to study the activity of cochlear outer hair cells *in vivo* without the generation of a traveling wave. The ability to rapidly and synchronously stimulate many hair cells should additionaly permit investigations requiring rapid simultaneous activation of hair cells. This aproach could be used to study synaptic fusion at the hair cell's ribbon synapse. Finally, irradiation can be used to verify that a hair cell's transduction apparatus is intact before further experimentation.

Although the bulk of this study was conducted with ultraviolet stimulation, the mechanism of hair-bundle movement relies on heat production. Ultraviolet light is inefficiently absorbed by water, the major biological chromophore. Future users of this method would be best served by using infrared light, which can generate hair-bundle motion at a power density two orders of magnitude lower than that required for ultraviolet illumination. Infrared light is also much less damaging to tissue, and thus better suited for long-term use.

Bibliography

[1] A J Hudspeth. Integrating the active process of hair cells with cochlear function. *Nature Reviews Neuroscience*, August 2014.

[2] P M Sellick, R Patuzzi, and B M Johnstone. Measurement of basilar membrane motion in the guinea pig using the Mössbauer technique. *The Journal of the Acoustical Society of America*, 72(1):131–141, July 1982.

[3] H Davis. An active process in cochlear mechanics. *Hearing Research*, 9(1):79–90, January 1983.

[4] H L De Vries. Brownian movement and hearing. *Physica*, 14(1):48–60, 1948.

[5] Murray F Spiegel and Charles S Watson. Performance on frequency-discrimination tasks by musicians and nonmusicians. *The Journal of the Acoustical Society of America*, 76(6):1690–1695, December 1984.

[6] M A Ruggero and N C Rich. Application of a commercially-manufactured Doppler-shift laser velocimeter to the measurement of basilar-membrane vibration. *Hearing Research*, 51(2):215–230, February 1991.

[7] T Gold. Hearing. II. The Physical Basis of the Action of the Cochlea. *Proceedings of the Royal Society B: Biological Sciences*, 135(881):492–498, December 1948.

[8] Anthony W Peng and Anthony J Ricci. Somatic motility and hair bundle mechanics, are both necessary for cochlear amplification? *Hearing Research*, 273(1-2):109–122, March 2011.

[9] Dáibhid Ó Maoiléidigh and A J Hudspeth. Effects of cochlear loading on the motility of active outer hair cells. *Proceedings of the National Academy of Sciences*, 110(14):5474–5479, April 2013.

[10] Julien B Azimzadeh and Joshua D Salvi. Physiological Preparation of Hair Cells from the Sacculus of the American Bullfrog (Rana catesbeiana). *Journal of Visualized Experiments*, 1(121):e55380–e55380, March 2017.

[11] R A Jacobs and A J Hudspeth. Ultrastructural Correlates of Mechanoelectrical Transduction in Hair Cells of the Bullfrog's Internal Ear. *Cold Spring Harbor Symposia on Quantitative Biology*, 55(0):547–561, January 1990.

[12] T Holton and A J Hudspeth. The transduction channel of hair cells from the bull-frog characterized by noise analysis. *The Journal of Physiology*, 375:195–227, June 1986.

[13] Piotr Kazmierczak, Hirofumi Sakaguchi, Joshua Tokita, Elizabeth M Wilson-Kubalek, Ronald A Milligan, Ulrich Müller, and Bechara Kachar. Cadherin 23 and protocadherin 15 interact to form tip-link filaments in sensory hair cells. *Nature*, 449(7158):87–91, September 2007.

[14] J A Assad, G M Shepherd, and D P Corey. Tip-link integrity and mechanical transduction in vertebrate hair cells. *Neuron*, 7(6):985–994, December 1991.

[15] A J Hudspeth D P Corey. Response latency of vertebrate hair cells. *Biophysical Journal*, 26(3):499–506, June 1979.

[16] D P Corey and A J Hudspeth. Kinetics of the receptor current in bullfrog saccular hair cells. *The Journal of neuroscience : the official journal of the Society for Neuroscience*, 3(5):962–976, May 1983.

[17] J Howard and A J Hudspeth. Compliance of the hair bundle associated with gating of mechanoelectrical transduction channels in the bullfrog's saccular hair cell. *Neuron*, 1(3):189–199, May 1988.

[18] Andrei S Kozlov, Thomas Risler, and A J Hudspeth. Coherent motion of stereocilia assures the concerted gating of hair-cell transduction channels. *Nature Neuroscience*, 10(1):87–92, 2007.

[19] A J Hudspeth. Making an effort to listen: mechanical amplification in the ear. *Neuron*, 59(4):530–545, August 2008.

[20] Jeffrey R Holt, Susan K H Gillespie, D William provance, Kavita Shah, Kevan M Shokat, David P Corey, John A Mercer, and Peter G Gillespie. A chemical-genetic strategy implicates myosin-1c in adaptation by hair cells. *Cell*, 108(3):371–381, February 2002.

[21] R G Walker and A J Hudspeth. Calmodulin controls adaptation of mechanoelectrical transduction by hair cells of the bullfrog's sacculus. *Proceedings of the National Academy of Sciences of the United States of America*, 93(5):2203–2207, March 1996.

[22] G M Shepherd and D P Corey. The extent of adaptation in bullfrog saccular hair cells. *The Journal of neuroscience : the official journal of the Society for Neuroscience*, 14(10):6217–6229, October 1994.

[23] Pascal Martin, D Bozovic, Y Choe, and A J Hudspeth. Spontaneous oscillation by hair bundles of the bullfrog's sacculus. *The Journal of Neuroscience*, 23(11):4533–4548, June 2003.

[24] S W F Meenderink, P M Quinones, and D Bozovic. Voltage-Mediated Control of Spontaneous Bundle Oscillations in Saccular Hair Cells. *The Journal of neuroscience : the official journal of the Society for Neuroscience*, 35(43):14457–14466, October 2015.

[25] M E Benser, R E Marquis, and A J Hudspeth. Rapid, active hair bundle movements in hair cells from the bullfrog's sacculus. *The Journal of neuroscience : the official journal of the Society for Neuroscience*, 16(18):5629–5643, September 1996.

[26] J Howard and A J Hudspeth. Mechanical relaxation of the hair bundle mediates adaptation in mechanoelectrical transduction by the bullfrog's saccular hair cell. *Proceedings of the National Academy of Sciences of the United States of America*, 84(9):3064–3068, May 1987.

[27] A C Crawford, M G Evans, and R Fettiplace. Activation and adaptation of transducer currents in turtle hair cells. *The Journal of Physiology*, 419:405–434, December 1989.

[28] Eunice L M Cheung and David P Corey. Ca2+ Changes the Force Sensitivity of the Hair-Cell Transduction Channel. *Biophysical Journal*, 90(1):124–139, January 2006.

[29] J Howard and A J Hudspeth. Compliance of the hair bundle associated with gating of mechanoelectrical transduction channels in the Bullfrog's saccular hair cell. *Neuron*, 1(3):189–199, May 1988.

[30] Y Choe, M O Magnasco, and A J Hudspeth. A model for amplification of hair-bundle motion by cyclical binding of Ca2+ to mechanoelectrical-transduction channels. *Proceedings of the National Academy of Sciences of the United States of America*, 95(26):15321–15326, December 1998.

[31] Y C Wu, A J Ricci, and R Fettiplace. Two components of transducer adaptation in auditory hair cells. *Journal of Neurophysiology*, 82(5):2171–2181, November 1999.

[32] A J Hudspeth, Y Choe, A D Mehta, and P Martin. Putting ion channels to work: mechanoelectrical transduction, adaptation, and amplification by hair cells. *Proceedings of the National Academy of Sciences of the United States of America*, 97(22):11765–11772, October 2000.

[33] D Bozovic and A J Hudspeth. Hair-bundle movements elicited by transepithelial electrical stimulation of hair cells in the sacculus of the bullfrog. *Proceedings of the National Academy of Sciences of the United States of America*, 100(3):958–963, February 2003.

[34] Jean-Yves Tinevez, Frank Jülicher, and Pascal Martin. Unifying the various incarnations of active hair-bundle motility by the vertebrate hair cell. *Biophysical Journal*, 93(11):4053–4067, December 2007.

[35] Jonathon Howard and J A Spudich. Is the lever arm of myosin a molecular elastic element? *Proceedings of the National Academy of Sciences of the United States of America*, 93:4462–4464, 1996.

[36] G C Ellis-Davies and J H Kaplan. Nitrophenyl-EGTA, a photolabile chelator that selectively binds Ca2+ with high affinity and releases it rapidly upon photolysis.

Proceedings of the National Academy of Sciences of the United States of America, 91(1):187–191, January 1994.

[37] Jonathan E Gale, Jason R Meyers, Ammasi Periasamy, and T Corwin. Survival of bundleless hair cells and subsequent bundle replacement in the bullfrog's saccule. *Journal of Neurobiology*, 50(2):81–92, January 2002.

[38] A J Hudspeth and D P Corey. Controlled bending of high-resistance glass microelectrodes. *The American Journal of Physiology*, 234(1):C56–7, January 1978.

[39] A B Kroese, A Das, and A J Hudspeth. Blockage of the transduction channels of hair cells in the bullfrog's sacculus by aminoglycoside antibiotics. *Hearing Research*, 37(3):203–217, February 1989.

[40] J A Assad, N Hacohen, and D P Corey. Voltage dependence of adaptation and active bundle movement in bullfrog saccular hair cells. *Proceedings of the National Academy of Sciences*, 1989.

[41] A J Hudspeth and R S Lewis. A model for electrical resonance and frequency tuning in saccular hair cells of the bull-frog, Rana catesbeiana. *The Journal of Physiology*, 400:275–297, June 1988.

[42] R S Lewis and A J Hudspeth. Voltage- and ion-dependent conductances in solitary vertebrate hair cells. *Nature*, 304(5926):538–541, August 1983.

[43] P Martin, A D Mehta, and A J Hudspeth. Negative hair-bundle stiffness betrays a mechanism for mechanical amplification by the hair cell. *Proceedings of the National Academy of Sciences of the United States of America*, 97(22):12026–12031, October 2000.

[44] Dáibhid Ó Maoiléidigh, Ernesto M Nicola, and A J Hudspeth. The diverse effects of mechanical loading on active hair bundles. *Proceedings of the National Academy of Sciences*, 109(6):1943–1948, February 2012.

[45] Joshua D Salvi, Dáibhid Ó Maoiléidigh, Brian A Fabella, Mélanie Tobin, and A J Hudspeth. Control of a hair bundle's mechanosensory function by its mechanical load. *Proceedings of the National Academy of Sciences*, 112(9):E1000–9, March 2015.

[46] J Howard. Mechanics of Motor Proteins and the Cytoskeleton (Sunderland, MA: Sinauer), 2001.

[47] Jing Yao, Beiying Liu, and Feng Qin. Rapid temperature jump by infrared diode laser irradiation for patch-clamp studies. *Biophysical Journal*, 96(9):3611–3619, May 2009.

[48] W D BUTT and D KEILIN. Absorption spectra and some other properties of cytochrome c and of its compounds with ligands. *Proceedings of the Royal Society of London. Series B, Biological sciences*, 156:429–458, November 1962.

[49] Bin Liu, Hongtao Liu, Dongping Zhong, and Chentao Lin. Searching for a photocycle of the cryptochrome photoreceptors. *Current Opinion in Plant Biology*, 13(5):578–586, October 2010.

[50] J M SIEGEL, G A MONTGOMERY, and R M BOCK. Ultraviolet absorption spectra of DPN and analogs of DPN. *Archives of Biochemistry and Biophysics*, 82(2):288–299, June 1959.

[51] Rosario Rizzuto, Diego De Stefani, Anna Raffaello, and Cristina Mammucari. Mitochondria as sensors and regulators of calcium signalling. *Scientific Reports*, 13(9):566–578, August 2012.

[52] Laura Contreras, Ilaria Drago, Enrico Zampese, and Tullio Pozzan. Mitochondria: The calcium connection. *BBA - Bioenergetics*, 1797(6-7):607–618, June 2010.

[53] T Hasson, P G Gillespie, J A Garcia, R B MacDonald, Y Zhao, A G Yee, M S Mooseker, and D P Corey. Unconventional myosins in inner-ear sensory epithelia. *The Journal of Cell Biology*, 137(6):1287–1307, June 1997.

[54] Christopher Batters, Dario Brack, Heike Ellrich, Beate Averbeck, and Claudia Veigel. Calcium can mobilize and activate myosin-VI. *Proceedings of the National Academy of Sciences of the United States of America*, 113(9):E1162–E1169, March 2016.

[55] Lana M Pollock and Brian M McDermott Jr. The cuticular plate: A riddle, wrapped in a mystery, inside a hair cell. *Birth Defects Research Part C: Embryo Today: Reviews*, 105(2):126–139, June 2015.

[56] Gregory M Dittami, Suhrud M Rajguru, Richard A Lasher, Robert W Hitchcock, and Richard D Rabbitt. Intracellular calcium transients evoked by pulsed infrared radiation in neonatal cardiomyocytes. *The Journal of Physiology*, 589(6):1295–1306, March 2011.

[57] Richard D Rabbitt, Alan M Brichta, Hessam Tabatabaee, Peter J Boutros, JoongHo Ahn, Charles C Della Santina, Lauren A Poppi, and Rebecca Lim. Heat pulse excitability of vestibular hair cells and afferent neurons. *Journal of Neurophysiology*, 116(2):825–843, August 2016.

[58] J Crank. *The Mathematics of Diffusion*. Clarendon Press, 1975.

[59] E A Lumpkin and A J Hudspeth. Regulation of free Ca2+ concentration in hair-cell stereocilia. *The Journal of neuroscience : the official journal of the Society for Neuroscience*, 18(16):6300–6318, August 1998.

[60] J Valat, C Griguer, J Lehouelleur, and A Sans. Motile responses of isolated guinea pig vestibular hair cells. *Neuroscience letters*, 127(2):231–236, June 1991.

[61] H S Carslaw and J C Jaeger. *Conduction of Heat in Solides*. Oxford at the Clarendon Press, second edition edition, 1959.

[62] J G Bayly, V B Kartha, and W H Stevens. The absorption spectra of liquid phase H2O, HDO and D2O from 0· 7 μm to 10 μm. *Infrared Physics*, 3(4):211–222, 1963.

[63] Michael W Berns, Nicolai Gamaleja, Robert Olson, Cecilia Duffy, and Donald E Rounds. Argon laser micro-irradiation of mitochondria in rat myocardial cells in tissue culture. *Journal of Cellular Physiology*, 76(2):207–213, October 1970.

[64] C Salet. A study of beating frequency of a single myocardial cell. I. Q-switched laser microirradiation of mitochondria. *Experimental Cell Research*, 73(2):360–366, August 1972.

[65] Mikhail G Shapiro, Kazuaki Homma, Sebastian Villarreal, Claus-Peter Richter, and Francisco Bezanilla. Infrared light excites cells by changing their electrical capacitance. *Nature Communications*, 3:376–10, March 2012.

[66] Thomas Voets, Karel Talavera, Grzegorz Owsianik, and Bernd Nilius. Sensing with TRP channels. *Nature chemical biology*, 1(2):85–92, July 2005.

[67] David P Corey. *A biophysical approach to sensory transduction by vertebrate hair cells (Dissertation thesis)*. PhD thesis, California Institute of Technology, 1980.

[68] A J Hudspeth. Hair-bundle mechanics and a model for mechanoelectrical transduction by hair cells. In D P Corey and S D Roper, editors, *Sensory Transduction Society of General Physiologists th Annual Symposium*, pages 357–370. 1992.

[69] S McLaughlin. The electrostatic properties of membranes. *Annual review of biophysics and biophysical ...*, 1989.

[70] Qiang Liu, Micah J Frerck, Holly A Holman, Erik M Jorgensen, and Richard D Rabbitt. Exciting Cell Membranes with a Blustering Heat Shock. *Biophysj*, 106(8):1570–1577, April 2014.

[71] Michael Schultz, Peter Baumhoff, Hannes Maier, Ingo U Teudt, Alexander Krüger, Thomas Lenarz, and Andrej Kral. Nanosecond laser pulse stimulation of the inner ear—a wavelength study. *Biomedical Optics Express*, 3(12):3332–3345, 2012.

[72] G Paltauf, H Schmidt-Kloiber, and M Frenz. Photoacoustic waves excited in liquids by fiber-transmitted laser pulses. *The Journal of the Acoustical Society of America*, 104(2):890–897, August 1998.

[73] S S Gupte and C R Hackenbrock. The role of cytochrome c diffusion in mitochondrial electron transport. *The Journal of Biological Chemistry*, 263(11):5248–5253, April 1988.